Master's thesis

2019

Idun Eiken

NTNU
Norwegian University of
Science and Technology
Faculty of Engineering
Department of Civil and Environmental Engineering

Idun Eiken

An experimental study of thermal properties and the influence on the ground thermal regime in permafrost soil

July 2019

NTNU
Norwegian University of
Science and Technology

NTNU
Norwegian University of
Science and Technology

NTNU

Norwegian University of
Science and Technology

An experimental study of thermal properties and the influence on the ground thermal regime in permafrost soil

Idun Eiken

Civil and Environmental Engineering
Submission date: July 2019
Supervisor: Gustav Grimstad
Co-supervisor: Arne Aalberg

Norwegian University of Science and Technology
Department of Civil and Environmental Engineering

Preface

This master's thesis in geotechnical engineering is the final part of the MSc in Civil and Environmental Engineering at the Norwegian University of Science and Technology (NTNU). The work with the thesis was done in the spring semester of 2019 and the thesis was finalized in July 2019. Cooperation with the University Centre at Svalbard (UNIS) has made the study possible. An experimental study including laboratory work was performed at UNIS during the first two months of the work. The rest of the work was performed in Trondheim at NTNU. The work has been supervised by Professor Gustav Grimstad and Professor Arne Aalberg.

The author was introduced to theoretical and challenging aspects with engineering in permafrost areas through a course at UNIS in 2016. This course evoked my interest for further studies on frozen soil and permafrost. Therefore, this was the topic of a project report that was written in the fall semester of 2018. The work with the report inspired further work to study how the ground thermal regime in permafrost is affected by climate change.

Trondheim, 2019-07-25

Idun Eiken

Acknowledgment

I would like to acknowledge my supervisors Professor Gustav Grimstad and Professor Arne Aalberg for supporting me through my work with this master's thesis. Arne was very helpful in introducing me to the lab and everything I needed during the experimental work at UNIS. Discussions and insight from Gustav has greatly improved my understanding of the topic. I would like to thank UNIS for hosting me as a guest master's student and giving me the opportunity to work in the laboratory. The NGTS project has supported me economically, which I am grateful for. Graham Lewis Gilbert and Arne Instanes, both connected to UNIS, have given me good advice through the experimental work and in understanding the results.

My stay at Svalbard was extra enjoyable because of Mari and Linda who hosted me. The last months in Trondheim would not have been the same without Kaja, Per-Christian and Ingrid. My fellow master students have made it a joy to be spending a lot of time studying. I appreciate all the lunch breaks, encouragement, relevant and irrelevant discussions and endless coffee rounds.

I want to thank my dad, Trond, for showing interest in my project, for discussions and encouraging me when that was necessary. In addition, I want to thank the rest of my family and closest friends for encouraging me and listening to my talk about permafrost.

I.E.

Abstract

Soil is a porous composite material consisting of soil grains and pores filled with air and water. The strength of soil increases when it freezes, and infrastructure in permafrost areas depend on the high compressive strength and high bearing capacity of frozen soil. Thawing of frozen soil will reduce its strength and can give stability problems and lead to increased settlements of infrastructure. Adsorption and capillary forces and solute content in the pore water cause a depression of the freezing point of the pore water and are the reasons why there is an amount of unfrozen water in frozen soil. When temperatures are lowered below the freezing point part of the pore water will freeze. The change in water and ice composition in the pores will cause a change in the soil thermal properties and affect the temperature dependent strength in the soil.

Determination of index properties and thermal properties of a fine grained saline permafrost soil from the site UNIS East at Svalbard has been performed. Frozen and unfrozen thermal conductivity and volumetric heat capacity of the soil samples have been measured by a KD2 Pro Thermal Properties Analyzer. The KD2 Pro is unsuitable to measure thermal properties around the freezing point since the melting of ice is not accounted for in the solver. Values for thermal conductivity obtained by direct measurements tend to be higher than the values found by empirical formulations taken from literature. Values by Kersten's empirical formulations indicate higher values than determined by Johansen's formulation.

The water potential of the soil samples has been determined using the WP4C Dew Point PotentiaMeter. By measuring the water potential for sub samples with a range of different water contents, the measurements can be used to estimate the amount of unfrozen water content in the soil at various temperatures. The estimation of unfrozen water content is based on a newly derived form of the Clapeyron equation. The soil water content, the pore water potential and the concentration of solutes in the frozen soil are addressed in the equation. The Clapeyron equation is used to determine the freezing point of soil based on the matric potential, the osmotic potential and the total pore water potential. Experiments have been performed to measure the freezing point temperature in soil, and the test results are compared to the calculated results by the Clapeyron equation. Calculations show that for a fully saturated unfrozen soil sample with a high salinity, the effect of solutes in the pore water dominates the magnitude of the freeze point depression. When the soil is fully saturated, the matric potential is small, but when water starts to freeze the saturation decreases and the matric potential increases. For the tested samples the matric potential exceeds that of the osmotic at temperatures between –5°C and –10°C. The osmotic potential decreases with lowering of temperatures and is negligible when it is exceeded by the matric potential. It is found that the matric potential is the reason why part of the pore water remain unfrozen even at very low temperatures. The Clapeyron equation is used to estimate the curve of unfrozen water content for the soil. Based on the unfrozen water content curve the volumetric heat capacity can be calculated and the thermal conductivity can be estimated as functions of temperature.

A model based on the estimated functions for unfrozen water content and thermal properties has been set up in the finite element program Geostudio 2018 where the TEMP/W analysis module was used. It was attempted to simulate the response in the ground thermal regime due to climate change and rising air temperatures. The boundary conditions applied to the model were adapted from measured air and ground temperatures to simulate the present conditions at the UNIS East site. The model was validated by comparing the simulated temperature profile to recorded thermistor measurements. For simulations of future ground conditions the predicted changes in air temperatures based on different scenarios for greenhouse gas emissions (RCP2.6, RCP8.5)

presented by Hanssen-Bauer et al. (2019) were applied as boundary condition at ground surface. In simulations over a period of 50 years with RCP2.6 scenario the conditions are not critical for existing infrastructure. This is because the increase in active layer thickness is small and the temperatures in near-surface-permafrost are still below the freezing point and therefore the strength of the soil will not be reduced significantly due to temperature increase. In simulations for 100 years with RCP2.6 scenario and for 50 years with the RCP8.5 scenario the temperature profiles from the simulations indicate a drastic increase in active layer thickness and thawing of near-surface-permafrost after. This will reduce the strength and bearing capacity of the soil and cause geotechnical challenges when concerning the ground conditions for infrastructure. The different scenarios show a big difference in development of the state of the near-surface-permafrost for the next 50 years. A sensitivity analysis of the model response to various soil parameters shows that the rate of temperature change is sensitive for changes in the freezing point and unfrozen water content. The freezing point is important for correct determination of the unfrozen water content curve which is decisive for how large fraction of the pore water that freezes at different temperatures. Latent heat must be added during phase change when ice melts or water freezes. The consumption of latent heat slows the rate of ground warming. The amount of latent heat that must be added at different temperatures in the model is determined by the unfrozen water content curve for the soil material. The effect of solutes must be included in the unfrozen water content curves and the temperature dependency of thermal properties should be included when predictions of temperatures in the ground thermal regime in permafrost areas for geotechnical purposes are to be performed.

Sammendrag

Jord er et porøst materiale som består av mineralkorn og porer som er fylt med luft og vann. Frossen jord har høy trykkstyrke og høy bæreevne. Infrastruktur som er etablert i områder med permafrost er avhengig av styrken i den frosne jorda. Når frossen jord tiner vil styrken i jorda reduseres og det kan føre til stabilitets problemer i skråninger og for fundamter. I tillegg kan tiningen forårsake setninger som kan være skadelig for infrastruktur. Adsorpsjons- og kapillærkrefter og saltinnhold i porevannet kan forårsake en senkning av frysepunktet i porevannet. Disse kreftene gjør også at en del av porevannet forblir ufrosset selv når temperaturene senkes under frysepunktet. Mengden med vann og is endres ettersom temperaturen i jorda endres og dette forårsaker at de termiske egenskapene endres med temperatur.

Det har blitt utført rutineundersøkelser og testing av termiske egenskaper på prøver av finkorning, saltholdig jord fra et borehull i permafrost på Svalbard. Verdier for ufrossen og frossen termisk konduktivitet og volumetrisk varmekapasitet har blitt målt med KD2 Pro Thermal Properties Analyzer. Målingene med KD2 Pro gir usikre resultater ved jord temperaturer på og under frysepunktet. Dette er fordi smeltingen av is forårsaket av varmeøkningen under målingen ikke er tatt hensyn til i løsningsalgortimen i måleren. Verdier fra direkte målinger av termisk konduktivitet viser en tendens til å være høyere enn verdiene beregnet med empiriske formuleringer. Verdiene for termisk konduktivitet beregnet med Kerstens empiriske metode gir noe høyere verdier enn ved bruk av Johansens metode.

Vannpotensialet i jordprøvene har blitt målt med WP4C Dew Point PotentiaMeter. Det målte vannpotensialet har blitt brukt til å beregne mengden ufrosset vann ved negative temperaturer i jorda. Beregninger av ufrosset vann er basert på en utvidet form av den generelle Clapeyron likningen. Verdier for vanninnhold, vannpotensial og saltkonsentrasjonen i porevannet brukes for å beregne frysepunktet i jorda. Det osmotiske potensialet og det kapillære potensialet gir bidrag til frysepunkts senkningen. Frysepunktet i jorda har blitt målt direkte og brukes for å kontrollere resultatene fra Clapeyron likningen. Når en betrakter en fullt mettet prøve med et visst saltinnhold, er det funnet at det osmotiske potensialet gir størst effekt på senkningen av frysepunktet. Når jorda er fullt mettet er kapillærpotensialet lite, men når porevannet begynner å fryse synker metningsgraden. Når metningsgraden synker øker det kapillæret potensialet. Forsøk viser at det kapillære potensialet blir større enn det osmotiske potensialet mellom –5°C og –10°C. Det osmotiske potensialet synker med synkende temperaturer og er neglisjerbart ved lave temperaturer. Det kapillære potensialet er avgjørende for mengden vann som forblir ufrosset på lave temperaturer under ca. –5°C. Den estimerte kurven for ufrosset vann ved negative temperaturer har blitt benyttet for finne de termiske egenskapene som funksjon av temperatur.

De estimerte funksjonene for ufrosset vann og termiske egenskaper har blitt benyttet som parametere i en elementmetode modell satt opp i programmet Geostudio 2018 og analyser er utført med TEMP/W. Modellen er brukt til å simulere hvordan det termiske regimet i jorda påvirkes av klimaendringer og økning i lufttemperaturer. Grensebetingelsene som er påført i modellen er basert på målinger av lufttemperaturer og bakketemperaturer for at modellen skal gjengi dagens situasjon. Modellen valideres ved å sammenligne et temperaturprofil fra en simulering med et profil fra termistor målinger. Simulering av fremtidige temperaturforhold i jorda er gjort ved at predikerte endringer i lufttemperaturer basert på forskjellige klimagasssenarioer er lagt til som grensebetingelser i modellen. Senarioene RCP2.6 og RCP8.5 er brukt i simuleringene. Etter 50 år med utslippssenario RCP2.6 kan en økning i aktivt lag observeres, men endringene er ikke kritiske for infrastruktur i området. Derimot viser temperaturprofilene fra simuleringene

etter 100 år under RCP2.6 senarioet og etter 50 år med RCP8.5 senarioet at aktivt lag vil få en drastisk økning og at permafrost ned til 10 m dyp vil være nær smeltepunktet. En sensitivitetsanalyse er utført for å se hvor sensitiv modellen er for endringer i jordegenskapene. Analysen viser at temperaturendring i grunnen er sensitivitet for hvor frysepunktet i jorda er og dermed mengden ufrosset vann på ulike temperaturer. Oppvarmingsraten blir betraktelig redusert når is må smeltes fordi det trengs energi i form av latent varme for å smelte isen før materialet kan varmes opp videre. Dermed er kurven for ufrosset vann eller mengden vann som fortsatt er is viktig for å bestemme hvor fort oppvarming av jorda vil skje på forskjellige temperaturer. Det er viktig å bestemme frysepunktet i jorda nøyaktig og effekten av saltinnhold må inkluderes i kurver for ufrosset vann og termiske egenskaper. Dette er viktig for å vite hvilken jordtemperatur som er kritisk for at jorda skal være frossen og kunne for å kunne beregne korrekt mekanisk styrke i permafrost med tanke på geotekniske utfordringer.

Contents

Chapter 1

Introduction

Anthropogenic climate change is one of the most pressing global issues in the 21^{st} century. The Arctic region has experienced more warming than any other region on earth the last 2 to 3 decades, and predictions show that this trend will continue toward the next century (Hanssen-Bauer et al., 2019). The amplification of global warming in the Arctic region can be due to feedback mechanisms from loss of sea ice or changes in atmospheric and oceanic circulation (Førland et al., 2011) but a part of it is likely caused by anthropogenic change (Nordli et al., 2014). In January a report about how climate will develop in Svalbard towards 2100 was released and predicts that mean annual temperatures can rise with up to 10°C the next 100 years with a representative concentration pathway 8.5 (RCP) emission scenario which is a scenario where climate gas emission will continue to increase and no measures are taken to reduce the emissions (Hanssen-Bauer et al., 2019). According to the report near-surface-permafrost in low altitude areas will thaw under the high emission scenario. Permafrost is defined as subsurface material with temperatures remaining below 0 °C more than two consecutive years (Isaksen, 2001). Heat and moisture exchange between the ground surface and the atmosphere conjointly with thermal properties govern the thermal regime in the near-surface layers of soil (Williams & Smith, 1989).

Meteorological records from weather stations in Svalbard are available from 1911. Including observations from trappers and scientific expeditions Nordli et al. (2014) have been able to extend the meteorological observations to 1898. These observations are used to create long term temperature series for the region. Mean annual temperatures (MAT) can be used when observing change in climate over time. Climate changes naturally, but is also influenced by human activity such as emissions of greenhouse gases. Many factors such as wind currents, oceanic circulation and sea ice coverage affect the climate and it is a complex task to predict how the climate will be in the future when concerning all the natural processes. In addition, the prediction is further complicated by including the effect of human influence. A warming period from 1910 with a maxima in the 1930s is known as the "early 20th century warming" (Nordli et al., 2014). This warming coincides with the end of the Little Ice Age in Svalbard (Etzelmüller et al., 2011). A period from 1943 to 1965 all observation stations at Svalbard show a cooling trend (Førland et al., 2011). After this cooling trend temperatures have increased, and the recorded temperatures from the last years are the highest in the recorded period (Nordli et al., 2014). The trend from the extended meteorological observations shows that MAT increase with 2.6°C/century with largest increase in spring temperatures (Nordli et al., 2014). Climate projections indicate that the decrease in sea-ice coverage will be the main reason for the large gradient in temperature increase in Svalbard (Førland et al., 2011).

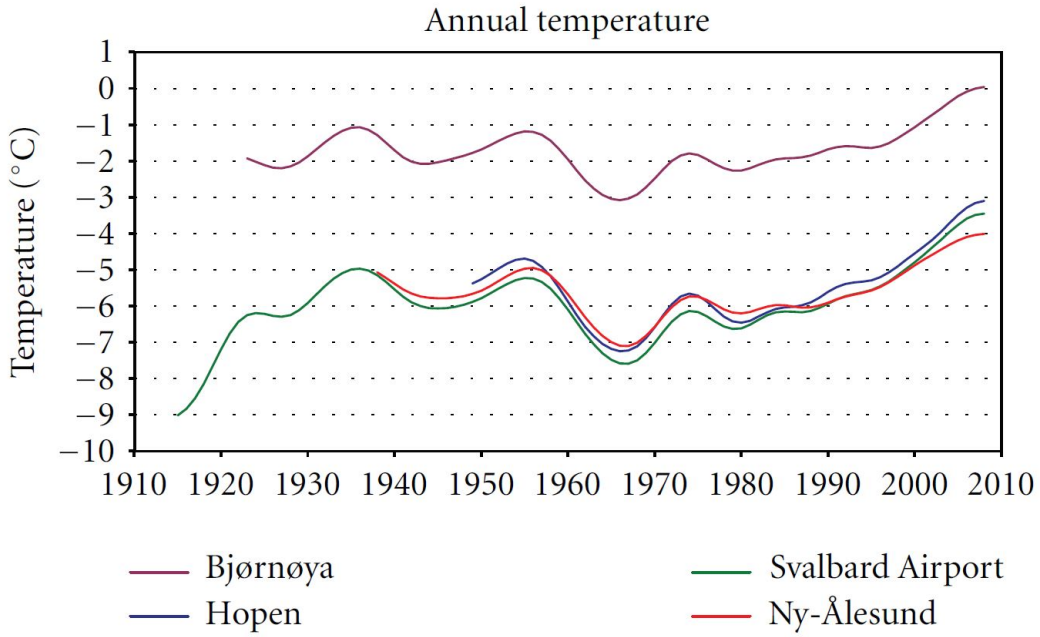

Figure 1.1: *Annual temperature development at weather stations in the Svalbard region (Førland et al., 2011).*

Model predictions of future ground temperatures reveal that near-surface layers are likely to warm significantly, active layer thickness (ALT) will increase and permafrost temperatures at depth where no annual temperature fluctuations occurs will also increase with climate change (Hanssen-Bauer et al., 2019). The active layer (AL) is the upper layer of soil that experience freeze and thaw throughout a year. The rate of warming depends on the present temperature state in the permafrost and the amount of water and ice present in the soil. The changes in the thermal state are necessary to account for in engineering solutions in present and future infrastructure design in permafrost areas since the strength and bearing capacity is dependent on the temperature state. To be able to predict how temperature change will occur in soil, the heat flow in soil must be studied and the thermal properties must be known.

Hazards arising from increased temperatures and degradation of permafrost are already seen in existing infrastructure in the Northern Hemisphere. In Longyearbyen in Svalbard, it has been common practice to use wooden piles for foundations. With increased temperatures and amounts of liquid precipitation and melt water, the existing pile lengths are too short to maintain bearing capacity and rotting of piles occurs (Larsen, 2016). To perform engineering work in permafrost areas it is necessary to know the temperature distribution with depth. The main principle for establishing infrastructure is to keep the disturbance of the permafrost at a minimum. This can be done by placing the structure on piles anchored in the permafrost with space between the ground and the structure, placing piles on concrete foundations placed below the AL or use artificial freezing of the foundation (Larsen, 2016). A study by Hjort et al. (2018) shows that one third of pan-Arctic infrastructure are in regions where thaw-related ground instability can cause severe damage to built environment because of ground subsidence and loss of bearing capacity. Climatic change and degradation of near-surface-permafrost has already caused damage to infrastructure in Arctic communities and studies show that infrastructure will be prone to thaw-related damage even if climate emissions are reduced drastically by 2030 as projected in the RCP2.6 scenario (Hjort et al., 2018). Thaw consolidation as a result of thawed

(a) (b)

Figure 1.2: *Permafrost related damage to structures in Longyearbyen. (a) The action of creep from thawing on foundation piles (Riksantikvaren, 2018). (b) The old hospital with cracks in the concrete due to soil settlements (Engås, 2018).*

ice can lead to differential settlements of foundations which is detrimental for the supported construction. Deformations or creep in thawed soil are especially large in sloped terrain as the saturated soil will move downwards. This can cause large loads and damage to foundations and piles. In addition, increase in permafrost temperature and ALT lead to more active slope processes. When thawing of frozen soil occurs, the void ratio changes and a new equilibrium must be adapted in the soil structure. Melted water can cause excess pore water pressure since it melts faster than it drains away and exceeds the absorption capacity of the grains. More active slope processes in combination with more precipitation and higher frequency of heavy rainfall events, will increase the instability in slopes and increase the likelihood of slides (Hanssen-Bauer et al., 2019).

1.1 Background

Frozen soil is a multiphase system and consists of mineral grains and pores filled with ice, water and air. Freezing of the pore water occur when temperatures are lowered below the freezing point (FP). Permafrost is defined by temperatures remaining below 0°C over two consecutive years. However, the FP of soil can be depressed with several degrees due to adsorption, capillary forces and solutes in the pore water. This means that the permafrost can thaw at temperatures below 0°C under certain circumstances. The freezing of soil increases the soil strength because ice forms bonds between the soil particles. Therefore, frozen ground has high compression strength, high bearing capacity and low permeability. The ice bonds that strengthens frozen soil disappear when it thaws and reduce the cohesion and the bearing capacity in the soil (Williams & Smith, 1989). The thermal state of the permafrost will drastically change when temperatures approach the FP. The mechanical properties of soil will change; the bearing capacity and strength will be reduced, because the ice bonds are lost.

Air temperature is of importance to the thermal regime in the ground because it governs the exchange of heat and moisture between the ground surface and the atmosphere. Most of the heat transfer in the ground happens by conduction. Therefore, thermal conductivity, heat capacity, and latent heat are important parameters in predicting conductive heat flow in the soil. Soil saturation, water content, density and grain size distribution are some of the soil properties that influence the thermal properties. To predict the heat flow through a porous composite

is more demanding than for a uniform medium. Soil is an inhomogeneous material, and the composition and properties vary within the soil stratum. Moreover, the thermal properties for a material change as temperature changes. Since soil is usually saturated with water, the change in properties is especially significant around the FP where water change phase to ice. Volumetric heat capacity can be directly found if the composition of soil grains, water, ice and air are known. The thermal conductivity is more complex to determine since the components cannot be linearly added. Direct measurement methods and empirical relations exist for determination of thermal conductivity. However, estimation by empirical models, such as those by Kersten and Johansen, inherit uncertainty and demands knowledge of soil properties for precise estimates. Measurement methods of thermal conductivity are not reliable to give the thermal conductivity around the FP. An efficient and precise way of determining the thermal properties as function of temperature with respect to unfrozen water content (UWC) and solutes in the pore water is not readily available.

The FP in soil is the temperature where ice nucleation is initiated and pore water start to freeze. Freezing is initiated at the FP, but part of the water content in the pores will remain unfrozen. This is due to negative water potentials in the pore water. Research has been done and is still going on to investigate what factors give rise to the water potential. Surface tension due to the soil grains, adhesive forces and solutes in the pore water are some of the influencing factors. The amount of ice and UWC affect the mechanical properties in the soil. Precise estimation of UWC will be important for obtaining the temperature dependent thermal properties. The ice and UWC is important when considering change in the temperature of the soil. When the soil is warmed, latent heat is needed to change the ice into water, requiring more latent heat than just warming ice.

> "The forthcoming infrastructure risk assessments would significantly benefit from applicable process-based transient models of ground thermal regime and high-resolution climate and ground-ice data. With the help of improved permafrost projections, hazard maps and verified infrastructure data, it would be feasible to quantify the economic impacts of climate change on infrastructure at the pan-Arctic scale." (Hjort et al., 2018).

Reading from this, climate data and knowledge about ground properties are needed to construct models of the ground thermal regime. Climate models can be used to predict future air temperatures (AT) in accordance with different climate gas emission scenarios. Since AT are influencing ground temperatures, they can be used in ground thermal models and thereby predict what changes this will cause in the ground temperature profile. The magnitude and rate of change in the temperature profile are important to predict in order to make good engineering solutions for infrastructure in the Arctic. Thickness of the active layer and temperatures of the near-surface-permafrost are the most important to observe regarding infrastructure.

Problem Definition

The aim of this thesis is to determine how thermal properties of frozen soil can be estimated and how thermal properties affect the heat flow in the ground thermal regime will be studied. Thermal properties are difficult to determine because soil is a porous composite and consist of different materials and the properties changes with temperature. Water, ice, soil and air all have different heat capacities and conduct heat at different rates. Especially, thermal conductivity is challenging to determine in frozen state where water can be both frozen and unfrozen. The thermal conductivity is essential to determine because the heat flow in soil is governed by

heat conduction and the thermal conductivity of a material is important for the rate of heat exchange. The freezing point depression and the amount of UWC at negative temperatures must be determined to obtain thermal conductivity and volumetric heat capacity as functions of temperature. Methods exist for determining UWC, but demands special procedures and instruments. Empirical formulations such as the liquid limit determination exist, but demands knowledge of characteristic soil parameters from liquid limit testing. It is desirable to derive a more efficient way that can be used to measure or predict the amount of UWC for a soil with a certain water and solute content. Therefore, a method to determine the UWC curve including water and solute content will be studied. Determined UWC curves will be used to establish temperature dependent curves for thermal conductivity and volumetric heat capacity. It will be studied how factors, such as solutes in the pore water, capillary and adsorption forces, influence on the UWC. Understanding of these relations can possibly result in easier ways to determine the freezing point depression and UWC curves for different soil types. The rate of temperature change in permafrost depend on the thermal properties which depend on the FP and UWC. The temperature change in permafrost is essential to determine for evaluation of ground conditions for existing and future infrastructure. The temperature change in the near-surface soil arise mainly du to changes in AT and heat exchange at ground surface. Therefore, predictions of how temperatures in soil change with change in AT are key factors.

Literature Survey

A preliminary literature study on permafrost and frozen soil was done in a project thesis. The theory and literature studied in the project is used in the work with this thesis. The two books, *Frozen Ground Engineering* by Andersland and Ladanyi (2004) and *The Frozen Earth* by Williams and Smith (1989) provide the basic theory regarding permafrost features, the ground thermal regime and thermal properties. For the experimental investigations, ISO Standards, handbooks from Statens Vegvesen, instrument manuals and descriptions from earlier investigations have been used. In lack of standard procedures for measuring thermal conductivity and water potential with the probe method and the dew point method respectively the results from the study of Bratlie (2018) and applications from Putkonen (2003) were used for the probe method, and for the dew point method the procedure explained by Campbell, Smith, and Teare (2007a) was used. The previous study of the UNIS East site by Gilbert et al. (2019) has been helpful in the experimental work. Several articles on the topic of thermal property determination of soil have been studied.

Farouki (1981c) evaluated different methods of determining soil thermal conductivity, explained measuring methods and how different soil properties affect the thermal conductivity. Empirical models based on experimental testing are made by Øistein Johansen (1975) and Kersten and the Kersten formulas are presented by Andersland and Ladanyi (2004). Putkonen (2003) has evaluated the probe method for measuring thermal conductivity in frozen soil and give recommendations for how this should be performed. Both Sun et al. (2016) and Aleksyutina and Motenko (2017) present experimental work on characterizing thermal properties of soil at sub-zero temperatures.

Determining ways to predict unfrozen water content has been revised by many authors such as Tice, Burrous, and Anderson (1978) and Black and Tice (1989). Anderson and Morgenstern (1973) describes the difference between bound and unbound water and how the amount of unfrozen water is related to the specific surface of soil particles. The Clausius-Clapeyron equation has many times been used to calculate FP and UWC. It has earlier failed to include

all factors that influence on the amount of UWC. Water potential is important in the determination of UWC and Campbell et al. (2007a) describe a procedure for how to use dew point detection measurements for deciding water potential. Istomin, Chuvilin, and Bukhanov (2017) present a way of fast estimation of UWC with the use of water potential measurements and measurements. Bing and Ma (2011) and Watanabe and Mizoguchi (2002) study the influence of solutes in the pore water and how this affects the FP. Zhou et al. (2018) use generalized forms of the Clausius-Clapeyron equation to include the effect of solutes and overburden pressure to estimate the FP and UWC.

To get a better understanding of the present and future climate at Svalbard several research articles have been used such as those by Hanssen-Bauer et al. (2019), Nordli et al. (2014), Førland et al. (2011), Isaksen et al. (2000) and (Etzelmüller et al., 2011). The work by Hjort et al. (2018), Hanssen-Bauer et al. (2019) and Instanes and Rongved (2017) give predictions for how the ground thermal regime can develop in the future and what consequences the predicted changes can give.

1.2 Scope and Objectives

The main scope of this thesis is to find how we can determine thermal properties of soil as functions of temperature and to use the temperature dependent properties in a soil model in order to predict how the ground thermal regime will respond to change in AT.

The following objectives are important to achieve this:

- Determine thermal properties of a fine grained permafrost soil from Svalbard.
- Determine thermal properties of soil as functions of temperature
- Compare the results of temperature dependent properties to theoretical and empirical relations
- Use the obtained results for temperature dependent properties in a finite element method (FEM) model to predict how the ground thermal regime respond to changes in air and ground surface temperature. Thermistor string measurements will be used to validate the model.

1.3 Limitations

The number of tests, trials for each test and amount of samples to be tested are limited due to lack of time. For the testing of thermal properties at different temperatures it is important to leave enough time for temperature equilibration. With only one TR–1 sensor available, it was difficult to take the desired amount of tests at different temperatures. Water potential testing was very time consuming. Ideally more sub samples at different water contents should have been tested. Tests are performed on different sub samples from a 40 cm long soil sample, but should ideally be tested on the exact same soil. Few tested samples give no basis for statistical deviation. More test results on the same soil are needed to give certain conclusions of the results. In addition, when performing tests, human error can affect the results and cause deviation between the tested and real value. Ideally, samples from two different sites should have been tested, but this was not possible to perform during the time available. With samples

from different sites a check of the applicability of the methods for various soil types would be possible. With tests from only one site it is difficult to say if the methods used would be applicable to other soil compositions.

There are no standardised procedures for the use of the probe method in frozen soil or the dew point detection method. With lack of standardised procedures, the test results may deviate from other tests because the test is performed differently. Methods were tested to find the best possible procedure for measurements. It is difficult to determine the accuracy of the results without a standard procedure and previous results to compare with. Moreover, the probe method used to measure thermal properties has proven to be inaccurate for measurements of frozen soil between –2°C and –10°C (Putkonen, 2003). The effect of phase change is not included in the algorithms in the control device. Therefore, it is difficult to validate the calculation of thermal properties at these values since values from measurements hold some uncertainty.

The mineral composition of soil should be determined to obtain more precise results with the use of the empirical formulations by Johansen. This was not done in the experimental testing. Therefore, correct values for soil thermal conductivity are lacking and make it more difficult to interpret the results of this empirical method. This empirical formulation is hence not sufficient to use for validation of measured results.

The unfrozen water content is determined by water potential and calculations. The unfrozen water content can be measured directly, but the necessary equipment to do this was not available. To be able to assess the results from calculations and to check the applicability of the calculation method direct measurements would be needed to compare the results.

Regarding modelling of the soil many limitations apply. The soil should be divided into more layers for a higher accuracy, but that demands testing of soil from more depths. The thermistor string measurements have an accuracy of ±0.25°C and give unrealistic fluctuations within the temperature profile. Thermistor measurements were available for 1.5 years. It would be desirable to have measurement series over a longer time period to be able to observe how the temperature profile change over time. Ground surface temperatures (GST) were not directly measured, but can be estimated by AT or thermistor measurements from 0 m depth. AT from a nearby site were used since there was no meteorological station at the site, but local variations may give different results and limits the applicability. A better understanding of the correlation between ground surface temperatures, surface conditions and AT are needed to improve the boundary conditions in the model.

Predictions of future climate change are very complex and many different models exist, and a simplified scenario is applied in the model. The predictions of future ground thermal regime given in this thesis is an indication of how the conditions will be in the future, but the results should be used with care.

1.4 Approach

An experimental study was be performed on soil samples from a site at Svalbard, UNIS East. The experimental study was performed in the laboratory at UNIS on core samples extruded from a bore hole at the site. Laboratory testing included index testing to determine basic soil properties. Measurements of thermal conductivity and volumetric heat capacity were done with the probe method and measurements of water potential were done with a dew point meter. In addition, soil salinity and freezing points were measured. Test results were used to

calculate the unfrozen water content curve for the soil samples. The unfrozen water content and basic soil properties were used to determine the thermal properties as function of temperature. Calculations are based on existing theory. The obtained results were compared to the measured values of thermal properties to check the compliance and for validation of the results.

The results from analysis of measured values and calculation of temperature dependent properties were compared to theoretical and empirical relations. This was done by using existing empirical formulations with the measured soil properties as input. Kersten's and Johansen's empirical formulations to determine thermal conductivity were used. The comparison is made to check that results coincide with theory and to find where the used method gives deviations from other determination methods.

The calculated unfrozen water content curves and thermal properties were used in a FEM model. The temperature profiles from model simulations were compared to thermistor measurements for validation. A sensitivity analysis was performed to check how sensitive the modelled ground thermal regime is to changes in the thermal properties. Predictions of how the ground thermal regime respond to changes in ground surface temperatures were made by output results from model simulations.

1.5 Structure of the Report

This report is divided into 9 chapters. The chapters consist of sections and subsections. Chapter 2 give theoretical background on permafrost and the ground thermal regime in soil. In Chapter 3, theory about thermal properties of soil is presented with emphasis on how the properties can be measured and estimated with calculations based on soil properties. Chapter 4 explains the concept of unfrozen water content, how it can be determined and different calculation methods. Chapter 3 and Chapter 4 give a description of the main topic of study in this report and is important for the following chapters. In Chapter 5 a description of the test site, the test samples and laboratory investigation methods used is presented. An overview of the test results are given in Chapter 6. The result analysis and calculation of thermal properties based on experimental test results are presented in Chapter 7. A proposed model for the ground thermal regime based on the properties from experimental testing is discussed in Chapter 8. Chapter 9, includes conclusions of the study and suggestions for further work to be done to advance in this research field.

Chapter 2

Permafrost and the Ground Thermal Regime

2.1 Permafrost Features

Permafrost is defined as subsurface material with temperatures remaining below 0°C more than two consecutive years (Isaksen, 2001). For permafrost to exist the mean annual ground temperature (MAGT) must be lower than the freezing point and it is assumed that the mean annual temperature (MAT) at ground surface must be –3°C or lower (Andersland & Ladanyi, 2004). If these criteria are fulfilled, permafrost exists at depths where the seasonal variation is insufficient to raise the temperature above freezing point (Williams & Smith, 1989). The cold regions of the earth, where permafrost exists, are found at high latitudes and in mountain areas. The definition of the boundary for cold regions can be determined in two ways. One definition is when the isotherm of average temperature of the warmest month is above 0°C and below 10°C (Bates and Bilello (1966) in Andersland & Anderson, 1978). Seasonal frost penetration of 300 mm into the ground once in 10 years is also an accepted definition (Andersland & Ladanyi, 2004). Concerning these two definitions, the southern boundary for the cold region in the Northern Hemisphere is found to be the 40th parallel which is at the latitude of Madrid in Spain.

According to studies of Anisimov and Nelson (1995), almost 25% of Earth's land area is underlain by permafrost. Permafrost areas can be continuous or discontinuous. Figure 2.1 indicate that large parts of Alaska, Siberia and Canada are covered with continuous permafrost. In Norway, Svalbard is completely covered with continuous permafrost while the mainland has patches of continuous and discontinuous permafrost. Terrain features such as ice wedges, pingos, thermokarst and patterned ground can be indicators of underlying frozen ground (Andersland & Ladanyi, 2004). Most of the permafrost originate thousands of years ago (Williams & Smith, 1989). Research on newly formed, degrading and disappearing permafrost is important today.

We distinguish between perennial or seasonally frozen ground, with perennially frozen ground being permafrost. Seasonally frozen ground is where the temperatures fluctuate around 0°C throughout the year. This is often seen in the top layer of the soil and is called the active layer. The active layer thickness (ALT) is dependent on many factors, e.g. winter temperatures, soil type, moisture content, snow cover, surface vegetation, drainage and the orientation and inclination of the slope (Andersland & Ladanyi, 2004). The active layer (AL) usually reaches the permafrost table in the continuous permafrost zone, but a layer remaining in the unfrozen state

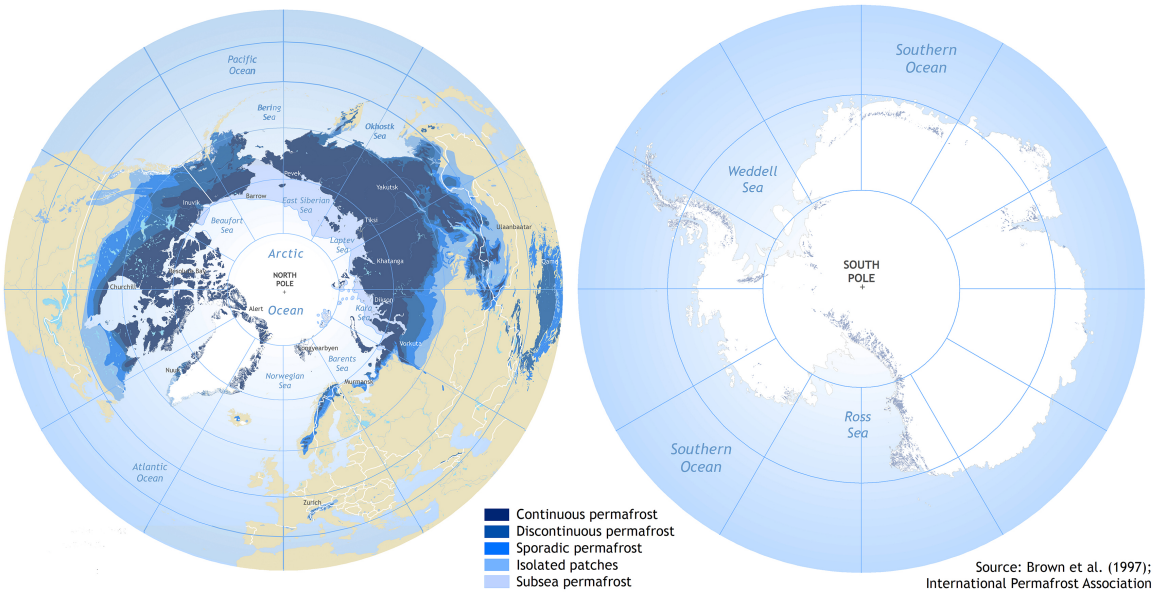

Figure 2.1: *Geographic distribution of permafrost and ground-ice (Brown et al., 1997).*

can also exist between the AL and permafrost. The ALT varies between 15 cm and more than 1 m with increasing thickness southward on the northern hemisphere (Andersland & Ladanyi, 2004). Figure 2.2 shows a ground temperature profile where it is seen that the AL is where temperatures rise above 0°C while the layer of permafrost remains below 0°C. As Figure 2.2 shows, soil temperatures will increase with depth and this is due to the geothermal heat flux, i.e. heat from the Earth's interior.

2.2 Soil Properties

The composition of soil grains and voids is important for description of frozen soil. The soil grains can be of various minerals with different shapes, sizes and strength properties. The pores between the soil grains can be filled with air, water and ice. This constitutes four components. The presence of unfrozen and frozen water content is dependent on temperatures and will be of importance to both mechanical and thermal properties. Soil is in classification often divided into coarse grained soils like sand and gravel and fine grained soils such as clay. To describe the composition of a soil, it can be divided into different phases. The soil phase relationship can be represented in fractions of mass or volume of the total soil sample (Figure 2.3). In thawed state, frozen soil is reduced from a four to a three component system. To obtain necessary knowledge about the composition, mechanical properties and thermal properties of soil drilling, sampling and insitu or laboratory testing must be performed. Drilling and sounding can give information about layering of the soil, strength and deformation parameters.

To describe the composition of the soil some definitions are necessary. The mass of water in a soil sample can be determined by the weight difference of the soil sample before and after drying the sample. Water content, w, is the ratio of mass of water, m_w, to mass of the solids, m_S.

$$w = \frac{m_w}{m_S} \tag{2.1}$$

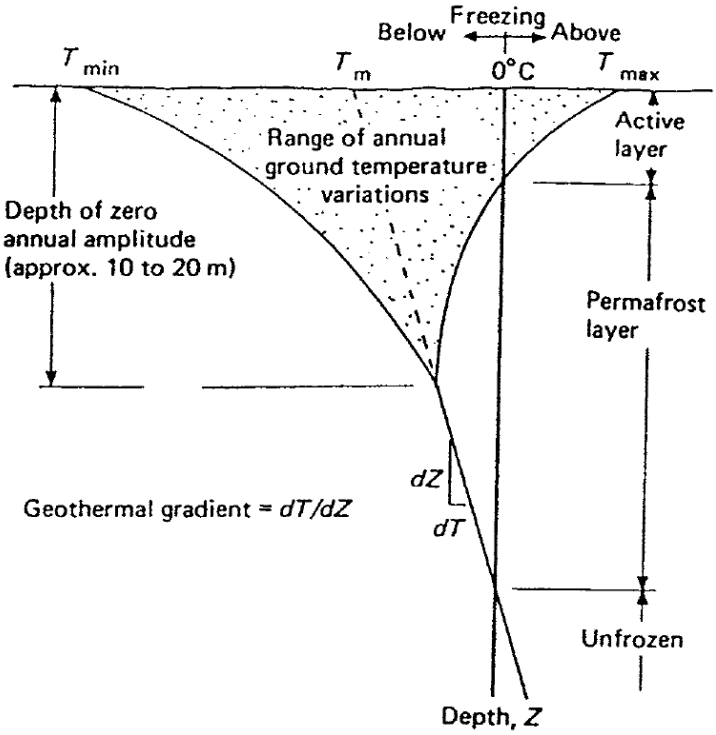

Figure 2.2: *Temperature profile in permafrost soil showing the temperature zones and range of temperatures (Andersland & Ladanyi, 2004).*

In frozen soil the total water content will consist of two components calculated as

$$w = w_u + w_i \tag{2.2}$$

where w_u is the unfrozen water content and w_i is the frozen water content, i.e. ice. The porosity, n, describes the ratio of pore volume to the total soil volume. Porosity is defined as

$$n = \frac{V_v}{V} = 1 - \frac{\gamma}{\gamma_s(1+w)} \tag{2.3}$$

where V is the total volume of a sample and V_v the volume of voids. The volume of voids can be determined from the phase relations in Figure 2.3 and the porosity can then be calculated by the last part of Equation 2.3. In the equation, γ is the unit weight of the sample and γ_s the density of the soil grain particles. The pores can be filled with water and air. The saturation describes the ratio of unfrozen water in the pores to the volume of pores. Saturation is defined as

$$S_r = \frac{V_w}{V_v} = \frac{w\gamma}{\gamma_w(1+w-\frac{\gamma}{\gamma_s})} \tag{2.4}$$

where V_w is the volume of water in the soil sample and γ_w the density of water. A fully saturated soil has S_r of 1 (100%). When pore water freezes, the saturation decreases. Ice accumulation in soil pores can cause expansions of pores and ice lenses can form. Where ice lenses accumulate the saturation of the soil can exceed 100% when the sample is thawed.

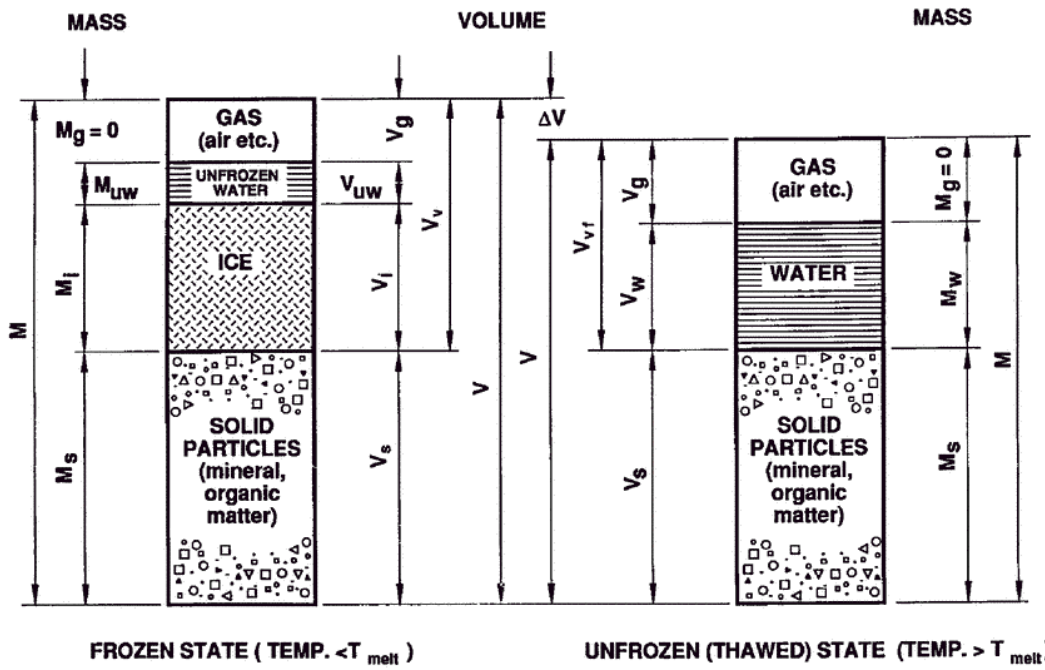

Figure 2.3: *Phase relationships in soil. Frozen soil is a four component system (Andersland & Ladanyi, 2004).*

2.2.1 Mechanical Properties

Bound water exists as films surrounding the mineral particles in soil even at very low temperatures, and this water is referred to as unfrozen water (Andersland & Ladanyi, 2004). Even if part of the water remains unfrozen, most of the pore space will be filled with ice. The ice acts as a bonding agent and increases the strength of the soil. The strength of ice will increase with decrease in temperature, and pressure and strain rate will also affect the mechanical behaviour (Andersland & Ladanyi, 2004). Size, structure and orientation of soil grains will also affect the strength of ice rich soil. The high compression strength of soil containing pore ice allows for it to carry relatively large foundation loads and makes the soil able to carry large foundation or pile loads. The shear behaviour of frozen soil is mainly controlled by pore ice strength, soil strength (inter particle friction and dilatancy effects), increase in effective stress due to the ice bonding and synergistic effects between soil and ice matrix. When loads are applied to frozen soil it will experience an immediate deformation and time-dependent deformations, called creep. At low strain rates ice shows a ductile yielding but as strain rates increase it becomes more brittle (Andersland & Ladanyi, 2004). Higher amounts of unfrozen water content cause a more plastic deformation. The strain rates and creep reduce the long term strength of ice rich soils and are important to consider in engineering designs. Infrastructure is often designed with a lifetime of approximately 50 years. Both strength and creep rates are temperature dependent, strength will be reduced and creep rates increase with increasing temperatures.

2.2.2 Experimental Testing of Frozen Soil

The properties of frozen soil are highly dependent on the insitu temperature and temperature gradients. It is important to reduce the thermal disturbance to a minimum when handling,

transporting or performing tests on frozen soil. It is convenient if some index tests, such as moisture content, unit weight and classification, can be performed at the sampling site to avoid disturbance. When samples need to be transported to a lab, special precautions must be made to keep the moisture content and temperature within acceptable limits. Andersland and Ladanyi (2004) describe that wrapping samples in cellophane and keeping them in deaired well-sealed polyethylene bags is a successful method to prevent moisture loss from the sample. They also describe that frozen samples can be kept at acceptable temperatures by storing them in portable refrigerators or insulated boxes packed with snow or ice.

2.3 The Ground Thermal Regime in Permafrost Areas

The depth of continuous ground freezing vary from more than 1000 m at maximum to some tens meter (Williams & Smith, 1989). The permafrost depth is limited by the heat flux from earth's interior where the temperature is very high. There is also energy transfer between the ground surface and air. This heat flux originates from solar radiation. Some of the solar radiation is absorbed and reflected in the atmosphere. A part of the solar radiation is received at the ground surface and is then reflected or absorbed, depending on the absorptivity of the ground. The absorbed heat will warm up the ground. When the ground surface has higher temperatures than the overlying air, heat will flow from the ground surface to the overlying air. Heat transfer will in this case happen by conduction but also convection (Andersland & Ladanyi, 2004). The heat flux from ground to air contributes to the cooling of the earth surface. The heat flow into and out from the ground surface should sum up to be approximately zero over a year. Figure 2.4 shows a simplification of the contributions to the heat flux equation. Because of this equilibrium, the MAGT will remain about constant at a specific place, unless significant changes in the energy balance occur (Williams & Smith, 1989).

In addition to air temperatures, other influencing factors are amount of radiation absorbed in the ground, degree of air turbulence, availability of water for evaporation, the thermal conductivity of the ground surface layer and micro climatic conditions (Williams & Smith, 1989). Vegetation and snow cover are micro climatic factors and influence the heat transfer between ground surface and air. The ground surface temperature can differ from air temperatures by several degrees, but the ground surface temperatures reflect the fluctuations in air temperature. The ground surface temperature is important for how temperatures in the near-surface ground thermal regime change. If ground surface temperature is warmer than the underlying soil, heat will be conducted and warm up the soil below, and the energy transfer will move the opposite way if ground surface temperature is colder than the underlying soil. Ground surface temperatures are not readily available in most sites and air temperatures are often used as calculation basis. Two soils with identical compositions can with different micro climatic boundary conditions freeze to different depths and hence the thermal regime can be different due to microclimatic conditions (Williams & Smith, 1989).

The daily and seasonal variations in ground surface temperatures can be described by the freezing index, describing the duration and magnitude of freezing. Air temperatures can be used to determine the air freezing index for a soil since ground surface temperatures are often not available. Freezing index is found by adding the product of average monthly temperature that are below 0°C and the respective number of days per month (Andersland & Ladanyi, 2004). That gives the freezing index in degree days (°C days). The thawing index can be expressed in the same way for months with positive average temperatures. A design freezing index should be based on recorded average temperatures from the three coldest winters during the last 30

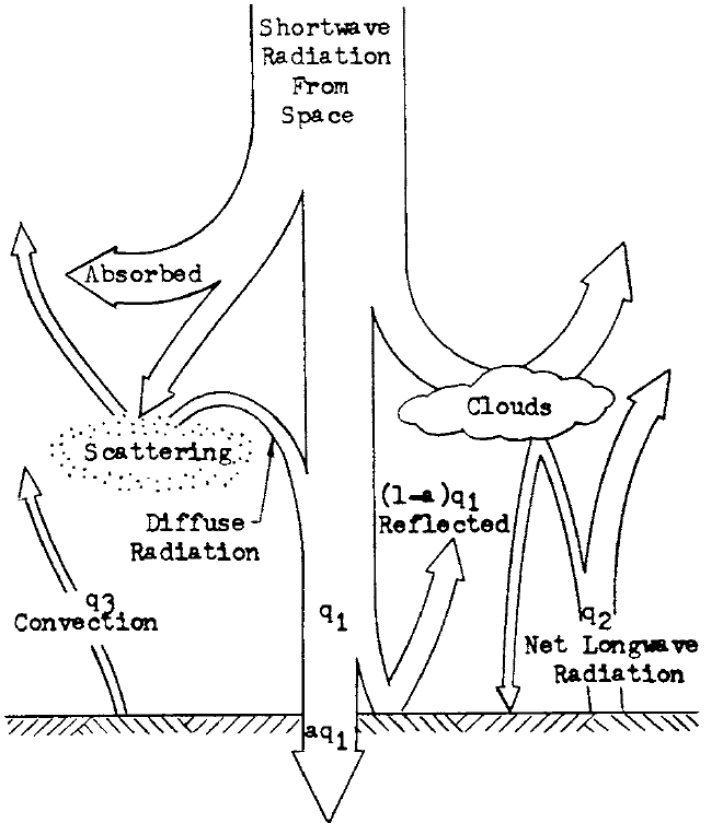

Figure 2.4: *Heat transfer between the ground surface and air on a sunny day (Andersland & Ladanyi, 2004).*

years (Andersland & Ladanyi, 2004). The following equation can be used to describe the state of permafrost

$$\frac{k_f}{k_u} = \frac{I_{st}}{I_{sf}} \tag{2.5}$$

and k_f and k_u are the frozen and unfrozen thermal conductivity and I_{st} and I_{sf} the thawing an freezing index for the ground surface (Carlson (1952) in Andersland & Ladanyi, 2004). A low number of these ratios (below 1) indicates stable permafrost, while with a higher number one can expect degradation of permafrost. Furthermore, the freezing and thawing indexes can be used to calculate the depth of seasonal freezing or thawing respectively. The depth of thawing is reciprocal to the ALT. The soil thermal and mechanical properties will experience variation within the depth of seasonal thawing, and when concerning soil as a foundation material it is important to estimate this depth. The Stefan equation has been developed for this purpose and yields

$$X = \left(\frac{2k_u I_{st}}{L}\right)^{0.5} \tag{2.6}$$

where X is the penetration depth of thawing or freezing and L the latent heat of the soil. The effect of latent heat at phase change is included in the equation, but not the effect of thermal energy stored as volumetric heat in the soil particles. Therefore, the equation underestimates

the thaw depth. Rising temperatures will cause an increase in thawing index, which according to the Stefan equation will increase the ALT. The rate of heat flow within the soil is highly dependent on the thermal conductivity. This is expressed in the Stefan equation in that the conductivity of the material is used to determine the thaw depth.

The MAGT at a specific place will remain constant given a constant mean annual temperature and the heat transfer sums to zero as described earlier. The sum is zero, but the heat transfer fluctuates periodically with seasons during a year and during day and night (Figure 2.5). A result of this is fluctuating ground surface temperatures. The time dependent temperature variation is greatest at the ground surface and attenuate with depth. The depth where there is no annual temperature fluctuation is called the depth of zero annual amplitude (ZAA) (Figure 2.2). The ground surface freezing index and the air freezing index can be used to describe the difference between mean annual air temperatures and mean annual temperature at ground surface (Andersland & Ladanyi, 2004). The difference is described by a surface n-factor that is defined by:

$$n_f = \frac{I_{sf}}{I_{af}} \tag{2.7}$$

Local wind speeds and surface types will affect the surface factor (Andersland & Ladanyi, 2004). The surface factor will be unique for different geographical locations and will vary from year to year.

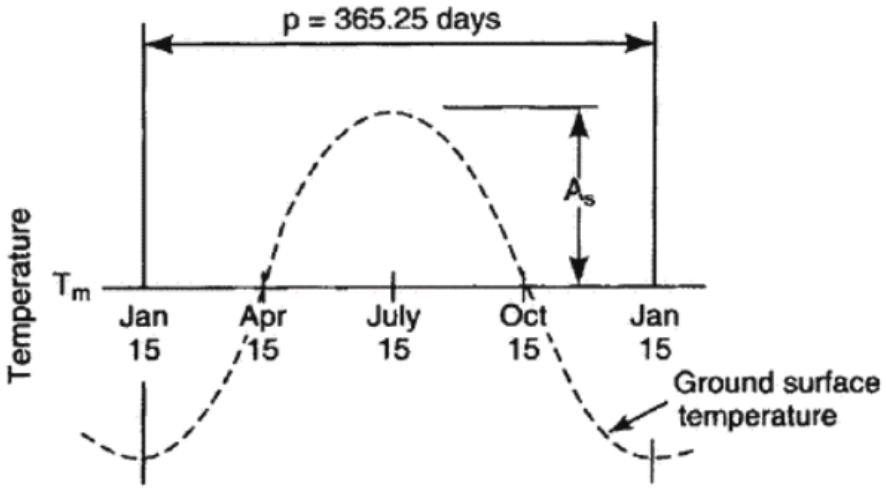

Figure 2.5: *The variation of ground surface temperature during a year. A_s is the surface temperature amplitude (Andersland & Ladanyi, 2004).*

The thermal regime in the ground can be theoretically presented by a set of equations. They are here given as presented by Andersland and Ladanyi (2004). The ground surface temperature can be estimated by

$$T_{S,t} = T_m + A_s sin\frac{2\pi t}{p} \tag{2.8}$$

where the period, p, can be given as 24 hours or 365 days, the time, t, can be given in hours or days accordingly depending on if fluctuations during a day or a year is to be found. T_m is the

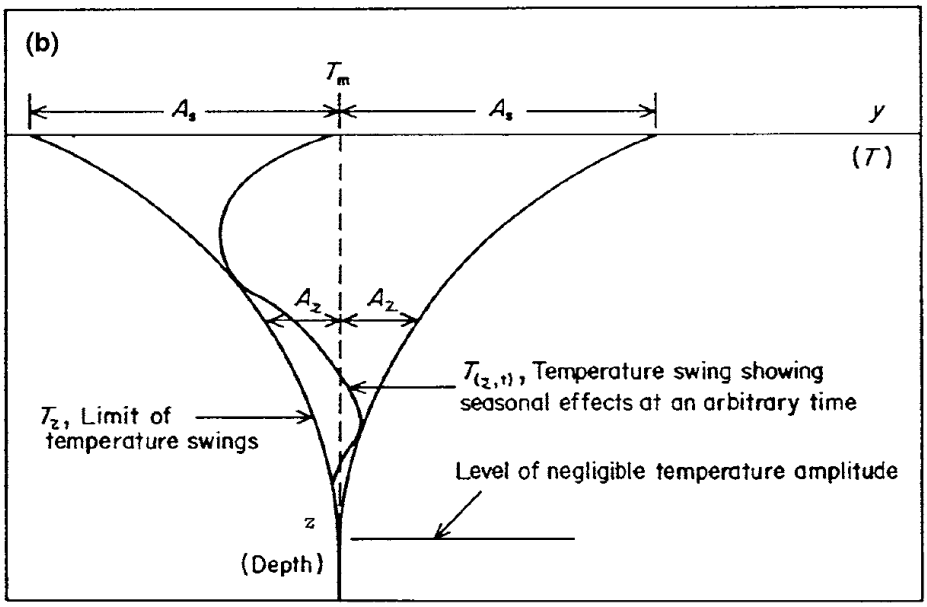

Figure 2.6: *The trumpet curve for the temperature attenuation with depth (Andersland & Ladanyi, 2004).*

mean annual temperature and A_s is the surface temperature amplitude. Equation 2.8 is based on the atmospheric climate and do not take into account the effects of micro climatic factors. It may be necessary to fit the temperature curve to measured data. The equation for ground surface temperature is then

$$T_{S,t} = T_m - A_s cos\left(\frac{2\pi t}{p} - \frac{2\pi\phi}{p}\right) \tag{2.9}$$

where ϕ is the phase lag. The phase lag must be given in hours or days according to the unit of the period, p. The temperature attenuate with depth and the temperature at a given depth can be calculated by

$$T_{z,t} = T_m + A_s exp\left(-z\sqrt{\frac{\pi}{\alpha_u p}}\right) sin\left(\frac{2\pi t}{p} - z\sqrt{\frac{\pi}{\alpha_u p}}\right) \tag{2.10}$$

where z is the depth and α_u the soil thermal diffusivity. Equation 2.10 is a simplification and can be applied to a homogeneous soil without phase change of materials and with negligible heat flow from Earth's interior. The temperature at a given depth will fluctuate between an upper and a lower limit that will have a trumpet shape as Figure 2.6 shows. $T_{z,t}$ at a given time will give the wave shaped function inside trumpet . The amplitude of the attenuation with depth is given by

$$A_z = A_s exp\left(-z\sqrt{\frac{\pi}{\alpha_u p}}\right) \tag{2.11}$$

and decrease with depth. The maximum and minimum limits for the temperature variation is given by

$$T_z = T_m \pm A_s exp\left(-z\sqrt{\frac{\pi}{\alpha_u p}}\right) \tag{2.12}$$

and give the trumpet shaped curves. The point where the amplitude is zero is the level of negligible temperature amplitude or ZAA. The depth to ZAA usually ranges from 15 to 20 m depth (Isaksen, 2001). Below the depth of ZAA, temperatures will increase with the geothermal gradient. The heat flow from Earth's interior yield temperature gradients of 0.02 to 0.03°C/m (Isaksen, 2001). The geothermal gradient limits the thickness of the permafrost layer from below.

Chapter 3

Thermal Properties of Soil

3.1 Thermal Properties

In a permafrost perspective it is important to know the thermal properties of the soil because heat conduction governs the heat flux through the soil. It is important to know the rate of heat flow to be able to understand the fluctuations in temperatures in the ground thermal regime. The thermal properties of soil are complex to determine. The thermal properties are not homogeneous in the soil layers but vary with soil type, organic content, density, moisture content and temperature (Williams & Smith, 1989). Estimates of thermal properties as function of temperature are necessary to know if accurate calculations on heat flow down in the soil profile are to be done.

3.1.1 Thermal Conductivity

Heat conduction governs the heat transfer in the ground, although circulation of groundwater can occur and contribute (Williams & Smith, 1989). Heat conduction means that heat or internal energy is transferred between particles of different temperature in direct contact by vibrating and colliding molecules. With temperature gradients present in the material, heat conduction will happen. This is an essential feature in the ground thermal regime. The rate of heat flow is dependent on the thermal conductivity, k, of the soil material. To describe heat conduction we can look at the heat flow, Q, over a given area, A, as shown in Figure 3.1. The heat will flow from the warm to the cold side until temperature equilibrium is reached (thus the minus-sign in the equation). The rate of heat flow is given by

$$q = \frac{Q}{A} = -k(\frac{dT}{dx}) \tag{3.1}$$

where $\frac{dT}{dx}$ is the temperature gradient in $°C/m$. The thermal conductivity is the rate of heat flow divided by the temperature gradient and is given in W/mK.

Different materials have different thermal conductivity and therefore the ability to conduct heat differs. The thermal conductivity for a material is temperature dependent. Water and ice are the same material but in different phases because of different temperatures. Table 3.1 shows the thermal conductivity of the materials that soil is composed of. Different types of soil minerals have different ability to conduct heat and the mineral composition should be

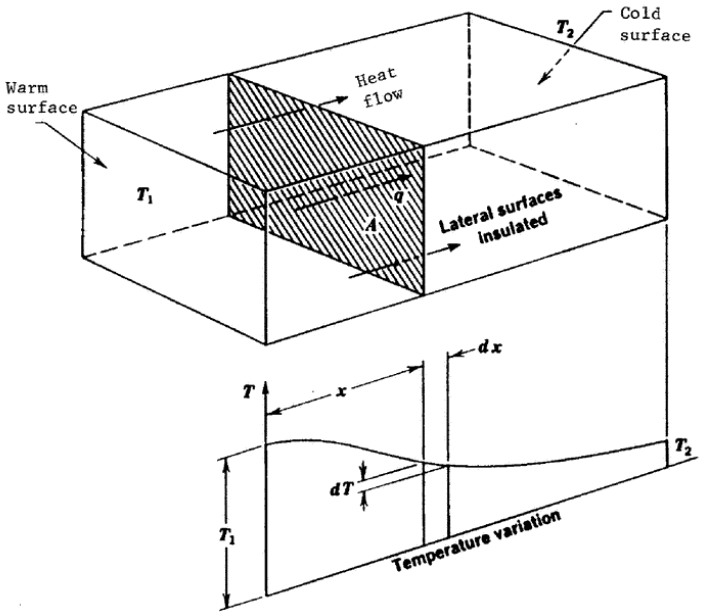

Figure 3.1: *Heat flow through a unit area due to temperature variations over the length (Andersland & Ladanyi, 2004).*

Table 3.1: *Thermal conductivity and heat capacity for materials in the soil composition (adapted from Andersland and Ladanyi (2004)).*

Material	**Thermal conductivity** (W/mk)	**Heat capacity** (kJ/kgK)
Air, 10°C	0.026	1.0
Water, 0°C	0.56	4.2177
Ice, 0°C	2.21	2.09
Granite	1.7 – 4.0	0.8
Quartz	8.4	0.733

known for precise thermal conductivity estimation. Quartz is the normal soil mineral with highest thermal conductivity. In frozen soil pore water exists in two phases. The thermal conductivity for a soil will be a combination of the different substances and the parameters must be determined through soil testing. The material's ability to conduct heat will depend on the density, mineral composition and saturation of the soil. The influence of each parameter on the thermal conductivity is important to determine and will indicate what parameter governs the heat flow by conduction. Andersland and Ladanyi (2004) describes that the heat transfer by conduction increase as dry density increase and degree of saturation increase.

Even though the thermal conductivity of each material is known, we cannot simply determine the total conductivity of soil material by adding properties of the parts together. This would be the case if the different materials were coupled in series and the materials were layered on top of each other, see Figure 3.2. The heat would be transferred through one material at the time. Furthermore, the materials are not coupled in parallel, that would be placing the materials in vertical layers next to each other. The total thermal conductivity for a composite will be found between the value of a series and parallel coupling and they represent an upper and lower boundary value. Thermal conductivity by series and parallel coupling can be represented by

$$k_{series} = \frac{1}{\frac{v_1}{k_1} + \frac{v_2}{k_2}} \tag{3.2}$$

$$k_{parallel} = v_1 k_1 + v_2 k_2 \tag{3.3}$$

where v_i is the volume fraction and k_i the thermal conductivity of each component in the composite. Figure 3.2 pictures the difference between parallel and series and also presents the concept of the Maxwell-Eucken model. The Maxwell-model considers a dilute dispersion of spherical particles of known conductivity, k_1, in a continuous matrix of conductivity k_m (Pietrak & Wisniewski, 2015). Eucken extended Maxwell's model to allow for different materials of the spherical particles (Pietrak & Wisniewski, 2015). The Maxwell-Eucken model gives a value between the series and parallel boundaries by the equation:

$$k_{ME} = k_m \frac{2k_m + k_1 - 2(k_m - k_1)v_1}{2k_m + k_1 + (k_m - k_1)v_1} \tag{3.4}$$

Gong, Wang, Cheng, Zhang, and Zhang (2013) studied how properties and structures of materials can be included in analytical models for thermal conductivity. They proposed a model for the thermal conductivity in porous materials by using a novel effective medium theory (EMT). They unified the Series and Parallel model, the Maxwell-Eucken models and the EMT into one equation. Figure 3.3 shows their concept where the material is considered as a large sphere of radius R with thermal conductivity k_e within a uniform medium with thermal conductivity k_m. The sphere can contain different materials with different volume fractions. The resulting equation from the study (Gong et al., 2013) is thus

$$\sum \nu_i \left(\frac{k_i - k_e}{k_i + X k_m} \right) = 0 \tag{3.5}$$

where ν_i is the volume fraction of a component, k_i the component thermal conductivity, k_e the system/sphere thermal conductivity and k_m the thermal conductivity of the uniform medium. The equation can represent the previously mentioned models by changing k_m. Equation 3.5 give thermal conductivity for series model with $k_m = 0$, parallel model with $k_m = \infty$, the Maxwell-Eucken model when k_m is the k for the continuous matrix or for an EMT model with $k_m = k_e$.

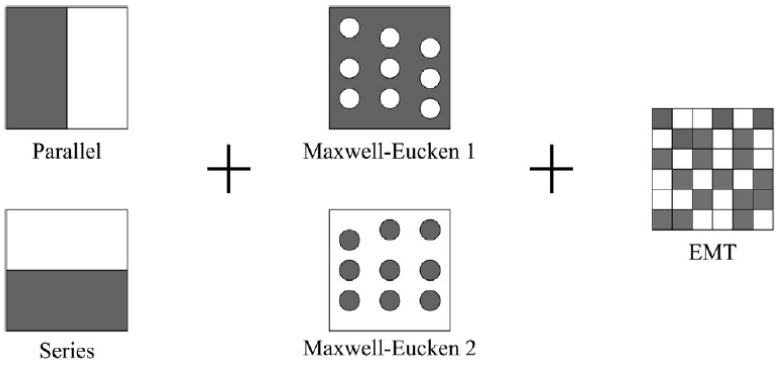

Figure 3.2: *Different models that describe thermal conductivity for composite materials (Gong et al., 2013).*

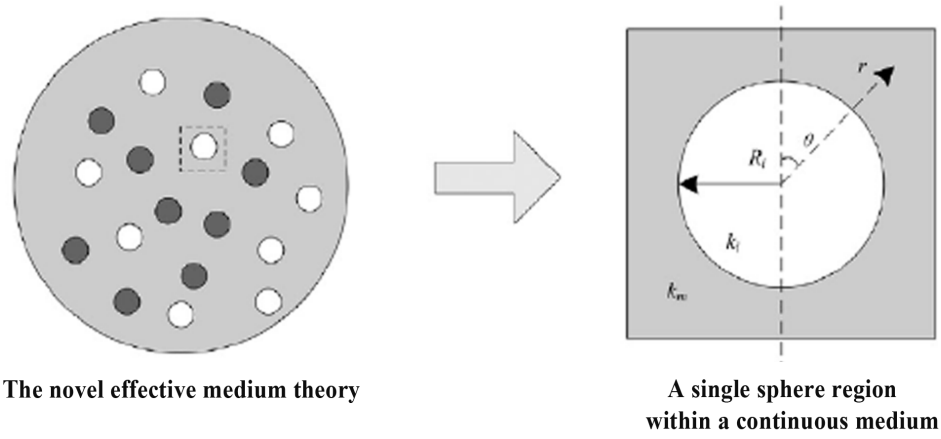

Figure 3.3: *The method of novel effective medium theory (modified from Gong et al., 2013).*

3.1.2 Heat Capacity

Heat capacity of a material is defined as the heat needed to add to or remove from a material to change the temperature with 1°C. Heat capacity, c, can, on the contrary to thermal conductivity, be calculated by adding the sum of heat capacity and mass of the constituents of the soil and dividing it by the total mass. Heat capacity [kJ/kg°C] of soil can thus be determined by

$$c = \frac{1}{m}(c_s m_s + c_w m_w + c_i m_i + c_{air} m_{air}) \tag{3.6}$$

where the heat capacities of solids, water, ice and air are added to determine the total heat capacity of the soil. The volumetric heat capacity [MJ/m^3°C] of the soil can be found in the same manner by dividing by volume:

$$c_v = \rho_{dry}(c_s + c_w w_u + c_i w_i) \tag{3.7}$$

Heat capacities for some materials are given in Table 3.1. To be able to compare the heat capacity of different materials more easily the specific heat, C_p, is often used. The specific heat is the ratio between the heat capacity of the material and that of water. Volumetric heat capacity for an unfrozen mineral soil can be determined by

$$c_{vuf} = (\frac{\rho_d}{\rho_w})(0.17 + 1.0\frac{w}{100})c_{vw} \tag{3.8}$$

where ρ_d and ρ_w are the densities of dry soil and water 0.17, 1.0, and 0.5 correspond to the specific heat of mineral soil, water and ice respectively (Andersland & Ladanyi, 2004). They also give the formula for the frozen soil volumetric heat capacity:

$$c_{vf} = (\frac{\rho_d}{\rho_w})(0.17 + 1.0\frac{w - w_u}{100} + 0.5\frac{w - w_u}{100})c_{vw} \tag{3.9}$$

3.1.3 Latent Heat of Fusion

Latent heat is related to the change of state in a substance. Latent heat of fusion, L, is the energy needed to go from solid to liquid state in a material without change in temperature. For water the latent heat of fusion is 333.55 kJ/kg. When heat is applied to ice, the energy will first be used to increase the temperature in the ice to the melting point, 0°C for bulk ice. When the melting point is reached, the latent heat needed for fusion of ice to water must be added. First when all ice is transformed to water, energy will go into increasing the temperature of water. Opposite, for the water to freeze again, the latent heat must be removed for the water to change phase (turn to ice). The latent heat describes the work needed to overcome forces that bind atoms in materials. Ice has a crystalline structure with stronger bonding than water.

3.1.4 Thermal Diffusivity

Thermal diffusivity, α, is the ratio of thermal conductivity to heat capacity multiplied by bulk density, ρ, of a material, and describes the rate of heat transfer to the rise in temperature (Equation 3.10).

$$\alpha_u = \frac{k}{c\rho} \tag{3.10}$$

Water has a thermal diffusivity of 1.4 $(m^2/s)\cdot 10^{-7}$ and ice has a much higher thermal diffusivity of 11.2 $(m^2/s)\cdot 10^{-7}$. Unfrozen soil will have a lower thermal diffusivity than a frozen sample. If the same amount of energy is added to a frozen and an unfrozen soil sample, the temperature increase will happen faster in the frozen sample due to the higher thermal diffusivity.

3.2 Determining Thermal Properties

Thermal properties can be determined in various ways, such as direct measurement or by empirical methods based on experimental testing. The properties of interest to determine are the thermal conductivity, thermal diffusivity and the heat capacity. The thermal diffusivity describes the transient situation where temperature varies over time and the thermal conductivity governs the steady state (Farouki, 1981b). It is generally time consuming to obtain the steady state where the temperature is constant within the material. A method to establish the steady state thermal conductivity of soil is the guarded hot plate (GHP) test. A flat plate main heater is placed between two test samples with known thickness. The sample is surrounded by an outer guard heater that prevents horizontal heat loss and force the heat to flow vertically through the soil samples (Farouki, 1981b). Temperature is measured by liquid-cooled heat sinks at each end. The temperature change over the sample height is used to calculate the thermal conductivity by Equation 3.1. In transient methods the temperature vary with time and it is not necessary to obtain temperature equilibrium in the sample before testing. Therefore transient measurements need less preparation and are more versatile. The probe method is a transient measurement and can be performed insitu or in a laboratory. The thermal properties can be modelled by theoretical or empirical formulas based on the soil properties. It is also possible to estimate soil thermal properties from temperature data where that exists.

3.2.1 The Probe Method

> "The probe is inserted into the soil to be tested and, being thin, should cause little disturbance. It consists of a heater producing thermal energy at a constant rate and a temperature sensing element. The rate of rise in the temperature of the probe depends on the thermal conductivity of the surrounding medium" (Farouki, 1981b).

The probe method can be used to measure the thermal properties of soil in an efficient way. With a hand-held device with connected probes it can easily be used insitu and in the laboratory. The probe is not suitable for determination of thermal properties for frozen soil at temperature between approximately –10°C and 0°C. This is because heat applied from the needle will cause phase change of ice and standard software does not account for melting of ice in the algorithms (Putkonen, 2003). The phase change will increase the apparent soil heat capacity and degrease the apparent thermal diffusivity. Putkonen (2003) found that the most reliable way to determine the frozen thermal properties was to measure with the probe at different temperatures with the most important temperature being the coldest one. The values of thermal properties vary from the freezing point to approximately –10°C, but the most significant change in thermal properties occur around the freezing point and vary little below this point. Therefore, values determined at temperatures colder than –10°C can be used for the temperatures up to about –2°C, depending on the freezing point temperature (Putkonen, 2003).

The KD2 Pro Thermal Properties Analyzer

In the experimental work in this thesis the KD2 Pro Thermal Properties Analyzer manufactured by Decagon Devices Inc. was used to measure the thermal properties in soil. The description of the device is adapted from the Operators Manual by Decagon Devices (2016). The KD2 Pro is the controller and it is used with different types of sensors. A single needle sensor (TR-1) can measure thermal conductivity and resistivity, and the dual-needle sensor (SH-1) measures volumetric heat capacity and thermal diffusivity in addition.

To perform measurements the needle is inserted into the material. The KD2 Pro will allow for 30 seconds equilibration time before heat is applied to the sensor. The KD2 Pro applies heat during half of the "Read Time" and takes 60 temperature measurements during the full read time. The different needles have different default settings for "Read Time" and hence the time between readings will differ. The heating of the sensor can cause convection and moisture migration in the sample and can cause the moisture conditions in the sample to change. The default setting for TR-1 and SH-1 is the high power mode which sends out a large heating current. This can be switched to low power mode where the current is small and cause less heating of the sensor. This could be an advantage in frozen materials to decrease the heat input and reduce melting of ice.

The sensors are suitable for doing measurements in different types of materials. The single needle TR-1 is 2.4 mm in diameter and 10 cm long. It is designed for use in soil and granular materials. In granular soil samples the contact resistance with the material and needle is an error source and the longer heating time (5 minutes) and larger diameter of this needle are chosen to minimize this error (Decagon Devices, 2016). The needles of the SH-1 are 3 cm long with 1.3 mm diameters and with 6 mm spacing. The heat pulse from the SH-1 needle is large and it is not suitable to use in liquids, but is compatible with solids and granular materials and is suitable to use in soil samples. The default read time is 2 minutes. It is important to keep

Table 3.2: *The table shows measurement range and accuracy for the KD2 Pro sensors (adapted from Decagon Devices (2016)).*

Sensor	**Property**	**Range**	**Accuracy**
TR–1	Thermal conductivity	0.1 to 0.2 W/mK 0.2 to 4.0 W/mk	$\pm 0.02 W/mK$ $\pm 10\%$
SH–1	Thermal conductivity	0.02 to 0.2 W/mK 0.2 to 2 W/mK	$\pm 0.01 W/mK$ $\pm 10\%$
	Diffusivity	0.1 to 1.0 mm^2/s	$\pm 10\%$
	Volumetric specific heat	0.5 to 4.0 mJ/m^3K	$\pm 10\%$

the spacing between the needles, so it should not be forced or bent into the material. The range and accuracy of measurements with the KD2 Pro are given in Table 3.2.

Algorithms for Determination of Thermal Properties

The KD2 Pro uses transient line heat source methods to measure thermal conductivity. The single needle TR–1 sensor has a heater and temperature sensor inside. In the dual needle SH–1 sensor the heater and temperature sensor are placed in the separated needles. A current is sent through the heater and the temperature sensors measures changes in temperature due to the current. The separation of needles in the SH–1 sensor makes it possible to measure the temperature and time relationship and through analysis of these measurements the thermal diffusivity, thermal conductivity and heat capacity of the material is found (Decagon Devices, 2016). The ideal sensor for these measurements should have very small diameter and a length multiple times the diameter. This is to have good contact with the material and have minimal impact on the change in the surrounding material. The KD2 Pro is designed to have a needle robust enough to use in tough materials while still having a dimension that works well for the measurements. The heating time is kept low and the heat input minimized to minimize thermally induced water movement and free convection (Decagon Devices, 2016). This is done by having a high temperature resolution (± 0.001°C) and special algorithms to analyse the temperature measurements.

In the dual sensor one needle is heated for a set time, t_h. The monitoring needle measures temperature during read time with a heating and cooling period. The temperature measurements are processed by

$$T^* = \frac{4\pi(T - T_0)}{q} \tag{3.11}$$

where T_0 is the temperature at time 0, T the measured temperature and q the heat per unit length. The dual needle algorithm uses a non-linear least square procedure to fit the data from measurement (Decagon Devices, 2016).

$$T^* = b_0 t + b_1 E_i \left(\frac{b_2}{t}\right) \tag{3.12}$$

$$T^* = b_0 t + b_1 \left(E_i \left(\frac{b_2}{t}\right) - E_i \left(\frac{b_2}{t - t_h}\right)\right) \tag{3.13}$$

The values determined by Equation 3.11 for T^* are fitted to Equation 3.12 for the measurements where the heat is on and to Equation 3.13 when the heat is off. Moreover, q is the heat input and

E_i is the exponential integral as presented by Abramowitz and Stegun (1972) (Decagon Devices, 2016). The constants b_0, b_1 and b_2 should be fit by minimizing the sum of squares error between the equations and measurements. KD2 Pro use the non-linear least squares procedure by Marquardt (1993) (Decagon Devices, 2016). When these constants are found the thermal conductivity is calculated by:

$$k = \frac{1}{b_1} \tag{3.14}$$

In addition, the KD2 Pro uses a method of minimizing the sum of squares of the measured and modelled values to give a dimensionless error value that describes how well the measured value fit to the modelled data (Decagon Devices, 2016). Putkonen (2003) has modelled the thermal behaviour in frozen soil measured by a heated needle probe. He found that phase change confound the measurement results with using the standard processing procedure, but with alterations to this procedure it is possible to obtain the frozen temperatures even at negative temperatures close to the freezing point (Putkonen, 2003).

3.2.2 Empirical Models

Kersten's Empirical Equations

M. S. Kersten was the first to perform tests on frozen and unfrozen soil to predict the thermal conductivity (Williams & Smith, 1989). He performed tests on nineteen natural soils from which he came up with four empirical equations and these were published in 1949 (Farouki, 1981c). The four equations are used to determine thermal conductivity for two soil groups, silt/clay and sandy soil and in frozen and unfrozen states. Frozen and unfrozen state is given by temperatures of –4°C and +4°C. The equations were converted to SI units by Farouki (1981b). For fine grained soil with more than 50% silt/clay content the equation for unfrozen thermal conductivity is

$$k_{fine,u} = 0.1442(0.9logw - 0.2)(10)^{0.6243\rho_d} \tag{3.15}$$

and for frozen thermal conductivity it is

$$k_{fine,i} = 0.001442(10)^{1.373\rho_d} + 0.01226(10)^{0.4994\rho_d}w \tag{3.16}$$

For coarse grained soils with less than 20% of fines Kersten estimates the unfrozen thermal conductivity as

$$k_{coarse,u} = 0.1442(0.7logw + 0.4)(10)^{0.6243\rho_d} \tag{3.17}$$

and the frozen thermal conductivity for coarse grained soil as

$$k_{coarse,i} = 0.01096(10)^{0.8116\rho_d} + 0.00461(10)^{0.9115\rho_d}w \tag{3.18}$$

The equations do not take into account variation in quartz content or unfrozen water content. Farouki (1981b) stated that these equations gave less than 25% deviation from measured results and are valid for soils with moisture content higher than 7%. He also stated that this average value was sufficient in most applications due to the inhomogeneity in natural soils (Andersland & Ladanyi, 2004). Andersland and Ladanyi (2004) presented the diagrams by Harlan and

Nixon (1978) that are based on Kersten's equations (Figure 3.4). The diagrams can be used to determine the thermal conductivity if the soil type, water content and grain density is known.

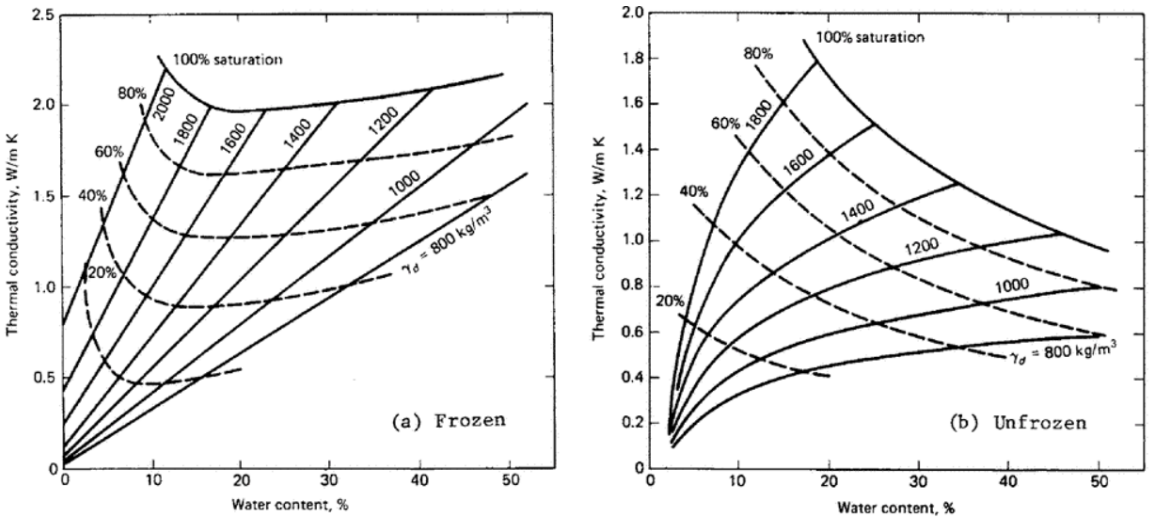

Figure 3.4: *Diagram for determination of average thermal conductivity for silt and clay soils (Andersland & Ladanyi, 2004).*

Johansen's Empirical Equations

The method by Øistein Johansen (1975) determines the thermal conductivity of mineral soils by interpolation between dry and saturated values. He introduced the Kersten number, K_e, that depend on the soil saturation. Andersland and Ladanyi (2004) and Farouki (1981c) agreed that the method of Johansen (1975) gave the best results for unfrozen and frozen soil for both coarse and fine grained soils with saturation above 0.1. The equations below are presented as by Andersland and Ladanyi (2004). Thermal conductivity computed from Johansen's method is denoted k_j. The main equation for determining the thermal conductivity is

$$k_j = (k_{sat} - k_{dry})K_e + k_{dry} \tag{3.19}$$

where the Kersten number for coarse grained unfrozen soil is

$$K_e = 0.7 log S_r + 1.0 \tag{3.20}$$

and for for fine grained soil it is

$$K_e = log S_r + 1.0 \tag{3.21}$$

The degree of saturation, must be >0.05 for Equation 3.20 and >0.1 for Equation 3.21. For frozen soil $K_e = S_r$. Furthermore, the dry thermal conductivity is found by the semi-empirical equation

$$k_{dry} = \frac{0.137\rho_d + 64.7}{2700 - 0.947\rho_d} \pm 20\% \tag{3.22}$$

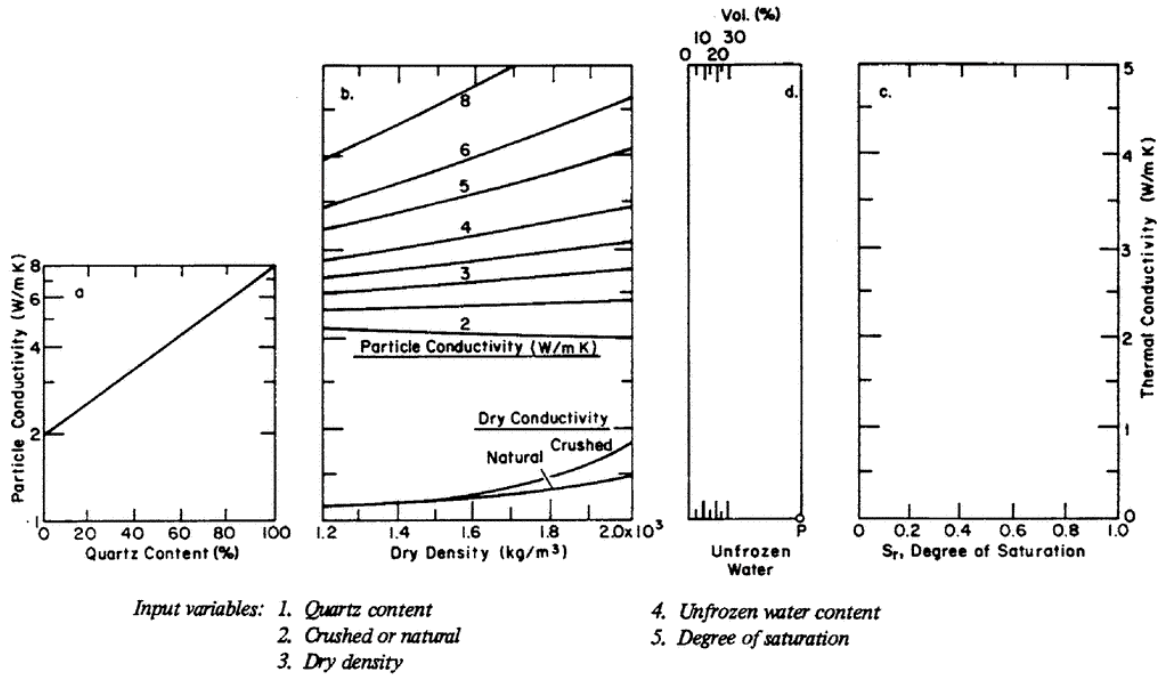

Figure 3.5: *Diagram by Johansen (1975) to determine thermal conductivity of frozen soils (Andersland & Ladanyi, 2004).*

with the dry density given in kg/m^3. The saturated conductivity will depend on frozen and unfrozen water content and for an unfrozen soil

$$k_{sat} = k_s^{1-n} k_w^n \tag{3.23}$$

where n is the porosity, k_w and k_s the thermal conductivity of water and soil grains respectively. Frozen soil thermal conductivity with inserted thermal conductivity values for ice and water is

$$k_{sat} = k_s^{1-n} (2.2)^n (0.269)^{w_u} \tag{3.24}$$

Johansen also included the effect of quartz content by the geometric mean equation

$$k_s = k_q^q k_0^{1-q} \tag{3.25}$$

where he differentiates between the thermal conductivity of quarts, k_q, and other minerals, k_0. The diagrams shown in Figure 3.5 are based on the equations by Johansen (1975). Quartz content, crushed or natural state of soil, dry density, unfrozen water content and degree of saturation are necessary input parameters to use the diagrams. Johansen's method demands the knowledge of more soil parameters than the Kersten method.

Research Findings

It is desirable to find an efficient way to determine the thermal conductivity whit the necessary accuracy. The empirical methods of Kersten and Johansen have been developed from testing of soils. Both methods have been tested by Farouki (1981b). For soil with saturation up to 0.9, it

was found that for frozen, fine grained soil Kersten's model give predictions with deviations less than ±30% (Farouki, 1981c). Above 0.9 it over-predicts the value (Farouki, 1981a). Johansen's method over predicts at saturations below 0.1 but give good agreement (±35%) at saturations above 0.1 (Farouki, 1981a). To be able to use Johansen's method to calculate values with good agreement it is necessary to have the proper value for the unfrozen water content. Furthermore, Farouki (1981c) has found that the unfrozen water content plays an important role in the heat transfer and that the bound pore water seems to have a higher thermal conductivity than bulk water. Other findings from his study are that frozen soil thermal conductivity is more sensitive to changes in moisture content than unfrozen soils. The thermal conductivity will increase if the moisture content is kept constant and the dry density is increased and the increase in thermal conductivity and moisture content is a linear relationship. Also, the thermal conductivity of soil grains in frozen soil has a considerable effect on the total thermal conductivity and the impact increase with increase of saturation. This means that the predictions of quarts content and mineral composition are important for precise predictions of the thermal conductivity.

A field and laboratory study on frozen and thawed soil from the Baydaratskaya bay coast was performed by Aleksyutina and Motenko (2017) and they studied the thermal properties with the KD2 Pro device. They found that in frozen soil the thermal conductivity increases with water content to a limit where the rate of change in thermal conductivity decreases. Their measurements showed that increase in organic matter caused a decrease in thermal conductivity due to the organic matters lesser ability to conduct heat. Furthermore, they found that the impact of salinity was most significant in frozen soil and lowers the thermal conductivity value.

A dramatic change in the soil thermal conductivity was seen between 0°C and –2°C in a study by Sun et al. (2016). They described that the effect of latent heat released or absorbed during thawing and freezing exceeded the effect of conductive heat flow at temperatures close to 0°C. The thermal properties of frozen soil were highly affected by phase change around the transition temperature (Williams & Smith, 1989). Figure 3.6 shows how the thermal conductivity has an abrupt change around the freezing point of the soil and how this can be connected to the amount of unfrozen water content. When the freezing point is reached, water start to freeze and the amount of unfrozen water decrease. This is in turn cause the thermal conductivity to increase, because ice has higher thermal conductivity than water. The freezing point for clay will be lower than for silt and the amount of unfrozen water content at same temperatures will be higher, as Figure 3.6 shows. As a result, the thermal conductivity of clay is lower than for silt. Under the same temperature gradient more heat will flow through the material with higher temperature gradient (Williams & Smith, 1989). That means that more heat will be transported and the material will warm faster.

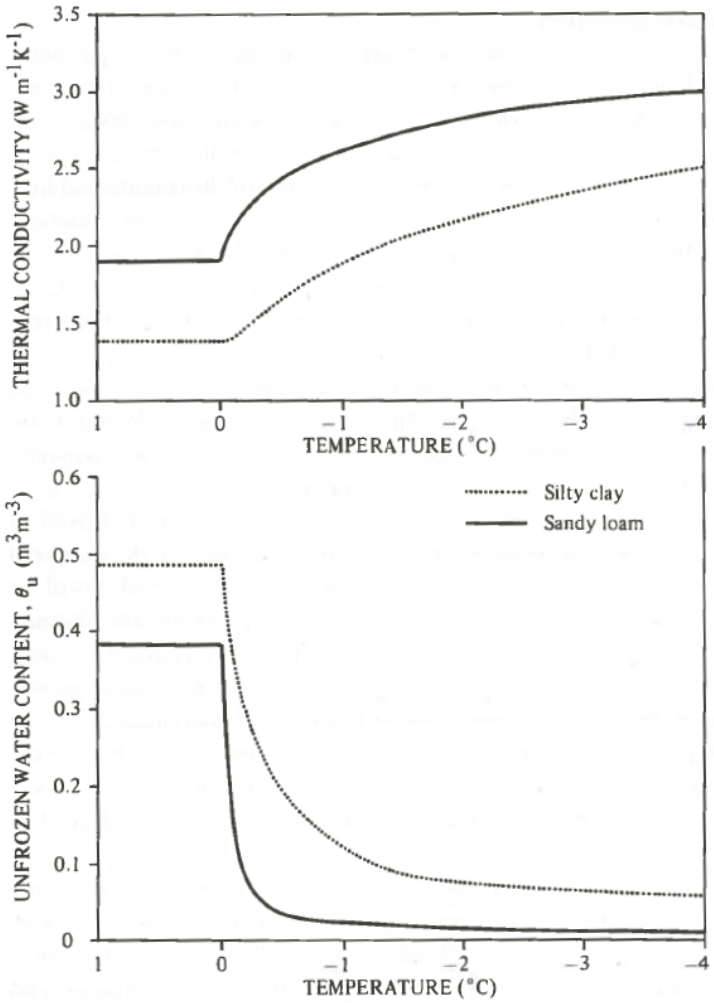

Figure 3.6: *Variation of thermal conductivity with temperature and the unfrozen water content with temperature for a silty clay and a sandy loam (Williams & Smith, 1989).*

3.2.3 Effective Medium Theory

Frozen soil is a porous composite medium and effective medium theory (EMT) can possibly be used to predict thermal conductivity and how it changes with temperature and soil composition. Equation 3.5 with $k_m = k_e$ give the EMT-equation. The advantage with using the EMT-model is that it in theory only has one unknown factor, X, that has to be determined. Both Kersten's and Johansen's equations for determining k contains several empirically determined numbers. The EMT-equation will give a solution for thermal conductivity that lies between the limits given by series and parallel heat flow. If a single factor can be verified for different soil samples, EMT will be an effective tool to predict thermal conductivity. It would be necessary to test soils with different mineral composition, porosity and saturation and with different temperatures to determine a general value for X that can be used in frozen soil thermal conductivity prediction.

The complexity of Equation 3.5 can be increased in different ways to reduce the deviations in predictions of frozen soil. Different factors such as mineral content, porosity, frozen water content and ice content give rise to different X factors in the EMT-equation. The equation equals the sum of the volume fractions of the different components and additional components

can easily be added. The soil grain fraction can be split in fractions for different mineral content. This is done in Johansen's equation by distinguishing between quartz content and other mineral content. Including different mineral fractions will give a more nuanced system thermal conductivity. In addition, the fraction of air can be added. That would make it possible to use the equation on soils that are not fully saturated. This would increase the number of the fractions in the sum and each fraction gives a contribution to the system conductivity. The X factor needs to be re-evaluated when adding more fractions in the sum. Other models distinguish between coarse and fine grained material, and it would probably be necessary to determine different X factors for coarse and fine grained material and maybe for several different soil types. Diagrams similar to those shown in Figure 3.4 and 3.5 could be established for different soil types.

Furthermore, it is possible to determine different factors for the components or give a weighting to the factor in a fraction. For example if change in the porosity and fraction of soil grains have a larger influence on the change in thermal conductivity than the mineral composition, this effect should be accounted for in the EMT-equation. One way to do this is to look at the relation between two components at a time, for example water-ice, ice-soil and soil-water. From these relations it is possible to see some indications on how the thermal conductivity and the unknown factor X relates within the two component system. Weighting can then be applied in the total system to components that seem to have larger effect on the system thermal conductivity. In a real soil the heat flow move through the composite material and the different materials affect the heat flow differently which can be reflected by the weighting.

Chapter 4

Unfrozen Water Content

The unfrozen water is referred to as the water that remains liquid when the soil is cooled below 0°C. Figure 4.1 shows how cooling of a soil-water system develop. First, the water will be super cooled to a temperature, T_{sc}, where the water starts to freeze (Andersland & Ladanyi, 2004). Secondly, when ice is formed, latent heat is released which cause a rise in temperature to the freezing point (FP), T_f. T_f is close to 0°C for coarse grained soil and can be depressed down to –5°C for fine grained soil (Andersland & Ladanyi, 2004). When T_f is reached, free water in the soil pores will continue to freeze at this temperature. The release of latent heat will slow the cooling rate also when bound water start to freeze. The bound water will appear as liquid layers around the soil grains. At temperature T_e (about –70°C) all water will be frozen. A standard method to determine the FP in soil does not exist. The freezing point depression, ΔT in Figure 4.1, in a soil depends on the size of soil pores, water content and solute content (Zhou et al., 2018). Even when the initial FP is reached a part of the soil will remain unfrozen. To determine the amount of unfrozen water content is important when studying the heat transfer in soil. Watanabe and Mizoguchi (2002) has found that the amount of unfrozen water content decrease with temperature and that in water saturated with solution the amount of unfrozen water content increase with increasing solute concentration. The amount of unfrozen water content affects the strength and the hydraulic and thermal conductivity of soil (Watanabe & Mizoguchi, 2002), mainly because not all the water freeze to ice and water exist in two different phases.

4.1 Determining the Amount of Unfrozen Water Content

There has not been established an efficient way to determine the FP in soil and the amount of unfrozen water content below the FP that includes the influencing factors. However, through experimental investigations qualitative evaluation methods have been developed. Dilatometry, adiabatic calorimetry, x-ray diffraction, heat capacity, nuclear magnetic resonance, differential thermal analysis, and isothermal calorimetry are some different methods that can be used to directly determine the unfrozen water content in soil (Anderson & Morgenstern, 1973). In addition several indirect and empirical methods have been established. Methods will be briefly presented.

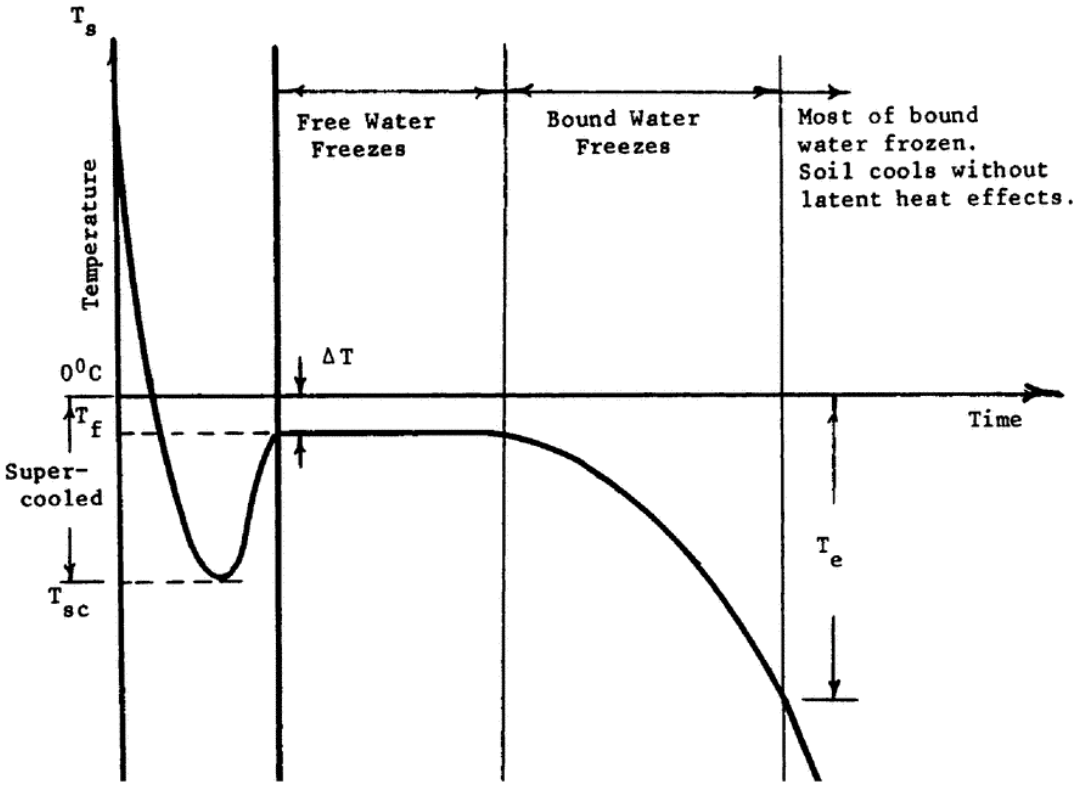

Figure 4.1: *Cooling curve for soil water and ice (Andersland & Ladanyi, 2004).*

4.1.1 Direct Measurement Methods

Calorimetry is based on measuring the change in enthalpy of a substance with a given change in temperature. In adiabatic calorimetry the heat capacities of the components in the soil must be known (Anderson & Morgenstern, 1973). Differential thermal analysis, also called differential scanning calorimetry (DSC), use temperature measurements and the fact that heat will be liberated or absorbed during a phase change. An electric thermometer measures temperature in the soil sample and a reference substance that are exposed to a uniform change in temperature. The temperature in the soil sample will lag behind or precede that of the reference substance when phase change occur and allows for prediction of unfrozen water content (Anderson & Morgenstern, 1973).

Dilatometer measurements are based on the assumption that soil water expand to the same extent as bulk water (Anderson & Morgenstern, 1973) and the dilatometer measures volume change. Dilatometry and adiabatic calorimetry is best to determine the amount of water that freeze in the range of 0°C to about –3°C, while the DSC method is useful to determine the unfrozen water content at low temperatures (–10°C to –30°C) (Anderson & Morgenstern, 1973).

Nuclear magnetic resonance (NMR) can be used to estimate the amount of unfrozen water content by measuring the changes in the magnetic field due to an applied pulse. The water in a sample will be aligned along a fixed external magnetic field due to the magnetic moment from water protons (Watanabe & Mizoguchi, 2002). A NMR analyser is used to apply the pulse and observe proton relaxation (Tice et al., 1978). The voltage induced by changes in the magnetic field is measured by NMR and the measurements give a free-induction decay curve (FID). The peak value of the FID curve represent the total amount of ice and water and the decay of the FID

curve is more rapid for ice than for water and this is used to determine the amount of unfrozen water (Watanabe & Mizoguchi, 2002). By use of the NMR method it was discovered that the total water content (ice content) in addition to temperature affect the amount of unfrozen water content (Tice et al., 1978).

4.1.2 Empirical Method

An Empirical equation based on experimental values of unfrozen water content have been suggested

$$w_u = \alpha\theta^{\beta} \tag{4.1}$$

where α and β are characteristic soil parameters and θ temperature expressed in positive Celsius below freezing (Tice, Anderson and Banin (1976) in Andersland & Ladanyi, 2004). The unfrozen water content will decrease with lowering of temperatures below the FP. The characteristic parameters α and β are defined for some soil types and can be determined on the basis of liquid limit data (Andersland & Ladanyi, 2004). When α and β are determined a curve of unfrozen water content at negative temperatures can be determined. Nybo (2017) used the liquid limit method on permafrost soil from Svalbard and found that the method under predicted the amount of unfrozen water content. She made alterations to the equations for α and β determination to obtain a better fit of the estimated unfrozen water curves.

4.2 Water Potential

Water potential, $\psi[MPa]$, is the potential energy per unit volume of water in a sample relative to bulk water in reference conditions. Pure, bulk water at atmospheric pressure under the same thermodynamic conditions will be the reference conditions and have a potential of zero. The potential energy in pore water in soil can be modified by physicochemical interactions between the pore water and the soil substance in a way that the potential energy of the fluid and species in the pores are different from the potential energy without the surface forces under the same thermodynamic conditions (Zhou et al., 2018). Water will move from higher to lower potential when there is a difference in potentials. The total potential is caused by forces due to earth's gravitational field, overburden pressure, osmotic effects and attraction of soil particles (Williams & Smith, 1989). When concerning water potential in relation to the FP and unfrozen water content we are mostly concerned about the matric potential, ψ_m,and osmotic potential, ψ_o, and the following equation will be used to describe soil water potential

$$\psi = \psi_o + \psi_m \tag{4.2}$$

The soil water potential can be related to the free energy of the soil water. Gibbs free energy or the chemical potential is used in physical chemistry to study the equilibria in chemical reactions, melting points and modification of melting points (Williams & Smith, 1989). Bulk water and pure ice has equal free energies at 0°C (Figure 4.2). The matric potential is numerically equivalent to the difference in Gibbs free energy of the soil water relative to the reference water at the same temperature (Williams & Smith, 1989). The free energy in soil water is lower than the free energy in bulk water. Therefore, the soil water and ice free energies will be equal

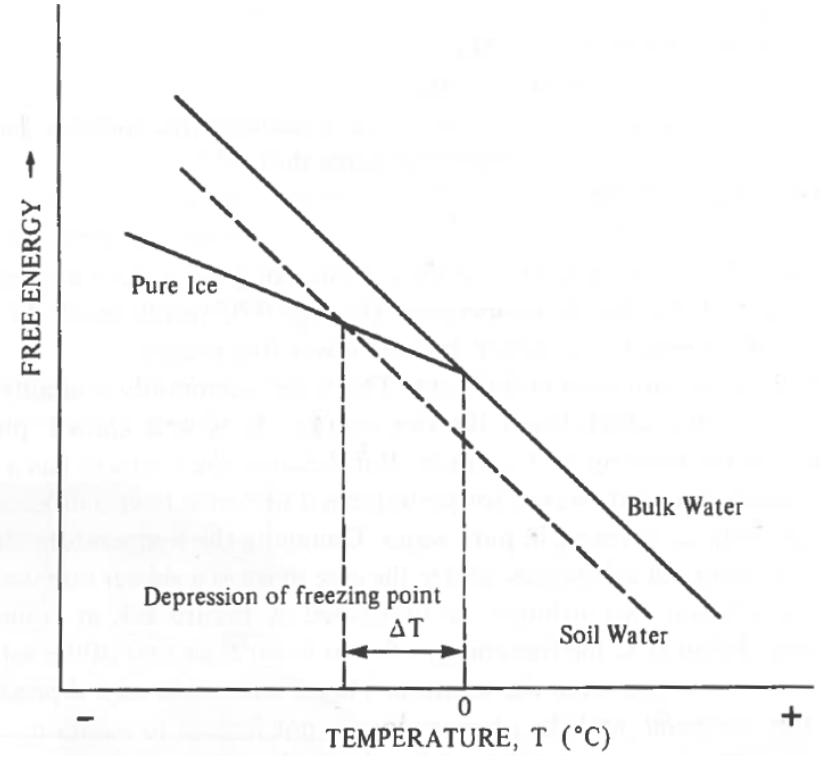

Figure 4.2: *The two parallel lines show how the free energy in bulk water and soil water changes with temperature, and the depression of FP in soil water compared to FP in bulk water is indicated (Williams & Smith, 1989).*

at a temperature below 0°C (Williams & Smith, 1989). The FP is where the free energy in the soil water is in equilibrium with the free energy of the ice. The FP in soil water will be depressed below zero due to the negative matric and osmotic potential. The interface between two phases is associated with surface tension which will influence the pressure and thus the soil water potential (Williams & Smith, 1989). The water potential is temperature dependent and when the temperature is lowered the water potential increase.

4.2.1 Matric Potential

Matric potential is the effect of capillarity and particle surface adsorption and is also referred to as soil suction (Williams & Smith, 1989). Electrostatic forces at the particle surface of soil grains affect the water and cause suction (negative pore water pressure). The adsorptive forces bind the water in thin films around the soil grains. The adsorptive effect is larger in fine grained soils because of larger relative surface area (M. Anderson & R. Tice, 1972). The capillary potential is not affected by the soil force field but by surface tension in unsaturated soils. In clays the pores are very small and when the soil grains are in contact with water a meniscus will form around the soil grains. The curvature of the meniscus indicates a pressure difference. Adhesive and cohesive forces in the water will cause the curvature and pressure difference in the water. The pressure under the meniscus will be lower than atmospheric pressure and the water is in tension which is characterised as negative pressure.

4.2.2 Osmotic Potential

The osmotic potential depends on the solute concentration in the pore water. In general the osmotic potential in a soluble can be calculated as

$$\psi_o = -icRT \tag{4.3}$$

where i is the van 't Hoff index, c [mol/l] the molar concentration of solute, R is the ideal gas constant (8.314 J/k mol) and T is the temperature in Kelvin. i is the number of ions an ionic compound brakes into when dissolved in water. For a NaCl solution $i = 2$. Coefficient factors can be applied to the van 't Hoff index for correction since solutions are usually not ideal, but this will not be done in this thesis. Seawater has a salinity of approximately 3.5% which can be expressed as 0.6 mol/l and would at 0°C have an osmotic potential of approximately –2.7 MPa. Seawater freeze at approximately –2°C. The osmotic potential decreases with temperature and increases with increase in molar concentration. When water in the soil pores freeze the molar concentration in the remaining pore water will increase because the salt ions are not included in the ice crystal lattice.

4.2.3 Determination of Water Potential

The WP4C Dew Point PotentiaMeter developed by Decagon Devices can be used to measure the water potential (ψ) in soil with varying particle sizes and moisture content. It uses the condensation method, also called dew point detection, to determine the potential. The measured potential in WP4C is the sum of matric and osmotic potential (Decagon Devices, 2018). The use of this method makes it possible to determine the unfrozen water content as a function of negative temperatures in a highly efficient, accurate and easily repeated way (Istomin et al., 2017). The WP4C measure the water vapour dew point of a gas phase in equilibrium with a porous medium with a certain moisture content (Istomin et al., 2017).

The water potential of a soil will wary with the change in water content. In a closed system where you have a medium in gas phase over a liquid there will exist a vapour pressure above the liquid. The vapour pressure is related to the rate of evaporation. Equilibrium vapour pressure is the pressure when the gas and liquid in the closed system is in thermodynamic equilibrium at a given temperature. When the soil sample is placed in the closed chamber the head space above the sample will reach the equilibrium vapour pressure. At the equilibrium point the water potential for the air above the sample will be the same as the water potential for the sample. The WP4C measures the vapour pressure when equilibrium is reached and the sample temperature is measured by a temperature sensor. A mirror inside the chamber is controlled by a cooler and detects the dew point by condensation and the mirror temperature where this occurs (Decagon Devices, 2018). This is used to measure the vapour pressure, p, of the air above the sample. The saturation vapour pressure at sample temperature, p_0, is calculated from sample temperature (Decagon Devices, 2018). Then the water potential is estimated by

$$\psi = \frac{RT}{M} ln \frac{p}{p_0} \tag{4.4}$$

where R is the universal gas constant (8.314 J/mol K); T is the Kelvin sample temperature (K) and M is the molecular weight of water (18.015 g/mol). The water potential measured depends on the sample moisture content and the temperature at the time of measurement.

4.3 Application of the Clausius-Clapeyron Equation

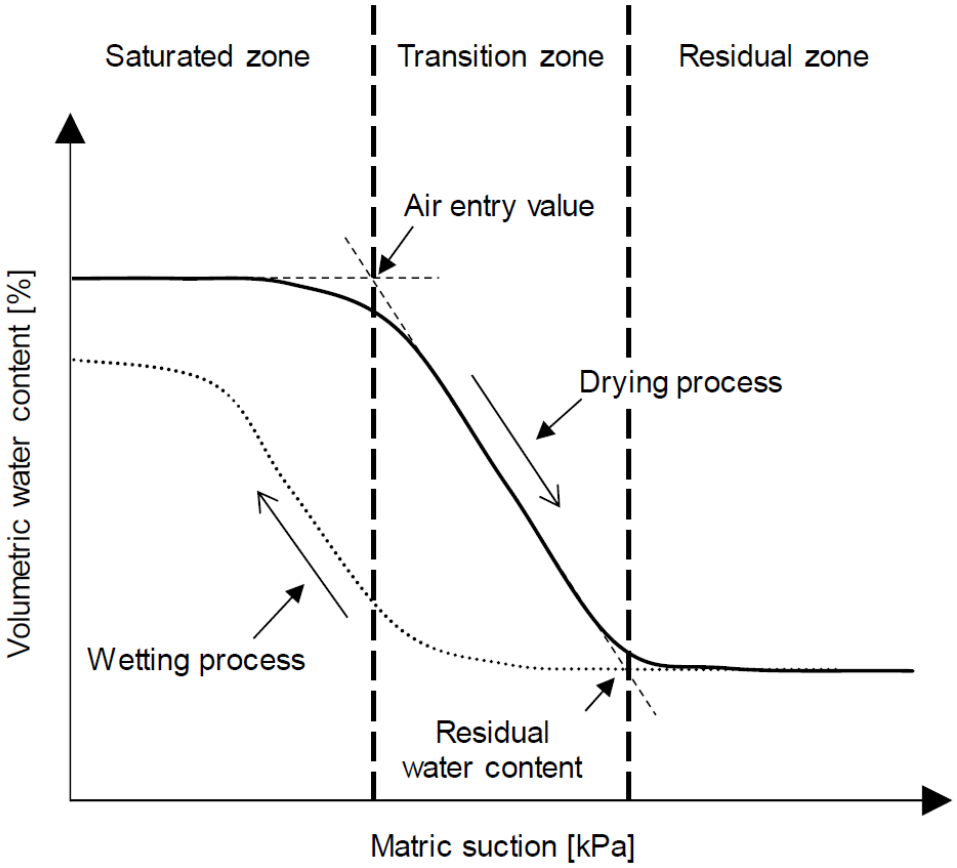

Figure 4.3: *Soil water characteristic curve for the wetting and drying process of an unfrozen soil (Hong et al., 2016).*

A soil water characteristic curve (SWCC) describes the relation between volumetric water contents in a soil and the matric potential or suction of the pore water. An example is shown in Figure 4.3. Mineralogy, particle size distribution, soil type, dry unit weight and permeability affect the shape of the SWCC (Hong et al., 2016). When a soil is dried, the water content is reduced and replaced with air and the opposite happens under wetting. The difference in the wetting and drying SWCC is called hysteresis. At full saturation the water potential is low or zero and as Figure 4.3 shows the water content will remain at or close to full saturation until the potential has reached the air entry value (Hong et al., 2016). The matric suction must reach to the air entry value before air will flow into the soil pores. When the air entry value is reached there is a transition zone where air flows into the sample because of increase in matric potential and water flows out from the sample. At a point a residual zone is reached and even with further increase in matric potential, the water content will remain constant (Hong et al., 2016). The soil freezing characteristic curve (SFCC) has been related to the SWCC by using the modified Clausius-Clapeyron equation (Black & Tice, 1989). The Clausius-Clapeyron equation expresses the relation between pressure and temperature during a phase change. The equation has an equilibrium requirement that must be fulfilled. That is, the chemical potentials of the two different phases must be equal at coexistence (Zhou et al., 2018). In an unfrozen soil the water potential is due to the pressure difference in the air entering the soil pores and the pore

water. For a soil that freeze it is the pressure difference between the ice that forms in the pores and the unfrozen pore water. The Clausius-Clapeyron equation can be expressed as

$$\frac{dT}{dP} = \frac{(V_w - V_i)T_{ref}}{L_f} \tag{4.5}$$

where dT is the freezing point depression, dP is the change in pressure, $V_w - V_i$ the volume difference between water and ice, L_f the latent heat of fusion and T_{ref} the reference FP of bulk water (0°C = 273.15K) (Williams & Smith, 1989). The equation describes that a change in pressure will cause a change in FP and relates ice pressure and water pressure to temperature in a freezing soil. The difference in ice pressure, p_i, and water pressure, p_w, can be expressed in terms of the water potential in an air-free frozen soil

$$\psi_{iw} = p_i - p_w \tag{4.6}$$

Another way to write the Clapeyron equation is

$$\Delta P = \psi_{iw} = \frac{L_f}{\Delta V} ln \left(\frac{T_f}{T_{ref}} \right) \tag{4.7}$$

where the soil water potential can be found if the freezing point depression is known. The volume change is due to the expansion of water when freezing (ca. 9% increase). If the soil water potential is known the FP can be estimated by the equation

$$T_f = T_{ref} \cdot exp \left(\frac{\psi_{iw} \Delta V}{L_f} \right) \tag{4.8}$$

The SFCC will have similar zones as the SWCC curve as shown in Figure 4.3. First, the potential must reach a certain potential before ice nucleation start. This potential is the ice entry value and is comparable to the air entry value. When initial freezing occur the pressure difference between the ice and the soil water will increase because of the reduction in unfrozen water. Even though the water content is the same, the forming of ice can be compared to entry of air in the sample. The temperature needed to freeze the remaining water is depressed as the water potential increase. How much the potential increase and what factors cause the increase is important to understand for establishing the SFCC. When comparing SWCC and SFCC, Black and Tice (1989) based the Clapeyron equation and the calculation of water potential on the effect of adhesion and capillary forces to drive water flow. They found that for a soil where adsorptive forces dominate they can be directly related with the Clausius-Clapeyron equation, but only for the same soil. However, their work did not include the effect of solute concentration and this limits the applicability of their results. Later on, it has been proven that the water potential used in the Clapeyron equation must include two effects; the osmotic pressure and other effects such as adsorption and capillarity (Zhou et al., 2018).

4.3.1 Thermodynamic Calculations for Fast Estimation of Unfrozen Water Content

A method for fast estimation of unfrozen water content in equilibrium with bulk ice at different negative temperatures is developed by Istomin et al. (2017). The method is also developed for nonclathrate water in equilibrium with the gas hydrate phase. Measurements at atmospheric

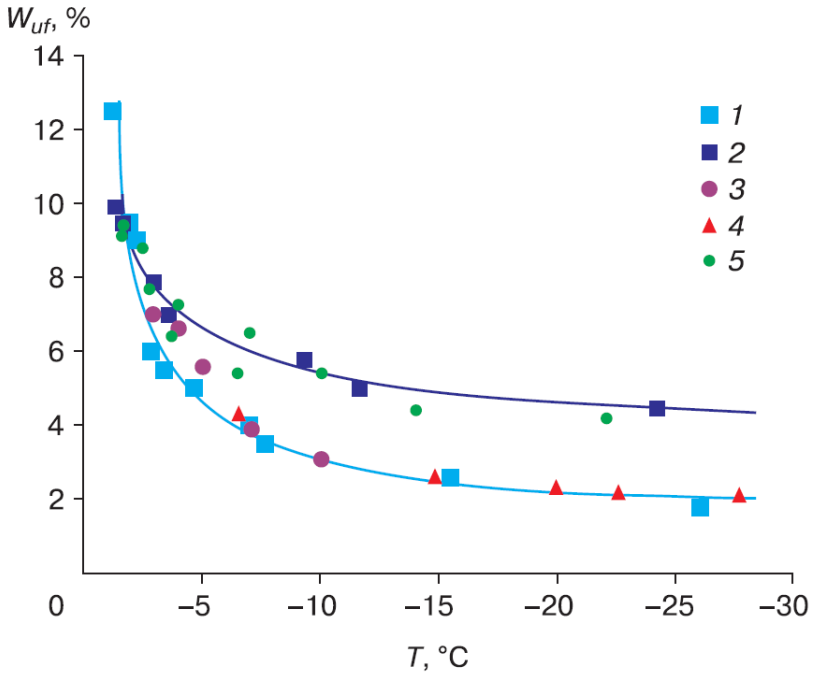

Figure 4.4: *Diagram of unfrozen water content for two different clay materials. The calculated curves based on water activity for kaolinite clay and polymineral clay, 1 and 2 respectively. The plotted data points 3 and 4 (kaolinite) and 5 (polymineral) show measurement by the contact method (Istomin et al., 2017).*

pressure are done to obtain the pore water potential of soil samples at different temperatures and moisture content. The water potentials are used in the thermodynamic calculations based on the concepts from the Clausius-Clapeyron equation. The change in volume can for phase change at low pressures and low temperatures be expressed by the general gas equation so that

$$\Delta V = \frac{RT}{P} \tag{4.9}$$

and (Istomin et al., 2017) use this and the translation of pore water potential to pore water activity in their calculations. The water activity, a, can be expressed in terms of the measured water potential and is then a function of the water content and temperature:

$$a(W,T) = exp(\frac{M\psi}{RT\rho}) = exp(\frac{2.167\psi(W,T)}{T}) \tag{4.10}$$

The water activity is expressed as the ratio of pressure difference between vapour pressure above the sample, p_{wpor}, and the vapour pressure of bulk water, p_w,

$$a = \frac{p_{wpor}}{p_w} \tag{4.11}$$

and is related to the water content. a is less than 1 when the sample is not fully saturated and will be 1 at full saturation (Istomin et al., 2017). The activity dependence on water has proven to be small. With the pressure difference related to the water activity, an altered form of the Clausius Clapeyron equation can relate water potential and temperatures for samples with determined water content

$$\psi = RT\frac{\rho}{M}ln\frac{p_{wpor}}{p_w} = RT\frac{\rho}{M}lna \tag{4.12}$$

where T is the sample temperature when testing, ρ is the water density (1.0 g/cm^3) and M the molecular weight of water (18.05 g/mol). The water activity at a given moisture content for the soil sample is used to calculate the temperature where bulk ice and pore water is in equilibrium, T_{eq}. The measured water content is equal to the unfrozen water content at the equilibrium temperature. An empirical relation for the difference in Gibbs free energy between super cooled water and bulk ice phase is used and by equating the chemical potentials of these two phases the following expression can relate the equilibrium temperature and pore water activity

$$-RTlna = 6008(1 - \frac{T}{T_0}) - 38.2(Tln\frac{T}{T_0} + (T_0 - T)) \tag{4.13}$$

where T_0 is the reference FP (273.15K) and T the temperature corresponding to the pore water-bulk ice equilibrium (t_{eq}). Equation 4.13 is rearranged to

$$t_{eq} = 103.25lna + 5.57(1 - a)^2 \tag{4.14}$$

where t_{eq} is calculated in °C based on the water activity (Istomin et al., 2017). By measuring the water potential at a range of different water contents and calculate the corresponding t_{eq}, the unfrozen water content curve can be established. Istomin et al. (2017) compare the results from the thermodynamic calculations to unfrozen water content measured by the contact method. Figure 4.4 shows the comparison of the results. The contact method measures water content in equilibrium with ice in a dried sediment plate placed in contact with two ice plates under isothermal conditions for two weeks (Istomin et al., 2015). The dried sample placed between the ice plates is weighed before the test, and re-weighed after saturation equilibrium with the ice plates under pressure is reached. The test is time consuming.

4.3.2 Estimation of unfrozen water content and freezing point depression with the Clausius-Clapeyron Equation with the Effect of Solutes

Zhou et al. (2018) has developed a new version of the Clapeyron equation to address the effect of solutes in the pore water on the FP and unfrozen water content. The explanations and derivations of equations described in the following section are adapted from the study by Zhou et al. (2018). Pore fluids have, because of surface forces, different potential energy from bulk water not affected by surface forces. If pore water and bulk water are in equilibrium, the thermodynamic conditions must differ, that is either the temperature or pressure. If thermodynamic equilibrium is reached for the system shown in Figure 4.5, the chemical potential for the reservoir solution, μ_R^w, and the pore solution, μ^w, must be the same, $\mu_R^w = \mu^w$. The pore solution is the pore water in the soil. The chemical potentials can be expressed as

$$\mu_R^w = \mu_{pure}^w + \frac{p'_R - p_0}{\rho_{pure}^w} + \frac{RT}{m^w}lna_R^w \tag{4.15}$$

$$\mu^w = \mu_{pure}^w + \frac{p' - p_0}{\rho_{pure}^w} + \frac{RT}{m^w}lna^w + \Omega' \tag{4.16}$$

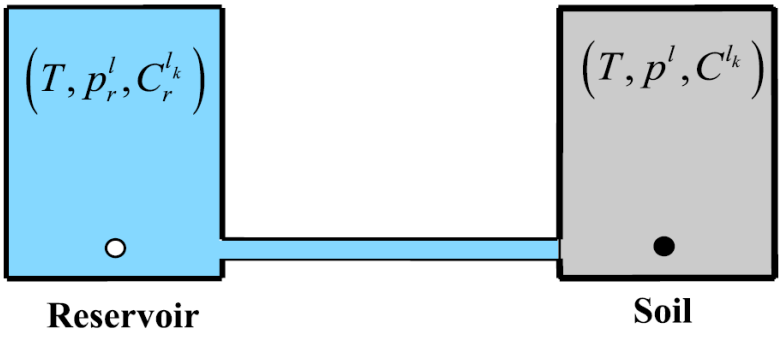

Figure 4.5: *Diagram of the equilibrium solution with a water saturated soil and a reservoir with water solution with the same composition as the water solution in the soil pores. The two are hydraulically connected and at the same elevation so they experience the same pressure (Zhou et al., 2018).*

where μ^w_{pure} is the chemical potential of water at its pure state, T is the temperature p is the liquid pressure where p_0, p'_R and p' is the reference pressure, equilibrium solution pressure and pore solution pressure respectively. Furthermore, ρ^w_{pure} is the mass density of pure water, m_w is the molar mass of water, a^w_R and a^w are the solvent activity in the reservoir and the soil and Ω' is the surface potential deriving from water and solid particle interaction in the soil. The solvent activity, a, ca be different in the reservoir solution and soil solution if the soil minerals are electrically charged. With a charge, the soil minerals must attract more positive ions to keep electrically neutral, and hence increase the solvent activity. From the equilibrium condition of the reservoir and soil chemical potential one obtain

$$p' = p'_R + \frac{\rho^w_{pure} RT}{m^w} ln \frac{a^w_R}{a^w} - \rho^w_{pure} \Omega' \tag{4.17}$$

$$\Pi_D = \frac{\rho^w_{pure} RT}{m^w} ln \frac{a^w_R}{a^w} \tag{4.18}$$

Π_D is the Donnan osmotic pressure and is the difference int the osmotic pressure in the pore solution and the reservoir solution. Of the three components of Equation 4.17, only p'_R is measurable and is what is usually termed the pore water pressure. The two other components accounts for the effect of capillarity, adsorption and osmosis.

When soil freeze the chemical potential of the pore solution and the pore ice must be in equilibrium and must be continuous across the interface between the two phases, $\mu^l = \mu^i$. From this equilibrium a generalized form of the Clapeyron equation can be expressed as

$$-Lln\left(\frac{T}{T_0}\right) = \frac{p^i}{\rho^i_{pure}} - \left(\frac{p^l}{\rho^l_{pure}} + \frac{RT}{m^w} ln a^w + \Omega'\right) \tag{4.19}$$

and is much similar to the equilibrium of Equation 4.16 and 4.15, but the latent heat released when water crystallize is included in Equation 4.19. In Equation 4.19, L is the heat of fusion or the difference in pore ice and water enthalpy; $T_0 = 273.15$°K is the FP of pure water under reference conditions of atmospheric pressure ($p_0 = 101.3$ kPa) and T is the equilibrium temperature. Ice will start to form at the equilibrium temperature. With a small change in FP the left hand side of Equation 4.19 can be approximated as $L \cdot \Delta_T / T_0$ where $\Delta_T = T_0 - T$ is the freezing point depression. Figure 4.5 must be altered to measure the pore water pressure

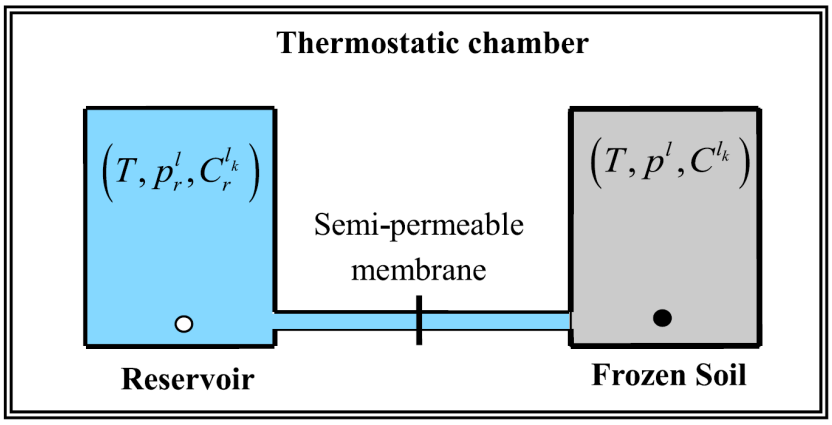

Figure 4.6: *Diagram showing the setup allowing for pore water pressure measurement in frozen soil (Zhou et al., 2018).*

in frozen soil, because the reservoir solution can freeze before the pore solution. By adding a chemical agent that depress the FP of the reservoir and a semi permeable membrane this can be resolved and this setup is shown in Figure 4.6. The p_r^l for the new reservoir solution can be directly measured. Then Equation 4.17 and Equation 4.18 can be solved for the new system shown in Figure 4.6. By subtracting these two equations from each other and assuming the equilibrium solution is ideal and dilute the expression

$$\frac{\rho_{pure}^w RT}{m^w} lna_R^w = -cRT \tag{4.20}$$

is derived. By substituting Equation 4.20 into Equation 4.19, with the assumption that the freezing point depression is small, gives:

$$p^i - p_R^l = \rho_{pure}^w \frac{L\Delta_t}{T_0} + cRT \tag{4.21}$$

The ice-liquid matric suction in a soil can be expressed by

$$\psi_m = p^i - p_R^l \tag{4.22}$$

where the ice pressure is assumed to equal the atmospheric pressure. By inserting Equation 4.22 into Equation 4.21 and rearranging the following expression is found

$$\eta(T_0 - T) = p^i(\beta - 1) + \psi_m + cRT \tag{4.23}$$

where

$$\beta = \frac{\rho_{pure}^w}{\rho_{pure}^i} \tag{4.24}$$

and

$$\eta = \frac{\rho_{pure}^w L}{T_0} \tag{4.25}$$

and η is 1.23 MPa/°C. The matric potential depend on pore solution concentration and ice pressure because these can alter intermolecular interactions and porosity. However, these effects are neglected because the dependence on the water content is much larger.

The unfrozen water content curve display the relation between unfrozen water content at different temperatures and the slope of the curve can be expressed by $w'_T = dw/dT$. The unfrozen water content depend on the matric potential and the temperature then depends on the matric potential through the unfrozen water content and this can be expressed by:

$$\frac{d\psi_m}{dT} = \frac{d\psi_m}{dw}\frac{dw}{dT} = w'_T\frac{d\psi_m}{dw} \tag{4.26}$$

It is assumed that the soil is a closed system so that the solutes do not move relative to the pore skeleton. Then the mass solute content, C, can be expressed as $C = m_c/m_s$ which is the ratio of mass of solute to mass of soil grains. The mass of solute will remain unchanged even if pore water solution change. Change in the water content will cause change in the molarity of the solution, c, by

$$c = \frac{n\rho^l C}{Mw} \tag{4.27}$$

where n is the number of ions released per solute molecule, ρ^l is the mass density of the pore solution and is equal to ρ^w_{pure} for a dilute solution (1g/cm^3). If Equation 4.27 is inserted in Equations 4.23, the derivative of the equation gives

$$\left(\eta + \frac{n\rho^l RC}{Mw}\right)dT = \left(\frac{\eta}{w'_T} + \frac{n\rho^l RCT}{Mw^2}\right)dw - \frac{n\rho^l RT}{Mw}dC \tag{4.28}$$

which express the FP in terms of water content and the mass solute content. Before the freezing process starts at T_f all water is unfrozen and is termed w_0. By integration of water content and solute content the FP can be determined from Equation 4.28

$$T_f(C, w_0) = T_{ref} + \int_{C_{ref},w_{ref}}^{C_{ref},w_0}\left(\frac{\left(\frac{\eta}{w'_T} + \frac{n\rho^l RCT}{Mw^2}\right)}{\left(\eta + \frac{n\rho^l RC}{Mw}\right)}\right)dw + \int_{C_{ref},w_0}^{C,w_0}\left(\frac{-\frac{n\rho^l RT}{Mw}}{\left(\eta + \frac{n\rho^l RC}{Mw}\right)}\right)dC \tag{4.29}$$

where T_{ref}, C_{ref} and w_{ref} is the FP, solute content and water content at at the reference state. The reference state yields atmospheric pressure conditions for bulk ice and bulk water, FP of 273.15 K and zero solute content. Th FP due to the capillary pressure can be found by Equation 4.29 if the solute content is set to zero, $C = 0$. That gives the expression

$$T_{f0} = T_{ref} + \int_{w_{ref}}^{w_0}\frac{1}{w'_T}dw = T_{ref} - \frac{1}{\eta}(\psi_m - \psi_{ref}) \tag{4.30}$$

where ψ_{ref} is the reference capillary pressure. Assuming an infinite water content at reference state gives zero curvature of ice-water interface which gives a reference capillary pressure of zero. The last part of Equation 4.30 is obtained by finding the temperature derivative of Equation 4.23, and using $C = 0$. That gives $d\psi_m/dT = -\eta$. By substituting this into Equation 4.26 give

$$d\psi_m = -\frac{\eta}{w'_T}dw \tag{4.31}$$

which give the last term in Equation 4.30. ψ_{m0} is the capillary pressure at the beginning of freezing.

Experimental data show that T_{f0} is always lower than T_0 and Zhou et al. (2018) explains that there are two reasons for this; the minimum capillary potential of the ice entry value must be reached before water and ice can coexist and impurity in natural soil pore water will lower the FP. When water starts to freeze, the water content, w, will be the sum of unfrozen water and ice. The water content does not change, but the solute content does, because the ice crystallisation does not include the solutes in the structure. This reduces Equation 4.28 to

$$\frac{dT_f}{dC} = \frac{\frac{n\rho^l RT}{Mw_0}}{\left(\eta + \frac{n\rho^l RC}{Mw_0}\right)} \tag{4.32}$$

which can be solved as an ordinary differential equation. By setting the FP to $T_f = T_{f0}$ at zero molarity Zhou et al. (2018) solve the differential equation. The solution give the FP of soi expressed by the FP due to matric potential and solute content and is:

$$T_f = \frac{Mw_0\eta T_{f0}}{\eta\rho^l RC + Mw_0\eta} \tag{4.33}$$

Zhou et al. (2018) develop these equations to calculate the FP as function of water content, solute content and temperature. The final equation that can be used to calculate the unfrozen water content curve, demands experimental results to decide curve fitting parameters. The necessary experiments were not performed in this thesis and makes it difficult to test these equations. The described equations for estimating FP temperatures will be used to establish unfrozen water content curves.

Chapter 5

Experimental Investigations

5.1 Site Description

5.1.1 Location

The Svalbard archipelago is located within the continuous permafrost zone (Gilbert et al., 2019). The site investigated in this study is one of the two Norwegian GeoTest Site (NGTS) developed in Svalbard. NGTS are reference field sites for long-term geotechnical field testing. Long series of observations of ground temperatures can give indications on how the ground thermal regime responds to warming trends in the climate. The site in this study is called UNIS East and is located immediately east of UNIS in Longyearbyen as shown in Figure 5.1. Longyearbyen is situated at 78°N. Figure 5.2 shows the location of the boreholes that have been drilled at the site. Borehole E5 with coordinates 78.2218°N 15.6601°E has been used for laboratory testing in this study. The elevation of the site vary between 1 and 8 m a.sl. (Gilbert et al., 2019).

5.1.2 Climatic Conditions

There are large inter annual variations, but it is evident that the average temperatures have increased. The mean annual air temperature at Svalbard for the period 1961–1990 was –6.7°C and increased to –4.6°C for the period 1981–2010 (Førland et al., 2011). These are temperatures from the Svalbard Airport series and show an increase in 2.1°C. Winter and spring temperatures have increased most, with 2.9°C and 3.9°C respectively (Nordli et al., 2014). The climate in Svalbard can be characterized by long, cold winters and short, cool summers. The winter season is dark and the polar night last for more than 2 months. In summer there is midnight sun. The increase in air temperatures also cause increase in air thawing index, increasing from approximately 400°C days to 575°C days from 1989 to 2018 (Gilbert et al., 2019).

Snow conditions are partially like the conditions at Janssonhaugen described by (Isaksen et al., 2000), thin due to strong redistribution by wind and low precipitation. Average precipitation is around 300–500 mm/year (Isaksen et al., 2000). Observations show that total annual precipitation has increased by roughly 14% the last century, with greatest increase in fall and winter (Førland et al., 2011).

Meteorological observations are not taken at the UNIS East site, but observational data from Adventdalen are available and adapted from UNIS (2018). The location of the Adventdalen

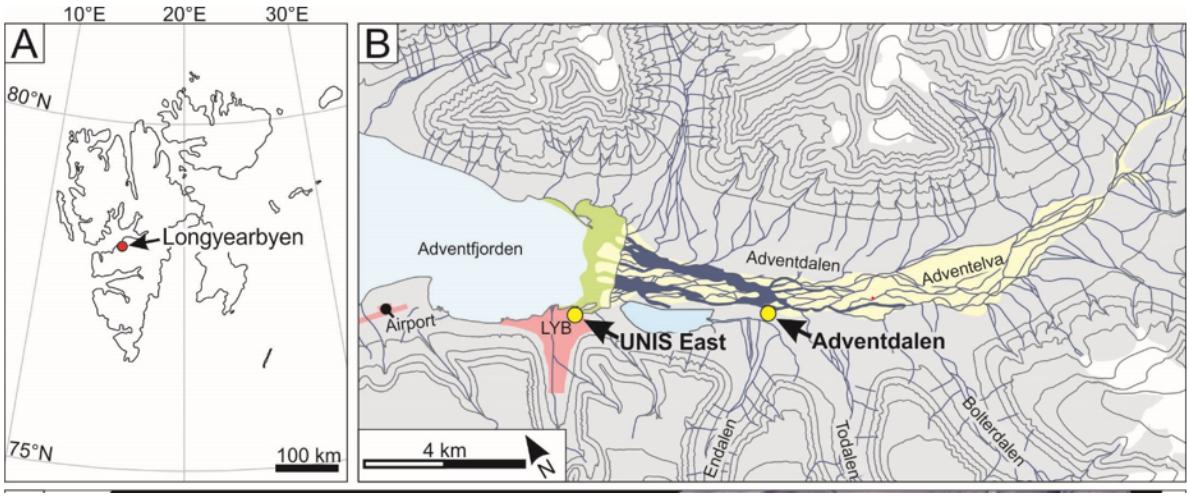

Figure 5.1: *a) Location of Longyearbyen in Svalbard and b) Location of the sampling site UNIS East and the Adventdalen site where meteorological observations are taken (adapted from (Gilbert et al., 2019)).*

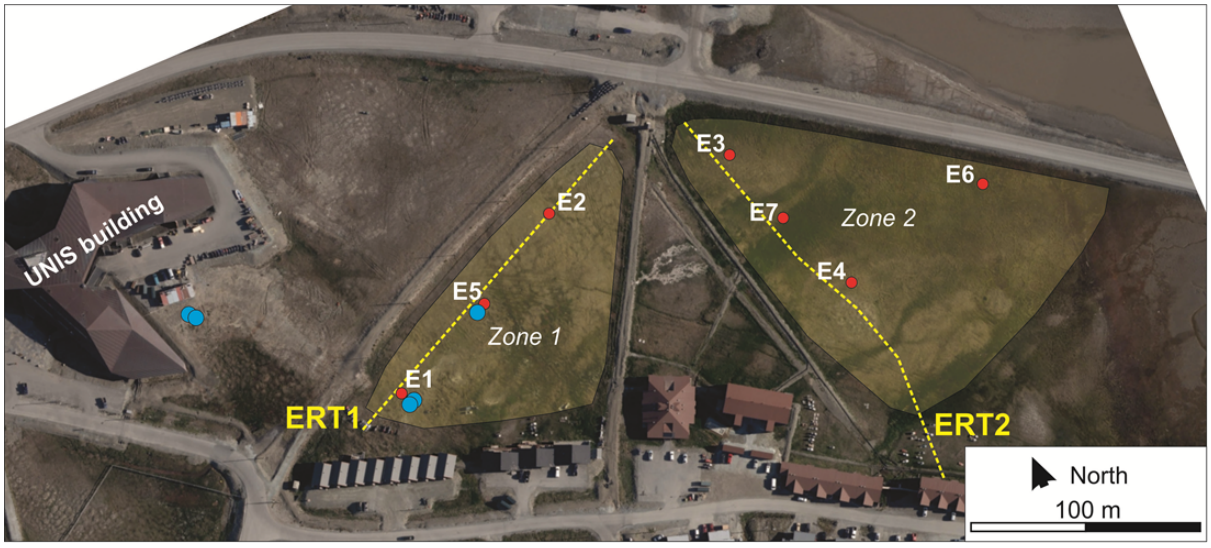

Figure 5.2: *Location of boreholes at the UNIS East site where samples have been extruded for experimental investigations (adapted from (Gilbert et al., 2019)).*

site is indicated in Figure 5.1 and is 4 km further in in Adventdalen and approximately at the same elevation as the UNIS East site. This is the observation station closest to the UNIS East site and the conditions are similar at the two sites. Therefore, the Adventdalen meteorological observations are used to describe the climatic conditions.

5.1.3 Geological Conditions

The UNIS East site is situated at 1 to 8 m above present sea level. As Figure 5.1 shows, the UNIS East site is located close to the Advent river. The soil at the site consists of former fjord bottom and the sediments are deposited as fjord-head deltas (Gilbert et al., 2019). After the deglaciation the sea level was approximately 62–70 m above the present level and the sites consist of marine sediments. Soil from the boreholes shown in Figure 5.2 have previously been tested, and based on these tests the soil has been categorized into three different layers (Gilbert et al., 2019). The top layer, down to approximately 2 m depth, consists of a coarser material of gravelly, silty sand. Below this layer the soil material is fine grained. The next layer is approximately 15 m thick and consists of silty clay. This layer is underlain by a coarser layer of diamicton, sandy, silty clay. Depth to bedrock ranges from 21 m to over 30 m (Gilbert et al., 2019).

5.1.4 Geotechnical Field Investigations

The samples were collected by SINTEF on the 17th of April in 2018. The borehole is 26.1 m deep. The first 0.5 m was pre-drilled. An auger was used down to 1.9 m depth and again at 21.5 m and 23.5 m to 26.1 m depth. From 1.9 m to 20.1 m depth a corer was used using a modified CRREL barrel (Figure 5.3. The samples were extruded from the CRREL barrel, placed in sealed plastic bags with cling film around and stored in a container with temperatures of –18°C. It is important to keep the samples frozen to keep moisture migration minimal. However, the temperature where the samples are stores is much lower than what it would be in the ground and this can have an effect on the test results, mainly because of changes in distribution and amount of water content.

5.1.5 Ground Temperatures

Thermistor strings are placed in plastic pipes installed in the boreholes. There are several sensors with varying spacing intervals on each thermistor string. The thermistors are closely spaced with 0.25 m the first 2 m, every meter down to 10 m depth and with 2 m spacing down to the bottom. The temperature is logged every 6^{th} hour. The accuracy of the thermistors is ±0.25°C. The thermistor strings were calibrated before they were placed in the ground. Figure 5.4 shows the temperature profile from thermistor readings from borehole E1 for 2017–2018. The irregularities in the temperature profile are likely due to the low temperature resolution of the thermistors. In addition, the thermistor string is placed in a pipe filled with air. Convection could occur inside the pipe and alter the temperature readings so they deviate from the temperatures of the soil at the same depth. This is the standard method used and is seen as adequate for engineering purposes. The monitoring of the ground temperatures makes it possible to study the ground thermal regime at the site and study response to climate variables and surface conditions (Gilbert et al., 2019).

Figure 5.3: *The drill rig with the CRREL barrel for drilling in frozen soil.*

Temperatures have been logged in the E5 borehole since September 2018. Temperatures in borehole E1 have been logged since August 2017 and provide a longer time series with data and will be used to describe the ground temperatures at the site. From the logged temperature data from borehole E1 from September 2017 to August 2018 it is observed that the mean annual ground surface temperature is –0.87°C, the active layer thickness is 95 cm, the depth of zero annual amplitude (ZAA) is 8 m where temperatures fluctuate less than 0.1°C. The temperature at ZAA is –3.1°C. The temperature at 30 m depth is –3.9°C. In addition Gilbert et al. (2019) has found that mean annual ground surface temperatures ranged from –1.6°C (E3) to –0.4°C (E4) and show a spatial variability for the site. Mean annual temperature at the permafrost surface ranged from –2.8°C (E3) to –2.2°C (E1) (Gilbert et al., 2019). The temperatures below ZAA are lower than the average temperatures at ground surface. This indicates that the permafrost has formed at a time where average air temperatures were much lover than they are today.

5.2 Index Testing

Laboratory experiments are performed to retrieve information about the soil in the study. The main focus has been on the thermal properties of the soil, but index testing has also been done to characterize the soil. Tests have been performed on samples from 2 m to 10 m. To represent the natural variability of soil deposition, structure and properties, the experimental testing has been performed on 8 samples down to 10 m depth and represent the soil above ZAA. Sample identification and respective depth are given in Appendix C. The samples retrieved from the CRREL barrel are 40 cm long and the diameter of the barrel is 50 mm. The depth given for each sample is the depth to the top of where the core was sampled. The samples have been stored in a container keeping –18°C after sampling. It was planned how much sample was needed for the different testing and the frozen samples were cut with a saw. Each sample was cut into pieces of approximately 12 – 2 – 5 – 4 – and 2 cm from the top. Some of the samples had fractures and the sequence was altered to fit the pieces. The upper two meters consist of coarse materials

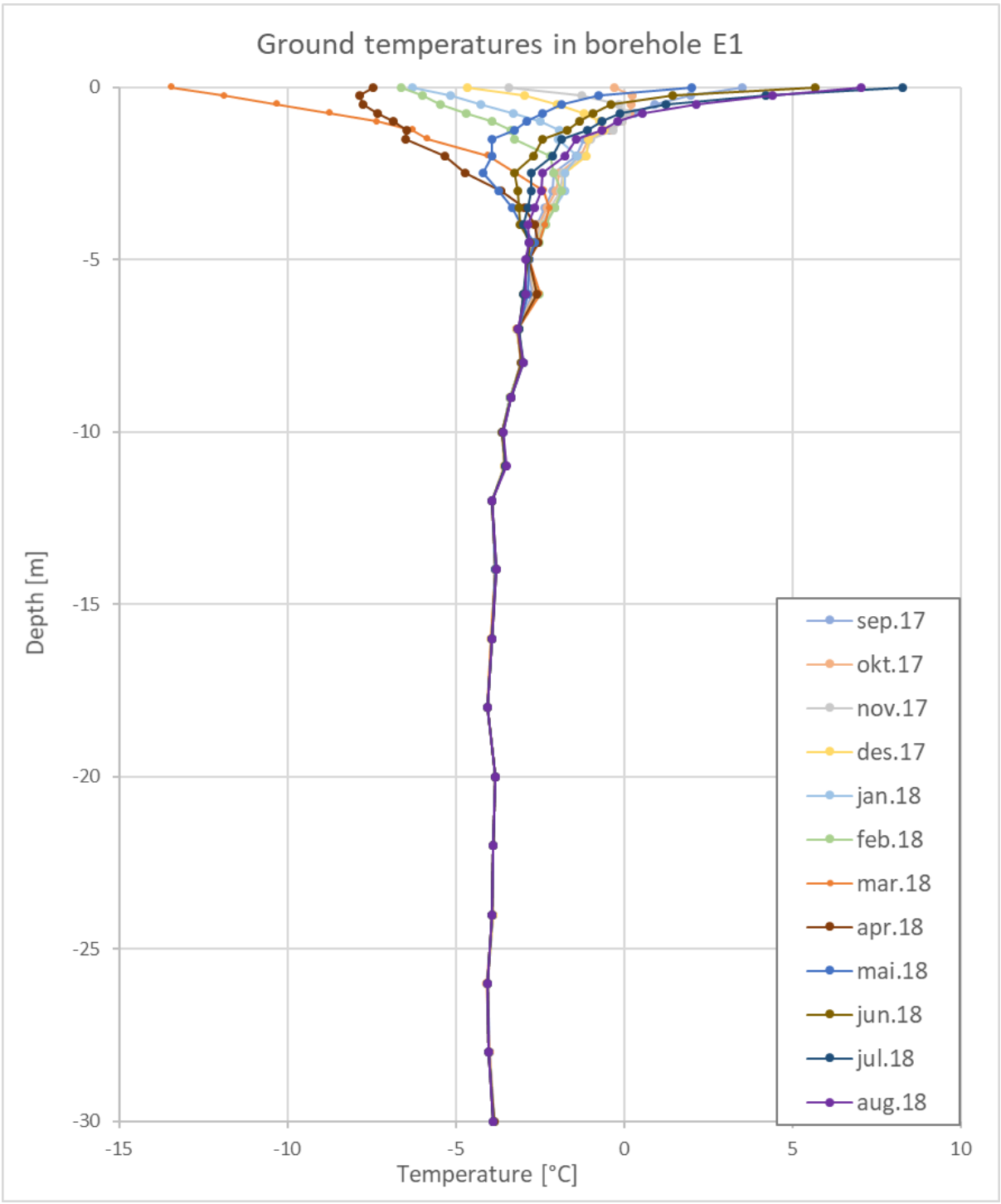

Figure 5.4: *The temperature profile based on average monthly values for borehole E1 at the UNIS East site.*

and some of the laboratory tests were different to perform on the sample from this layer. There were some small pieces of intact core. Most of the sample was not intact core, but loose sand and gravel. It was attempted to use the pieces of intact core from this sample. The sample fell more apart when thawed and this is likely to have affected the results from measurements on this sample.

The index tests performed were the estimation of water content, density, dry density, density of solid particles, grain size distribution, organic content and pore water salinity. The laboratory testing follows the standard "Geotechnical investigation and testing – Laboratory testing of soil" (ISO 17892). The handbook for laboratory investigation by (Vegdirektoratet, 2016) R210 has been used as a guideline for testing procedures. Some alterations have been necessary where to adapt the procedures to frozen samples. Some of the tests demand thawed samples. The samples were wrapped in cling film and placed in plastic bags in the fridge to thaw to avoid evaporation and water migration of the moisture content. The scale used has a precision of 0.01 g.

5.2.1 Water Content

The test was performed after NS–EN ISO 17892–1:2014 (Standard Norge, 2015). Samples of approximately 2 cm length were cut and immediately weighed. After the sample weight, m_1, was determined the sample was placed in a clean, dry container with known weight. The samples were placed in a drying oven maintained at 110°C and dried to a constant mass for at least 16 hours. After cooling, the dry samples were weighed to find the dry weight, m_2. The water content, w can then be calculated by

$$w = \frac{m_1 - m_2}{m_2} = \frac{m_w}{m_d} \tag{5.1}$$

The water content was also determined for the samples used in the bulk density test and an average value from the two tests calculated. Small drops of ice were seen on the cling film prior to cutting and testing of the soil samples. This can indicate that there has been some moisture evaporation in the sample prior to testing. This can result in a lower water content from testing than the actual natural water content insitu.

5.2.2 Bulk Density and Dry Density

The test was performed after NS–EN ISO 17892–2:2014 (Standard Norge, 2015). The total or bulk density of the soil is found by weighing the sample with a known volume. The linear measurement method is suitable to use due to the regular shape of the cylindrical core samples. A ca. 4 cm long specimen is cut with the saw from the frozen, cylindrical soil sample. The saw gives plane edges normal to the specimen axis. The sample is kept frozen to prevent deformation when determining the volume. The length, L, and the top, middle and bottom diameters of the sample are measured using a digital calliper with 0.01 mm precision. The average diameter, d, is calculated. The volume, V, is calculated by

$$V = \pi \frac{d^2}{4} L \quad [mm^3] \tag{5.2}$$

The volume should be at least 50 cm^3. The specimen is weighed to the nearest 0.01 g. The bulk density, ρ is then calculated by

$$\rho = \frac{m}{V} \quad [\frac{g}{cm^3}] \tag{5.3}$$

To determine the dry density of the specimen the procedure described in Subsection 5.2.1 was used to determine the water content. The dry density, ρ_d, is calculated by

$$\rho_d = \frac{\rho}{1 + (w/100)} \quad [\frac{g}{cm^3}] \tag{5.4}$$

The dry density can also be calculated by Equation 5.3 with substituting the mass with the dry mass of the sample.

5.2.3 Density of Solid Particles

The test was performed after NS–EN ISO 17892–3:2015 (Standard Norge, 2015). The purpose of the test is to determine the dry mass of the particles and the volume of the particles to determine the density of the solid particles. This is done by finding the difference in the volume required to fill a pycnometer with and without sample material present. Method B for moist specimens was used and the samples were thawed prior to testing. The calibrated pycnometers were weighed and the volume noted. The specimen should be approximately 15% of the pycnometer volume. Thin threads of the material were rolled out and threaded into the pycnometer. The mass of the pycnometer and sample is determined. The pycnometer was filled with distilled water and placed in a vacuum desiccator to evacuate all air from the sample and left until no more air bubbles appear. If all the air is not extruded the density of the particles will be underestimated because the air filling enclosed voids will give a larger volume than the solids. When the air was removed, the pycnometer was filled with distilled water and the glass stopper with capillary rising tube placed in the neck of the pycnometer. The pycnometer was placed in a water bath of approximately 20°C for an hour and the capillary rising tube was controlled before the pycnometer was taken out and dried on the outside. The pycnometer with content and glass stopper was weighed. After weighing the material was poured into a beaker and dried in the drying oven at 110°C to constant weight and weighed to determine the mass off the solids. The density of the solid particles, ρ_s is determiend by

$$\rho_s = \frac{m_4}{(m_1 - m_0) - (m_3 - m_2)} \times \rho_w \tag{5.5}$$

where m_4 is the dry mass of the test specimen, m_3 is the mass of the pycnometer filled with water and specimen, m_2 is the mass of the pycnometer and the dry specimen, m_1 is the mass of the pycnometer filled with water, m_0 is the mass of the pycnometer and ρ_w is the density of water which is 0.9982 at 20°C (Vegdirektoratet, 2016).

5.2.4 Grain Size Distribution

The test was performed after NS–EN ISO 17892–3:2016 (Standard Norge, 2015). The procedure 215 described in (Vegdirektoratet, 2016) was followed. The sieves used are from the American Standard Test Sieve Series (ASTM). Some of the sieve openings for the ASTM sieves differ slightly from the descrption in the ISO standard, and this has been accounted for in the

Table 5.1: *The numbers of the sieves in the ASTM series and the sieve openings.*

Sieve No.	**Sieve opening** [mm]
3/4 in.	19.0
3/8 in.	9.51
4	4.76
8	2.38
16	1.19
30	0.595
50	0.297
100	0.149
200	0.074

test. Table 5.1 shows the corresponding sieve number and sieve opening sizes. The particle size distribution test results give the basis for classification of the soil and are important for determining geotechnical properties. The material that was tested contain >50% fines and the sieving and sedimentation procedure was used.

Samples used for the density measurements with known weight and water content were used in the test. Firstly, the specimen was wet sieved on sieve No. 30 and the beakers containing the material with particles >600 μm and <600 μm was dried in a drying oven of 110°C. Secondly, the material >600 μm was then sieved on sieves No. ¾ , ⅜ , 4, 8, 16 and 30 and the retained mass on each sieve was weighed. The dried material with particle size <600μm was weighed, pulverised and sieved through sieve No. 30 again. Representative samples of approximately 100 g were taken out for the hydrometer test. The samples were mixed with 20 ml dispersant agent and 100 ml water and were left for drenching for at least 16 hours in a beaker covered with cling film. Then, the mixture was dispersed in a mixer for 1 minute and then poured into sedimentation cylinders. The cylinders were refilled to the 1000 ml mark with water keeping room temperature. The cylinders were covered with rubber and shaken for 1 minute and then turned upside down 10 times. The timer was started at the instant when the agitation was complete. A hydrometer was put down in the mixture and read at times 1 – 1 3/4 – 4 – 15 – 30 – 60 minutes and 4 and 24 hours to the nearest 0.5 g at the upper rim of the meniscus. After the hydrometer measurements were taken the fines were washed through the 75 μm sieve. The material was then put in the drying oven and then sieved on sieves No. 50, 100 and 200. The retained material on each sieve was weighed. The results of the weighing were used to calculate the grain size distribution.

5.2.5 Organic Content

The test method follows NS–EN 1744–1:2009+A1:2012 (Standard Norge, 2013) and the procedure 218 described in handbook R210 is followed (Vegdirektoratet, 2016). The dry samples that were used to determine the water content were used in this test. First the samples were crushed by a hammer and the crushed material was sieved through a 600 μm sieve. 20 g of the sieved material was put in porcelain cups and dried for another two hours at 110°C to ensure dry samples. The samples were taken out and left over night to cool to room temperature. 10.00 g of the prepared material was weighed and put in numbered crucibles. The crucibles were placed in the electric furnace keeping 480°C for 24 hours. After the crucibles had cooled

in an desiccator the samples were weighed and the organic content found by the loss of mass.

5.2.6 Salinity

The test method follows the standard ISO 11265:1994 (Standard Norge, 1994). The salinity of the soil is determined by measuring the concentration of soluble salts in the soil. For the testing a SG7 – SevenGo pro conductivity meter by Mettler Toledo was used. Samples of ca. 2 cm were cut from the core samples. The samples were thawed as it would be easier to dissolve them in water in unfrozen state. The thawed samples were weighed and approximately 50 g were used and 500 ml of distilled water was weighed and added. Next, the sample was mixed and soaked in the solution for an hour to let the salt dissolve completely. The conductivity meter was first calibrated with a standard conductivity solution of 1413 μS/cm. Then the measuring probe was rinsed with distilled water before taking the measurement in the soil mixture. The measured salinity for the solution was noted. This procedure was performed three times in each soil mixture. The conductivity meter measures the conductivity of the solution and converts this to salinity readings in part per thousand (ppt), which is approximately convertible to g/l. After the salinity had been measured, the bowl with soil mixture was left in the drying oven for the weekend. The dry weight of the sample was found by weighing.

When the initial soil weight, m, and dry weight, m_s, is known the initial water content, w, and the weight of water, m_{w1}, in the sample can be found. With known water content, the weight of initial pore water is

$$m_{w1} = \frac{w \cdot m}{1 + w} \tag{5.6}$$

The salinity measurements of the soil mixture, S_1, are the salinity of the added water and the soil water, M_{w2}. To convert this into the salinity of the pore water, S_2, the following equation is used

$$S_2 = \frac{m_{salt}}{m_{w1}} = \frac{m_{w2} \cdot S_1}{m_{w1}} \quad [g/l] \tag{5.7}$$

5.3 Experiments on Frozen Soil

5.3.1 Freezing Point Depression

Temperature loggers were used to measure the freezing point depression in the centre of the samples. Samples were thawed and wrapped in cling film and aluminium foil prior to testing. The probe was carefully inserted into the middle of the core sample. The probe was connected to a Testo 164 temperature logger. Temperatures were measured and logged every 5 seconds. The sample and the temperature logger were placed in a cold lab maintained at –18°C while logging. The measurements were continued until the core temperatures had reached –18°C. The data from the temperature logger was transferred to a computer and treated with the Testo software. The temperature loggings plotted as function of time give curves showing rate of temperature change. The plotted curves resemble the curve shown in Figure 4.1. The flat parts of the plotted curves are used to identify the freezing point, T_f.

(a) (b)

Figure 5.5: *Equipment used in laboratory testing. (a) The conductive meter used to measure the salinity in the soil and a bowl with soil sample mixed with water. (b) WP4C Dew Point PotentiaMeter.*

5.3.2 Water Potential

The purpose of finding the water potential at different saturation levels is to use it in calculations to determine the amount of unfrozen water content at negative temperatures. To determine the water potential the WP4C Dew Point PotentiaMeter from Decagon Devices was used. The measured water potential is a combination of matric and osmotic potential and depends on water content in the sample and the temperature at which measurements are taken. There is no available standard for how this experiment should be performed. The WP4C Operator's manual (Decagon Devices, 2018) describe how the instrument should be set up and used to give accurate readings of water potential. The procedure described by Campbell, Smith, and Teare (2007b) was used to obtain water potential measurements suitable for the unfrozen water calculations.

Correct preparation of soil samples is critical to obtain good results with the WP4C. The samples were left in a tin cup to air dry and obtain moisture equilibrium with the air. A part of the sample was dried in the drying oven at 110°C. The sample was weighed before and after drying to find the air dried water content, w_{ad}. The rest of the sample was crushed and sieved on sieve No. 8 with 2.38 mm sieve openings. Sub samples of the air dried sample were prepared so the sub samples have a range of different water contents. To obtain this the sub samples were first weighed in aluminium tins. Then, the necessary amount of water, m_w, needed to obtain the desired final water content, w, was added. m_w is calculated by

$$m_w = m_{ad}\frac{w - w_{ad}}{1 + w_{ad}} \tag{5.8}$$

where m_{ad} is the weight of the air dry sample. Approximately 10 sub samples with water content ranging from air dry to fully saturated were prepared for the 8 samples. The water was added to the sample and thoroughly mixed with the soil. The tins were covered with cling film

and left to equilibrate for approximately 24 hours. After equilibration sub samples were placed in the sampling cups that fit in the WP4C device. Then, the water potentials of the prepared samples were measured with the WP4C. How the WP4C takes water potential measurement is explained in Subsection 4.2.3. The sample cup must be colder than the temperature inside the device chamber to prevent condensation inside the block chamber (Decagon Devices, 2018). The reading can be started when the temperature difference between the sample and chamber temperature is less than 1°C. The WP4C device was connected to a computer so the values were stored automatically. The measurements were performed in a laboratory with air temperature of about 22°C and the chamber temperature in the WP4C was approximately 24.5°C when measurements were taken. Measurements were only taken at one temperature as previous studies have shown that the results of measurements at different temperatures does not give significant differences in the results (Nybo, 2017). For sample 1 – 6 the precise method on the WP4C was used and the fast mode was used for Sample 8. Sample 7 was not tested with the dew point method. The precise mode is very time consuming and takes approximately 20 minutes per sub sample. The fast estimation mode takes approximately 5 minutes, but there seem to be a significant difference in the water potential measurements from the two methods. It is recommended to use the precise mode. After WP4C readings were done the samples were weighed, oven dried for 24 hours and then reweighed to determine the water content. Samples prepared in steel sample cups could be dried directly in the cup. Where plastic sample cups were used they had to be put in crucibles before drying. The water content was noted with the according water potential.

5.3.3 Thermal Properties

Thermal properties of the soil were measured with the KD2 Pro device, by Decagon Devices Inc., with two different sensors, the dual needle SH–1 and the single needle TR–1. The sensors measure volumetric heat capacity, thermal diffusivity, thermal conductivity and thermal resistivity. There is no ISO standard for the procedure of determining thermal conductivity of soils and rock, but the KD2 Pro complies fully with ASTM D5334–14 (Decagon Devices, 2016). The Operator's manual (Decagon Devices, 2016) give insight in what sensor you should use for different materials, how needles should be inserted and how best measurements are achieved. The theory for how the device and sensors work is described in Subsection 3.2.1. Previous experimental studies by Putkonen (2003), Sun et al. (2016) and Bratlie (2018) have been reviewed to obtain a good test procedure to obtain the most accurate measurements possible.

The K2D Pro manual does not inform how sensors should be inserted in frozen soil material. Bratlie (2018) has found that pre-drilling holes for the sensors does not give the desired accuracy due to challenges with the contact resistance. Furthermore, she explains that pre-drilled holes with thermal grease also fail to give the desired accuracy. If the samples were thawed the sensor could be inserted in the material without drill holes. Decagon Devices (2016) suggest to minimize contact resistance in granular materials by drilling holes and applying thermal grease. They also suggest to increase read times to reduce the effect of contact resistance. The thaw-insert method was proven by Bratlie (2018) to be the best practice and seemed to give precise results. In this study experimental tests were performed to see which sensor and what procedures give the desired accuracy in measurements. The thaw-insert method was chosen to be used for the measurement of thermal properties of the soil samples.

Before starting the testing, the sensor performance was verified by testing the sensors with standard materials as explained by Decagon Devices (2016). The TR–1 needle was tested

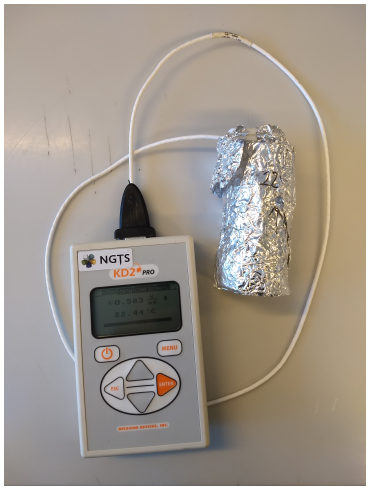

Figure 5.6: *The KD2 Pro device and TR–1 sensor inserted in a soil sample wrapped in cling film and aluminium foil.*

with a block of Verification Standard and the SH–1 needle with a two-hole Delrin block. The sensors were inserted into the verification material, left to equilibrate for 15 minutes before the measurements were taken. The measured value was compared to the recorded value on the Certificate of Quality Assurance. If the measured value is within 10% of the value on the certificate the sensor performance is verified. All needles were verified before measurements on soil samples were performed.

The frozen core samples were cut to about 12 cm to be long enough for the TR–1 sensor. The samples for SH–1 were cut to be 3–5 cm. The samples were wrapped in cling film and aluminium foil to prevent moisture evaporation and to prevent samples from deforming and falling apart when thawed. The samples were thawed and the needles were inserted in the centre of the core. For the SH–1 samples, the holes were stuck out with drill bits to get a good placement and the right distance between the two needles. It is important to not bend the needles as a 1% change in the distance between the needles can result in 2% measurement error (Decagon Devices, 2016). Measurements were taken at several different temperatures to determine the temperature dependency of the thermal properties. The temperatures around the freezing point are the most essential in this study. After inserting the sensor it was left in the sample for at least 20 minutes to obtain temperature equilibrium with the sample before measurements were taken. The sensor is connected to the KD2 Pro control device which takes the measurements. It is desirable to take three measurements of a sample at a given temperature. This is to check that the measurements give the same value. A 15 minute equilibration time is allowed between each measurement to reduce the heat disturbance from the measurements. After 3 readings were done at a temperature, the temperature was adjusted and the sample left to cool or heat to the adjusted temperature for approximately 12 hours. The temperatures were adjusted by placing the samples in room temperature (22°C), the fridge (4°C –7°C) and a cold lab where temperatures were adjusted from –1°C to –20°C. The samples in the cold lab reach a temperature approximately 1°C higher than the set temperature for the room after 12 hours equilibration time. After measurements were taken the KD2 Pro was connect to a computer and the KD2 Pro Utility software was used to download the data.

Chapter 6

Experimental Test Results

The results from the index testing, measurements of thermal properties and water potential are presented in this chapter. Some error sources and how these have affected the measurements are discussed. More detailed test results are summarised and presented in tables in Appendix C.

6.1 Index Testing

6.1.1 Soil Classification

Soil can be classified according to the size of the grains. Grain size influences the behaviour and mechanical properties of the soil. The grading system presented in NS-EN ISO 14688-1:2018 (Standard Norge, 2018) was used to describe the particle size distribution. The presented results are from the sieving and hydrometer tests.

One sample from the top layer was classified as gravelly sand. The top layer is of coarser material than the underlying soil and is approximately 2 m thick. The underlying soil has a high content of fines with variable sand content. The content of sand, silt and clay vary with depth, and five samples were classified as sandy, clayey silt. At depth 3.2 m and 6.0 m the clay content was $> 15\%$ and the soil was denoted as silty clay. Table 6.1 shows the percentage of each particle size fraction and the classification of the different depth samples. The experimental

Table 6.1: *Distribution of particle size fractions for the different samples based on sieving and hydrometer analysis.*

Sample ID	**Depth [m]**	**Clay [%]**	**Silt [%]**	**Sand [%]**	**Gravel [%]**	**Classification**
1	1.9	–	6	58	36	Gravelly sand
2	2.7	14	47	39	–	Sandy, clayey silt
3	3.2	22	60	18	–	Silty clay
4	4.4	10	57	33	–	Sandy, clayey silt
5	5.2	14	54	32	–	Sandy, clayey silt
6	6.0	25	61	14	–	Silty clay
7	6.8	13	55	32	–	Sandy, clayey silt
8	9.5	10	54	36	–	Sandy, clayey silt

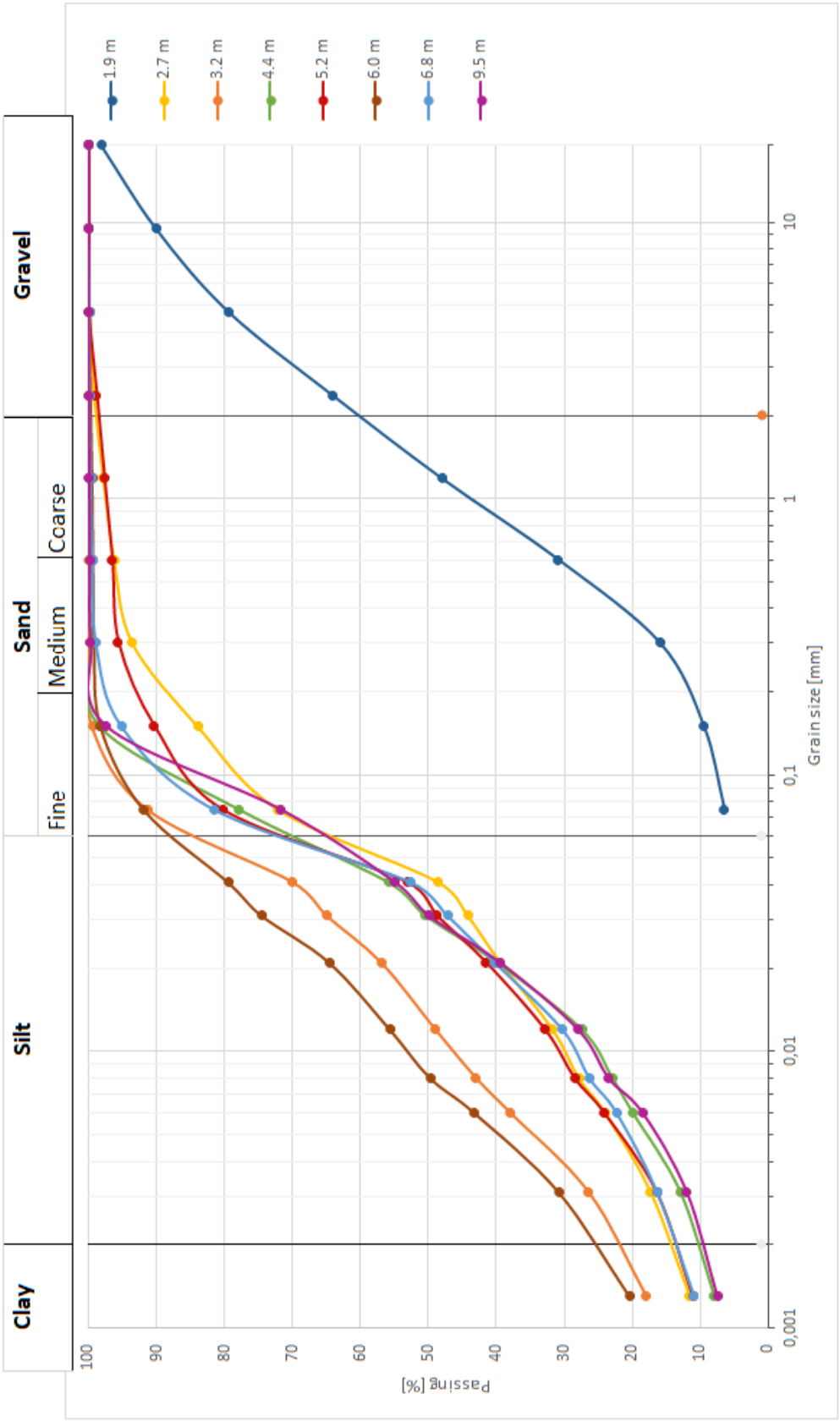

Figure 6.1: *The grain size distribution of the soil samples from borehole E5 that were investigated in the experimental analysis.*

testing performed on samples from borehole E5 down to 10 m depth are in the layer described as silty clay by Gilbert et al. (2019). Testing showed that some samples from this layer had clay content lower than 15%. When a soil has a clay fraction >15% it is defined as a clay. The clay fractions were very close to 15% in the samples, but fell into the silt category. The established grain size distribution curves are shown in Figure 6.1.

6.1.2 Water Content

The natural water contents for the tested samples range from 24% to 30% for the fine grained samples. The coarse sample at 1.9 m depth had a lower water content, around 15% to 18%. Because of lack of intact samples it was difficult to estimate the water content precisely for sample 1. Samples were studied in order to observe if there were ice lenses. Ice lenses could give very high water contents, but were not observed in the core samples from borehole E5.

6.1.3 Bulk and Dry Density and Density of Solid Particles

The estimate of the volume has errors due to geometrical irregularities on the core surfaces and this may influence the estimation of the densities. The volume of water expand up to 9% when it freezes and this can affect the volume and densities compared to unfrozen samples. Sample 1 was more irregular than the other samples and there was therefore a larger uncertainty in the measured sample volume. This will impact the bulk and dry density values as well. The calculated densities are tabulated in Table C.1 in Appendix C. The bulk density for sample 1 was 1.77 g/cm^3 and for sample 2–8 it ranged from 1.85 g/cm^3 to 1.98 g/cm^3. The low bulk density for sample 1 is likely due to the volume measurement. Sample 3 and 6 were classified as silty clay and both had a unit weight of 18.5 kN/m^3. For the sandy, clayey silt samples the unit weights were estimated to range from 18.1 kN/m^3 to 18.9 kN/m^3. Sample 8 was an exception with a unit weight of 19.4 kN/m^3.

The dry density for sample 1 was 1.39 g/cm^3. For sample 2 to 7 the dry density ranged from 1.45 g/cm^3 to 1.54 g/cm^3 while it was 1.58 g/cm^3 for sample 8.

The soil grain densities obtained from the pycnometer test ranged from 2.63 g/cm^3 to 2.66 g/cm^3. The density estimated for sample 2 was 2.59 g/cm^3 and was discarded. This sample was not left long enough in the vacuum desiccator so there was still air in the sample, which is the most likely reason for the low calculated grain density. The value for the grain density is expected to be around 2.65 g/cm^3 and this value was in the further used also for sample 2. The pycnometer test was not performed on sample 1.

6.1.4 Porosity and Saturation

The porosity and saturation were calculated from Equation 2.3 and 2.4 respectively. The porosity and saturation calculations are based on the unit weight, dry unit weight and the water content estimated for the samples. The uncertainties in the estimation of these parameters will affect the results for porosity and saturation. From calculations the samples have porosities in the range of 40% to 45% and a saturation of 80% to 99%. Saturation for sample 1 was 61%. A soil under the ground water table will be fully saturated. It is likely that the soil should have a saturation of 100% and that the deviation is caused by inaccuracy in the measurements of properties related to the saturation. The unit weight for sample 2 was the lowest of the fine

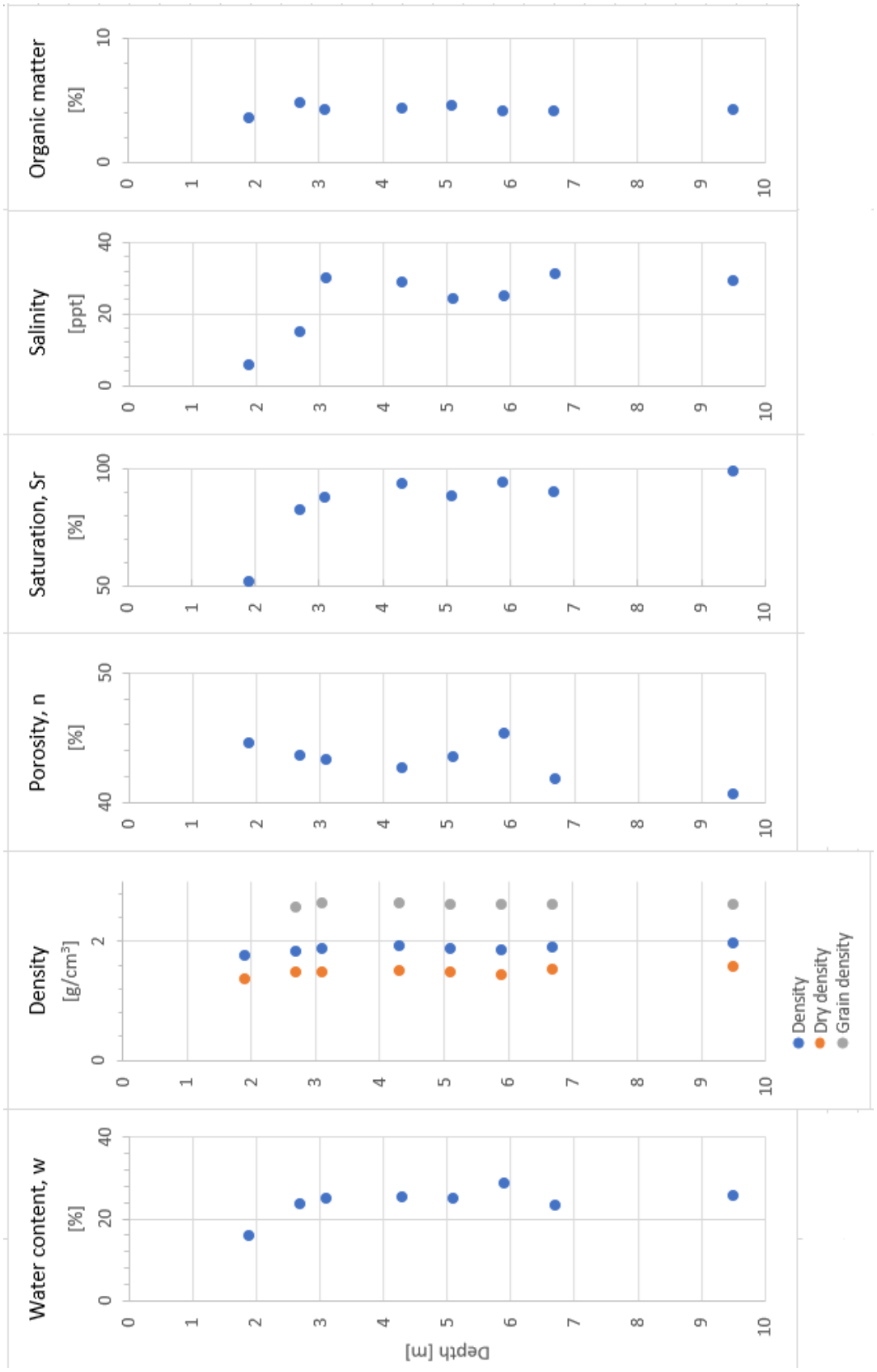

Figure 6.2: *Index parameters for the soil samples in borehole E5.*

grained samples (18.1 kN/m^3) and had the lowest saturation value of 80%. If the unit weight for sample 2 is set to be the same as for sample 8 (19.4 kN/m^3), the saturation would increase to 94%.

6.1.5 Organic Content

The organic content found by the ignition method was 3.6% for sample 1 and in the range 4.2% to 4.8% for the rest of the samples. Moss and shell fractions were observed in some of the samples under sieving. Organic material is not as good a conductor as soil and the organic content can have some impact on the thermal properties.

6.1.6 Salinity

Solutes in the pore water affect the freezing point and the unfrozen water content. The salinity measurements gave lower values for the upper part of the soil. This is not unexpected as the salt may have been washed out in the top. Sample 1 had a salinity of 6 ppt and sample 2 a salinity of 15 ppt. In the samples from 3 m to 10 m depth the salinity varied slightly from 25 ppt to 31 ppt. Sea water has a salinity of approximately 35 ppt. The permafrost is marine clay, deposited in the sea. The solutes are likely residual from the time of deposition and downwards growth of permafrost causing pore-water expulsion can have caused redistribution of the solutes (Gilbert et al., 2019). The redistribution of salt can result in salinity higher than that of sea water.

6.2 Experiments on Frozen Soil

6.2.1 Freezing Point Depression

Figure 6.3 shows the cooling curves for the soil samples. The logged temperatures from the soil cores plotted against time are used to study the rate of temperature change which is the inclination of the curve. The temperature decreased rapidly until the freezing point (FP) was reached. The flat parts of the curves indicate the freezing points of the soil samples. The freezing point depression is the difference between freezing of bulk water and the FP for the soil. After a time, part of the water had frozen at the FP and the temperatures decreased, but at a lower rate than before the FP was reached. The cooling curve for sample 1 did not indicate a FP temperature or temperature plateau. This is likely due to contact issues with the sample and measurement probe. The coarse sample fell apart when thawed and the water was redistributed. There was not enough water left in the sample for a FP to appear. Furthermore, the FP decreases with depth. The FP for sample 2 was –1.1°C and –2.1°C for sample 7. The other freeze points were between these two temperatures as summarised in Table 6.2.

6.2.2 Thermal Properties

The results from the measurements with the KD2 Pro device are directly read from the Excel files imported to the computer. The measurement results for different temperatures vary as expected, but variations in measurements taken at the same sample and temperature were also observed. It is desirable to determine which of the sensors and what procedure provide the most

Table 6.2: *The table shows results of salinity and FP measurements for the tested samples.*

Sample ID	**Depth [m]**	**Salinity [ppt]**	**Freezing point [°C]**
1	1.9	6.2	–
2	2.7	15.3	–1.1
3	3.2	30.3	–1.5
4	4.4	29.0	–1.6
5	5.2	24.5	–1.8
6	6.0	25.2	–
7	6.8	31.4	–2.1
8	9.5	29.7	–2.0

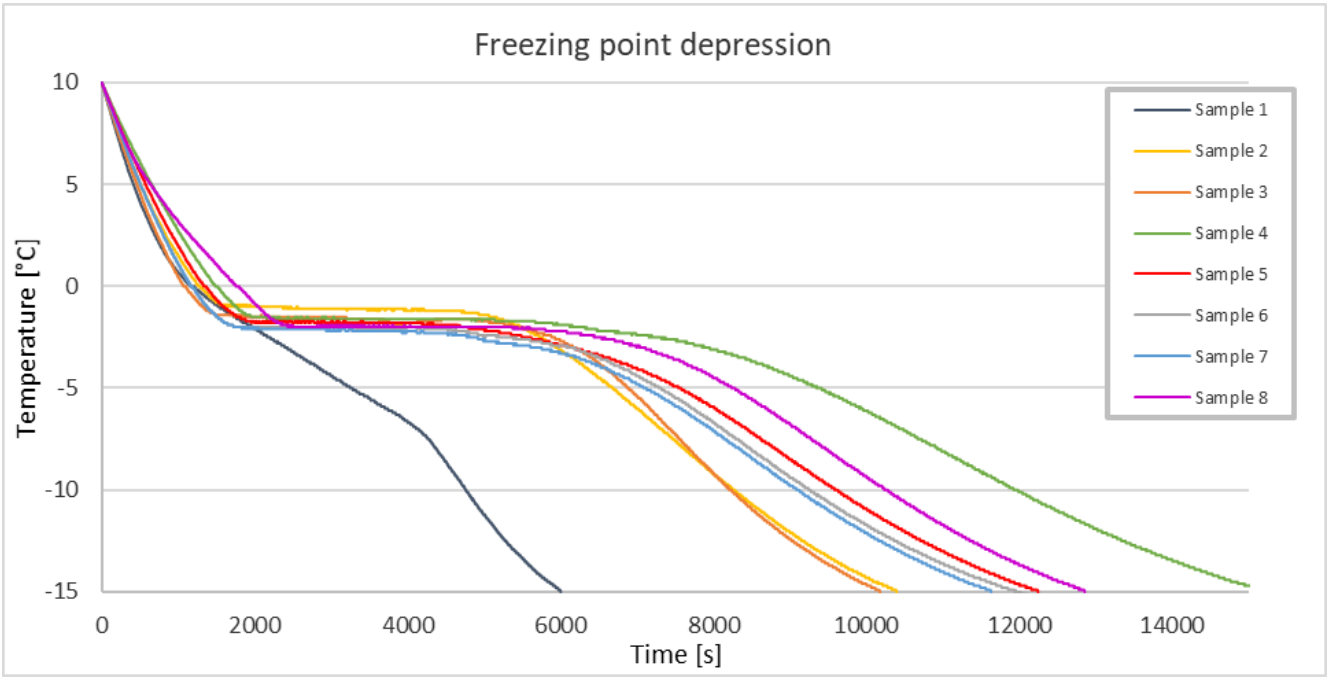

Figure 6.3: *The curve shows rate of cooling for the tested soil samples and indicate the freezing point depression for the samples.*

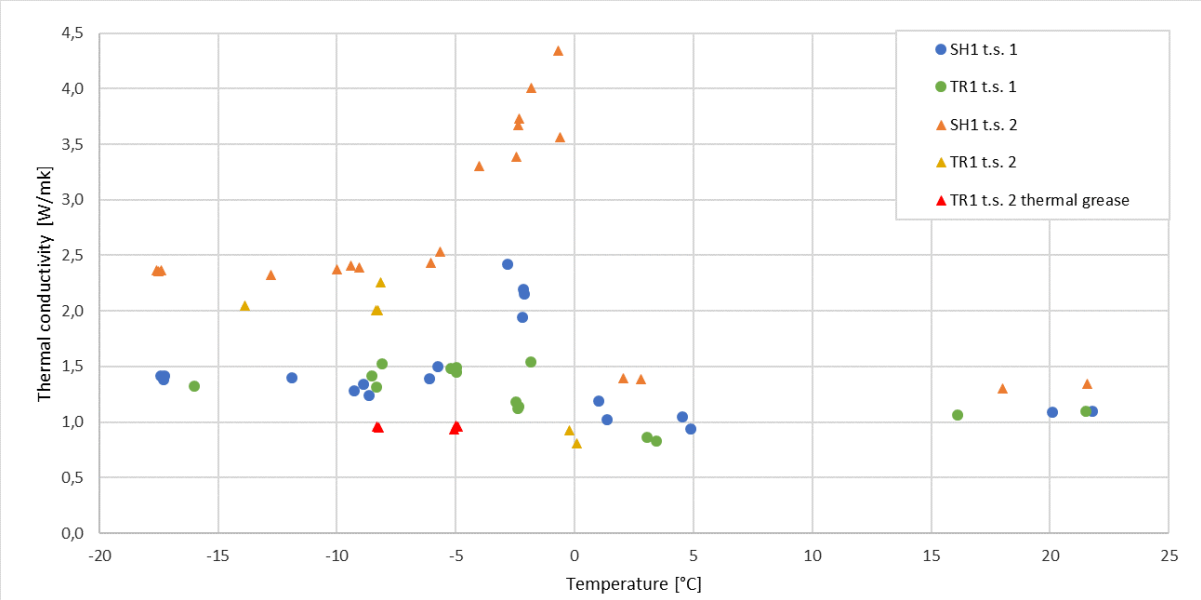

Figure 6.4: *Test results of sensors TR–1 and SH–1 at different temperatures. The tests were performed on separate samples, not the ones used for index testing. T.s. 1 and t.s. 2 are the name of the two different test samples that were used for testing.*

accurate measurements for the thermal conductivity. Measurements with high error factor or those that otherwise seemed to deviate from the other measured values have been discarded. Average values for unfrozen and frozen properties are determined for each sample.

The exact values for the thermal properties are not known and it is therefore difficult to evaluate the test methods. The values from different methods have therefore been compared to evaluate the test methods. To keep a constant temperature while measuring was very important for accurate measurements. If the sample was taken out from the cold lab into room temperature the measured value clearly gave a much higher value than at constant cooled temperature. Applying thermal grease gave measurements with low values for the thermal conductivity compared to readings on specimens without grease (Figure 6.4). High power mode is the standard mode for both the SH–1 and TR–1 sensors. Low power mode was also tested, but seemed to give too low measurement values. The measurement time was also changed, but it was not possible to observe any significant change. In sample 1 the needle did not have good contact with the material since it fell apart because of the coarser structure of the sample. Also, the state of the sample does not represent insitu state when thawed. The measurements for sample 1 should thus be interpreted with care. Test measurements from the SH–1 on frozen samples around –2°C to –5°C gave very high values for thermal conductivity as Figure 6.4 shows. Measurements from 0°C and up and below –5°C seem to give reasonable results. The results from TR–1 seem to be more accurate around –2°C, but the variations between measurements are larger around the FP with the TR–1 as well. The TR–1 gave slightly lower value for thermal conductivity, but the measurements from SH–1 and TR–1 coincided quite well.

The volumetric heat capacity was only measured by the SH–1 sensor. Figure 6.5 shows curves for how the measurements of volumetric heat capacity changed with temperature. The points plotted represent the determined average value for measurements at approximately the indicated temperature. It was expected that the volumetric heat capacity would decrease when the pore water started to freeze since ice has a lower heat capacity than water. The measurement

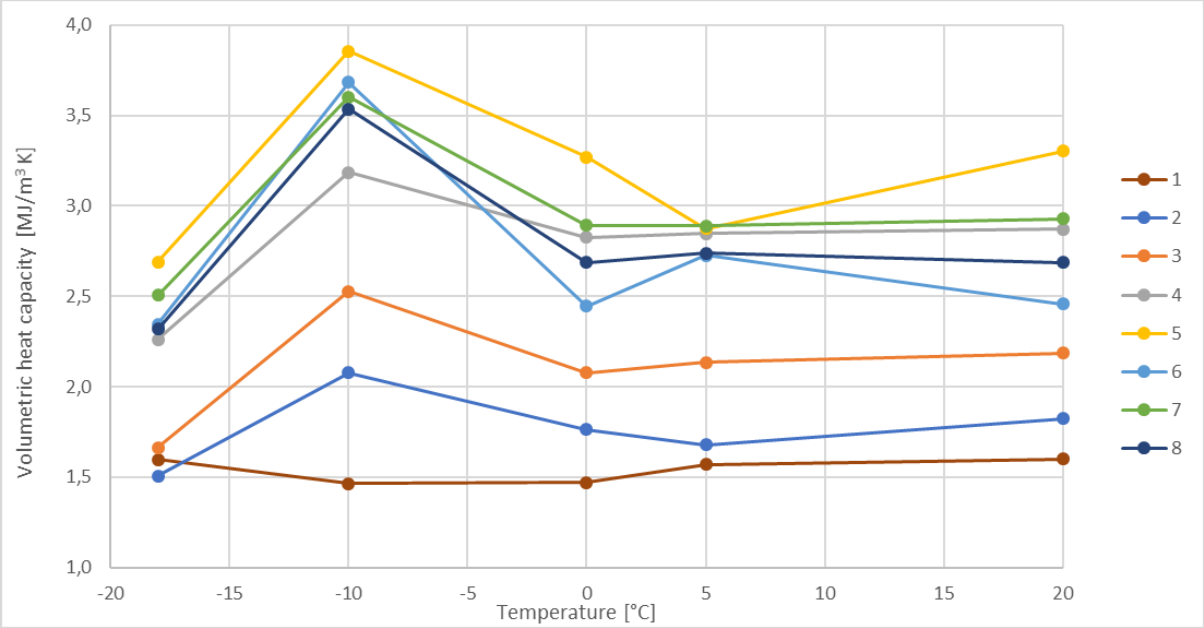

Figure 6.5: *Average measured values for volumetric heat capacity with sensor SH–1 with the KD2 Pro device.*

of volumetric heat capacity when the temperature dropped below the FP was not correctly determined by the KD2 Pro device. However, the measurements at –18°C were consistently lower than the 5°C and 0°C measurements. The sensors apply heat to the material and phase change of materials is not included in the algorithms to determine the thermal properties and this can have a significant effect on the results. Sample 4, 5, 6, 7, 8 have values close in magnitude for the volumetric heat capacity at 5°C and –18°C. The mean values are approximately 2.8 MJ/m^{3}K and 2.5 MJ/m^{3}K respectively. The values for sample 1 are clearly lower than for the other samples and this could be due to problems with contact between the sensors and the material since it was gravelly and fell apart when it was thawed. Values for sample 2 and 3 are lower than for the other samples and have an unfrozen heat capacity around 2 MJ/m^{3}K and a frozen value at –18°C of 1.5 MJ/m^{3}K.

Figure 6.7 shows the measurements of thermal conductivity at different temperatures for the different samples. The values are higher for the frozen conductivity and lower at positive temperatures. This is as expected since the thermal conductivity for ice is higher than for water. Sample 1 is an exception and is likely due to problems with contact between sensor and material. The magnitude of measurements on sample 4, 5, 7 and 8 are similar, except for the value at 5°C for sample 5. For these 4 samples the unfrozen thermal conductivity is ca. 1.6 W/mK. The frozen conductivity at –18°C is ca. 2.3 W/mK. The values for sample 2 and 3 are about 1.0 W/mK and 1.3 W/mK. The average calculation from thermal conductivity measurements are compared in Figure 6.6. In general the values measured by the TR–1 sensor are slightly higher than for the SH–1. In addition, the measurements by the TR–1 vary more for the measurement taken at the same temperature. This can be due to the long measurement time and larger influence of the moisture migration.

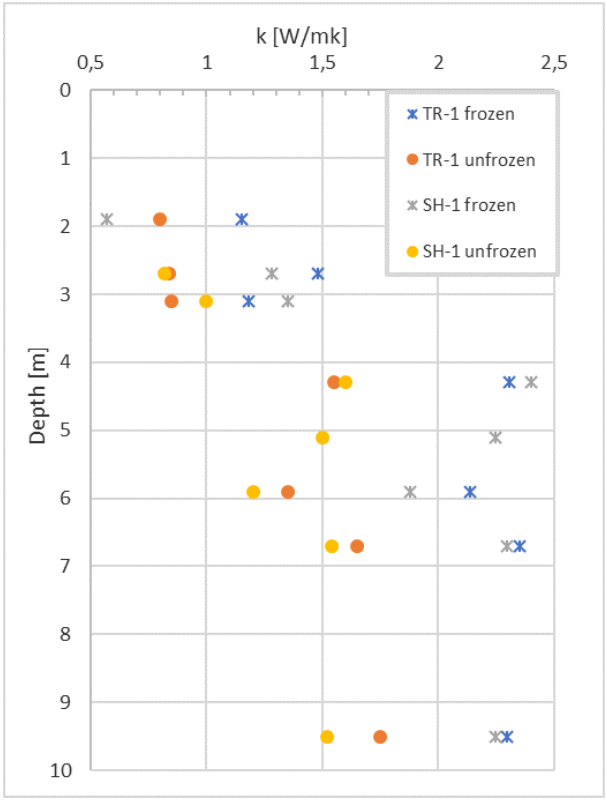

Figure 6.6: *Comparison of measured thermal conductivity by the SH–1 and TR–1 sensors.*

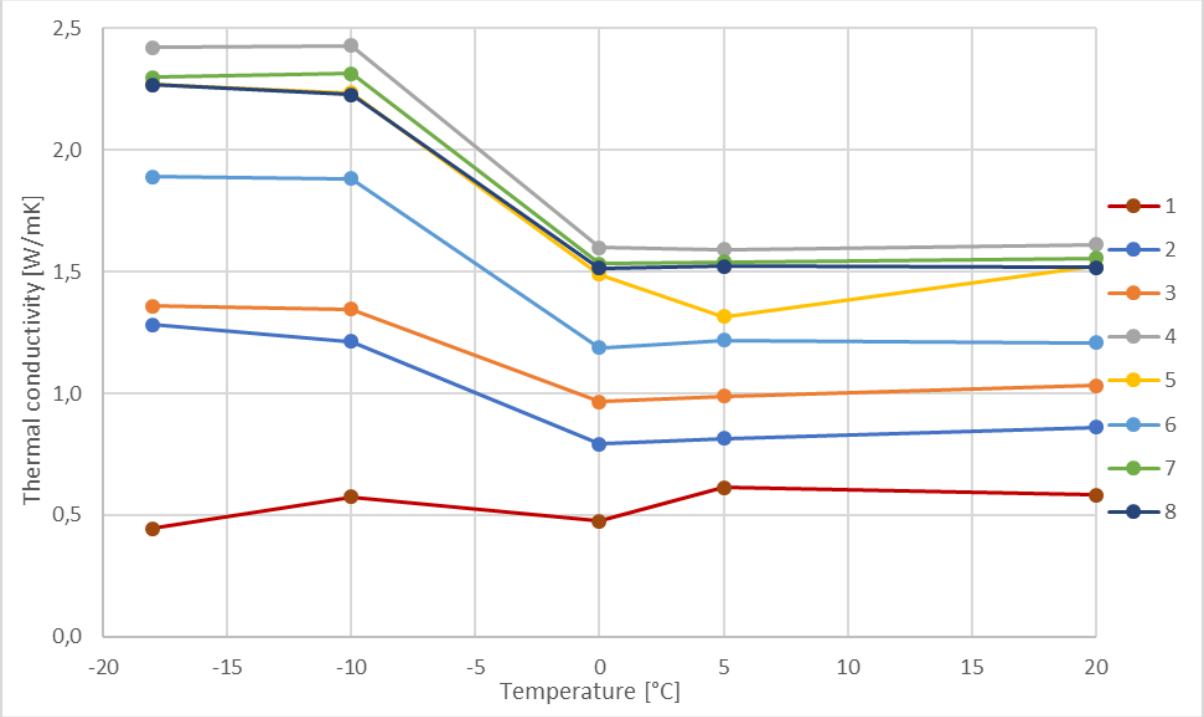

Figure 6.7: *Measured values for thermal conductivity with sensor SH–1 with the KD2 Pro device.*

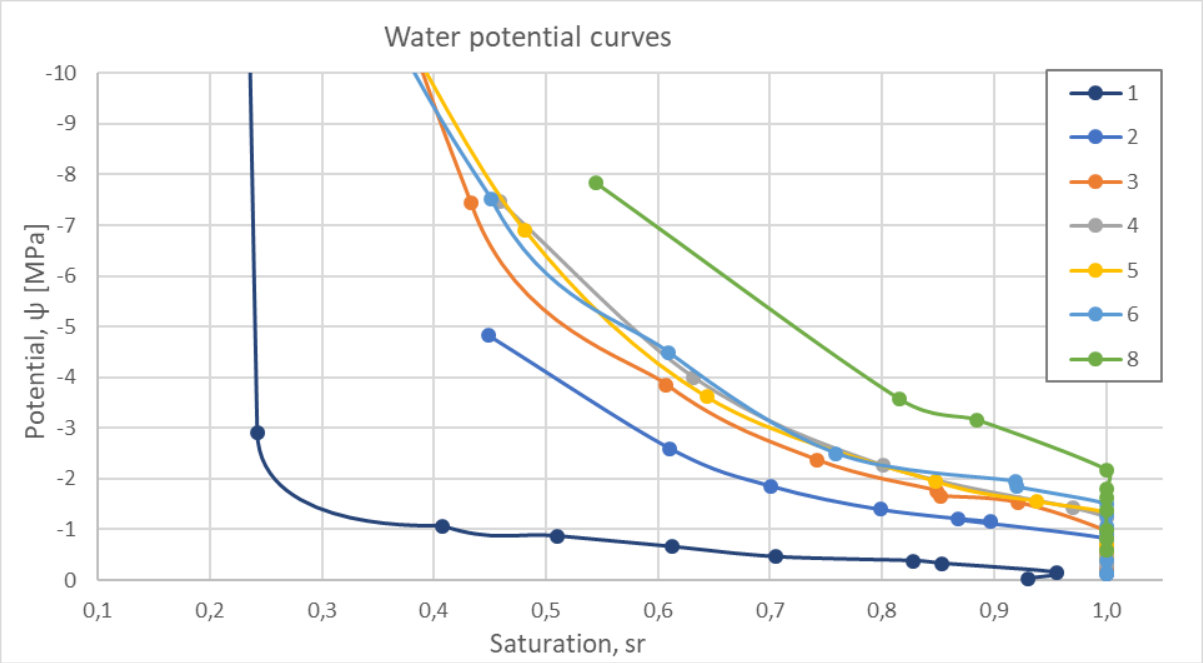

Figure 6.8: *Curve for the water potential measured by the dew point method against soil saturation. The soil saturation is estimated from water content, unit weight and grain density determined for the samples.*

6.2.3 Water Potential

The results from the WP4C Dew Point PotentiaMeter are shown in Figure 6.8 with potential plotted against saturation. The air dry water content for the soil samples was around 1.5%. The potentials measured for air dry samples were in the range of –300 MPa to –350 MPa. The potential decreases with the increase in water content and for water contents approximately at full saturation the water potential obtained is about –1.5 MPa and decreases when the water content is increased above full saturation. The saturation is calculated by Equation 2.4 by using the estimated water content for each sub sample. When the water content increases above 100% saturation the potential will continue to decrease, as the curves in Figure 6.8 shows. The vertical line at full saturation indicates the ice entry value discussed in Section 4.3. However, determination of the ice entry value from the potential curves is not very precise. First of all, the estimation of saturation depends on water content and density estimations which hold some uncertainty. Therefore, the point where full saturation occurs is uncertain. Secondly, the measurements of water potential close to full saturation have some variability. There will be an abrupt change from the inclined part of the curve to the vertical part and it is difficult to determine this exact point with variability in the measurements and difficulty with measuring all water potentials. Therefore, it can seem like the inclined curve should in some cases be extrapolated up to the full saturation point and that the ice entry value is higher than what the curve in Figure 6.8 indicates. It is a large change in water potential from measurements of an air dry sample and to a sample with a little higher water content. The range of potential measurements for the WP4C is 0 to –300 MPa and the values below –300 MPa are uncertain. More measurements should have been performed at low saturation levels to obtain a more accurate curve for the potential. It is difficult to prepare clay samples with water content just above air dry, because it is difficult to obtain equilibrium when a very small amount of water is

added to the sample. This could have been done by an absorption method, but was not done in this test. At high saturation the increase in potential is very small compared to the increase in saturation and the potential curve change from being vertical to approaching horizontal. Potential measurements should have been performed at more saturation levels to provide more accurate saturation curves.

The water potential is clearly dependent on particle size. This is clearly seen in Figure 6.8. Sample 1 had a high content of sand and gravel particles and the water potential is much higher for this sample than for the fine grained sample at the same saturation level. Sample 2 had higher potentials compared to sample 3, 4, 5 and 6. This can be explained by the lower salt content for sample 2, which reduced the magnitude of its osmotic potential. The difference in measurement mode is thought to be the reason for the deviation in results for sample 8 compared to sample 3, 4, 5 and 6.

The measured water potential should be a combination of the matric and osmotic potential according to Decagon Devices (2018). The osmotic potential is estimated from the salinity measurements and then the matric potential could be estimated by equation 4.2. This equation shows a linear relation between the osmotic and matric potential, but in reality this relation might be more complicated, but has not been studied in this thesis. The salinity is not measured from the exact same part of the sample as the water potential and this brings in elements of uncertainty. The osmotic potential in a sample with salinity around 30 ppt is around –2 MPa and the matric potential is likely in the range of –50 kPa to –200 kPa for fine grained samples. The matric potential is about 1/10 of the osmotic potential. With uncertainties in the measurements it is difficult to obtain a precise value for the matric potential from Equation 4.2.

Chapter 7

Analysis of Test Results

7.1 Calculations of Unfrozen Water Content

The purpose of measuring the water potential is to use it to calculate the temperature where freezing is initiated and estimate the unfrozen water content (UWC) as function of negative temperatures. The total water potential is a combination of osmotic and matric potentials. It is important to understand how change in temperature affect these potentials in order to find the freezing point (FP) and UWC. The osmotic potential decreases with lowering of temperature, but increases as water freezes and the concentration in the remaining unfrozen water increases. It is also important to determine which of these effects that dominates when temperatures are lowered. When ice nucleation is initiated in the pores, ice is formed and the saturation due to unfrozen water decreases. The decrease in saturation causes an increase in capillary tension forces, which causes the matric potential to increase.

7.1.1 Fast Estimation of Unfrozen Water Content

The fast method by Istomin et al. (2017) as presented in Subsection 4.3.1 was used to obtain the FP and UWC. The measured water potential was used to calculate the water activity by Equation 4.10 and the water activity was used in Equation 4.14 to determine the freezing point where the water content in the sample was in equilibrium with bulk ice. The water potential is a function of temperature and water content. The variation in water potential due to change in water content gives t_{eq} as a function of water content, approximating the soil freezing characteristic curve (SFCC) for the respective sample. The method does not distinguish between the matric and osmotic potential in the estimation of t_{eq}.

The curves for the water potential in Figure 6.8 have a vertical part at full saturation. Where the potential curves bend of to the left at the top of the vertical part can be interpreted as the ice entry value. It is the point where ice nucleation initiates in the soil pores and is the initial FP. With the use of the equation by Istomin et al. (2017) the calculated FP is too high. The curves indicate an initial freezing point around –1°C at full saturation. For example, the water content for sample 6 is measured to be 30% and the freezing point was measured at –2°C with the Testo temperature logger. The FP temperature derived by the Istomin equations is correspondingly –1.1°C for the sample with water content of 28%, as Figure 7.1 shows. This is clearly higher than the measured. From the calculations it seems like the measured potential is too low, which cause too high FP and a too low UWC. The steep part of the curve should converge towards the

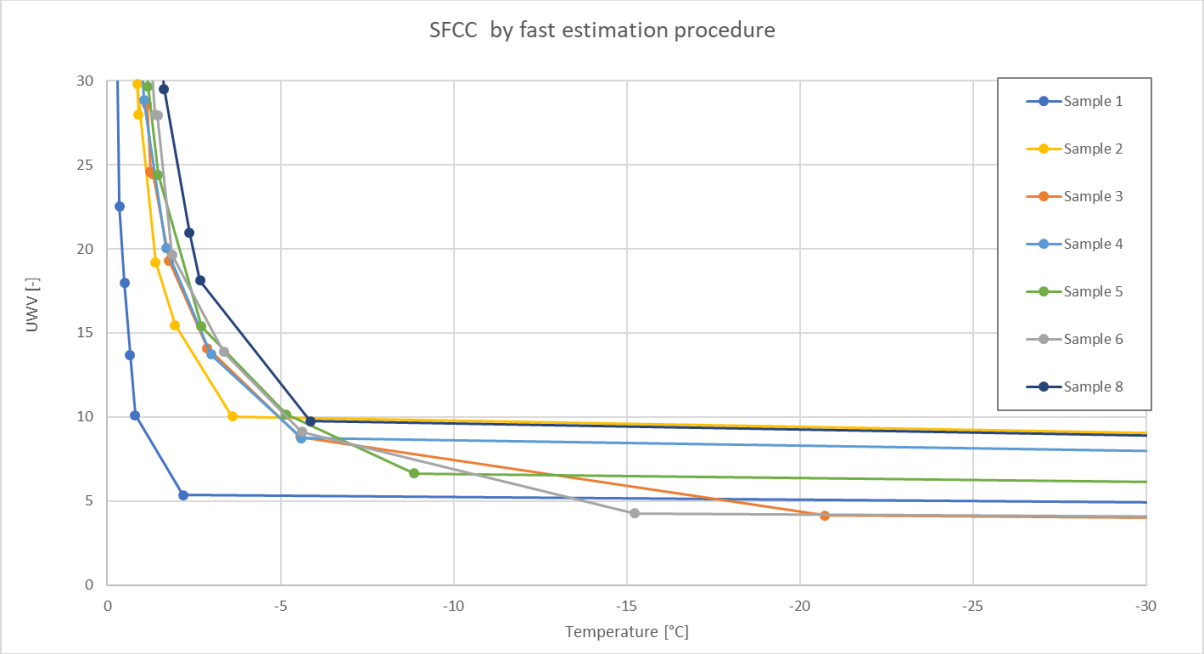

Figure 7.1: *The SFCC calculated with the fast estimation of UWC by (Istomin et al., 2017).*

freezing point, but converges towards a higher temperature (around –1°C). Therefore, it can be that the equation by Istomin et al. (2017) does not include the effect of solutes in a correct way or that the Dew Point PotentiaMeter underestimates the total potential and does not include the full effect of matric and osmotic potential. It might also be that the two potentials should not be linearly added, but coupled in a different way. The measurements wetter than –1 MPa are discarded because the samples are usually fully saturated at this potential. Higher potentials, closer to zero, will give smaller freezing point depression. For sample 1 the potential is –1 MPa before full saturation.

The SFCC by the fast estimation method indicate that there is approximately 15% UWC at –3°C, 10% UWC at –5°C and 5–7% UWC at –10°C. The WP4C Dew Point PotentiaMeter can measure down to –300 MPa, but the potential and water content at this level is uncertain. The UWC approach 0 as temperature and potential decrease. A potential of –300 MPa gives a FP of –250°C. What is most important is to estimate the amount of UWC at the temperatures the permafrost soil at UNIS East will experience. The upper layer can experience temperatures down to –30°C, but further down, the temperatures are around –4°C. Therefore, the temperature range from –5°C to freezing point is the most important to study. Samples 3, 5 and 6 all seem to have a lower water content at –10°C than samples 2, 4 and 8. The main reason for this is that samples 3, 5 and 6 have measurements for a low water content that give t_{eq} below –8°C. For samples 2, 4 and 8, there are no measurement points between approximately 10% water content at –6°C and the air dry water content with potentials around –250 MPa. The line is simply drawn straight between these two points. The curves with more potential measurement points give a better estimation of the unfrozen water content curve.

7.1.2 Calculations of Unfrozen Water Content with the Generalized Clapeyron Equation

The equations by Zhou et al. (2018) presented in Subsection 4.3.2 was used to estimate the freezing point and includes the effect of solutes in the pore water. For this method the osmotic and matric potentials must be known. The osmotic potential was calculated from Equation 4.3. The salinity measurements were used to estimate the molar concentration, c, of salt at different water contents in the soil. The mass of salt, m_{salt}, in the sample was calculated by equation 5.7 when the salinity was measured. The molar concentration was then calculated by

$$c = \frac{m_{salt}}{M} / \frac{m_w}{1000} \tag{7.1}$$

where M is the molar mass of a chemical compound and is 58.5 g/mol for NaCl and m_w is the mass of water in the sample at a certain water content. The salt should be included in the mass of water, but a dilute solution is assumed and the salt is not included in the mass in these calculations. The volume is determined by converting the water mass from grams to litres by dividing by 1000. For the initial FP the osmotic potential is calculated using the measured temperature for FP. For the following calculations of the temperatures below initial freezing point the previous value calculated for combined freezing point is used to estimate the osmotic potential. This can give a slightly higher estimation of osmotic potential. The freezing point depression was not possible to detect for sample 1 and the value estimated by the Istomin equations is used to predict the osmotic potential at the freezing point. The molarity increases when the sample freeze and the molarity is calculated for the water content at the measured potential. The calculated osmotic potentials are in the range –1 MPa to –2 MPa for the samples, except for sample 1 which was less saline and the osmotic potential was –0.4 MPa.

When the osmotic potential is determined the matric potential can be derived by using Equation 4.2 and the potential measured by the WP4C. It is assumed that the sample is fully saturated at the measured water content for each sample (except sample 1). The potential measurement taken at full saturation is ideal to use for the estimation of the initial freezing point. If a measurement of potential at the desired water content is lacking, a potential value can be interpolated from the two closest measurements of water content and potential. Subtraction of the calculated osmotic potential from the measured total potential should give an indication of what the matric potential should be. In some cases the matric potential got a positive value. The matric potential transpires from adhesion and capillary forces which cause the water to be in tension, which give a negative potential value. The estimation of a positive matric potential is wrong and must be corrected for. The reason for the wrong estimation of matric potential can be that the total potential measurement is too low, that the salinity measurement is too high or that the matric potential is so small compared to the osmotic potential that it is difficult to obtain its correct value.

To be able to evaluate the osmotic potential and matric potential the calculated freezing point for the total potential, combined FP, must be evaluated against the measured FP. The direct measurement of freezing point is assumed reliable as the instrument is precise. The first step to obtain the combined FP is to calculate the FP due to the matric potential. This is done by Equation 4.30. For the case where estimated matric potential is estimated with a positive value this is set to zero. Secondly, the freezing point due to the osmotic pressure is calculated with Equation 4.33 with T_{f0} being the reference freezing temperature (273.15 k). The initial FP by osmotic potential is within 0.5°C of the measured FP for all samples. To calculate the combined FP, including matric and osmotic potential, Equation 4.33 is used again, but with

T_{f0} as the freezing point due to matric potential. This combined freezing point is evaluated against the measured freezing point. For the cases where the matric potential was set to zero, the freezing point was not changed. A trial method was used to obtain an estimated value for the matric potential. The matric potential was given a negative potential between 0.1 MPa to 0.3 MPa to see what gave the best approximation of freezing point depression compared to the measured. The estimation of matric potential is accepted when the estimated FP fits with the measured. For sample 2, 5 and 8 matric potential of –0.2 MPa gave a good fit. Sample 6 had a higher clay content and a slightly lower value of –0.3 MPa gave a good fit for this sample. This is reasonable, as the matric potential is assumed to be higher when the clay content increases. For sample 3 and 4 the estimated freezing points were too low with estimated matric potential of –0.1 MPa. The salinity measurements for these two samples were compared to salinity measurements performed by Gilbert et al. (2019) on the same soil (Figure 7.10). At depth of approximately 3.5 m, which is between sample 3 and 4, the salinity measured by (Gilbert et al., 2019) was ca. 20 ppt. This is lower than the salinity measured in this experimental testing which was approximately 30 ppt. For sample 3 the salinity used in the calculations was changed from 30 ppt to 19 ppt and then matric potential of –0.25 MPa gave a good fit for FP. Sample 3 is also a clay sample. For sample 4 the salinity value used in calculations was changed from the measured value of 29 ppt to 25 ppt and then a matric potential of –0.2 MPa is suitable. The procedure by calculating the initial freezing point was repeated for potential measurements at lower water contents to establish the SFCC. Adjustments in the matric potential must be done accordingly for lower water content as well.

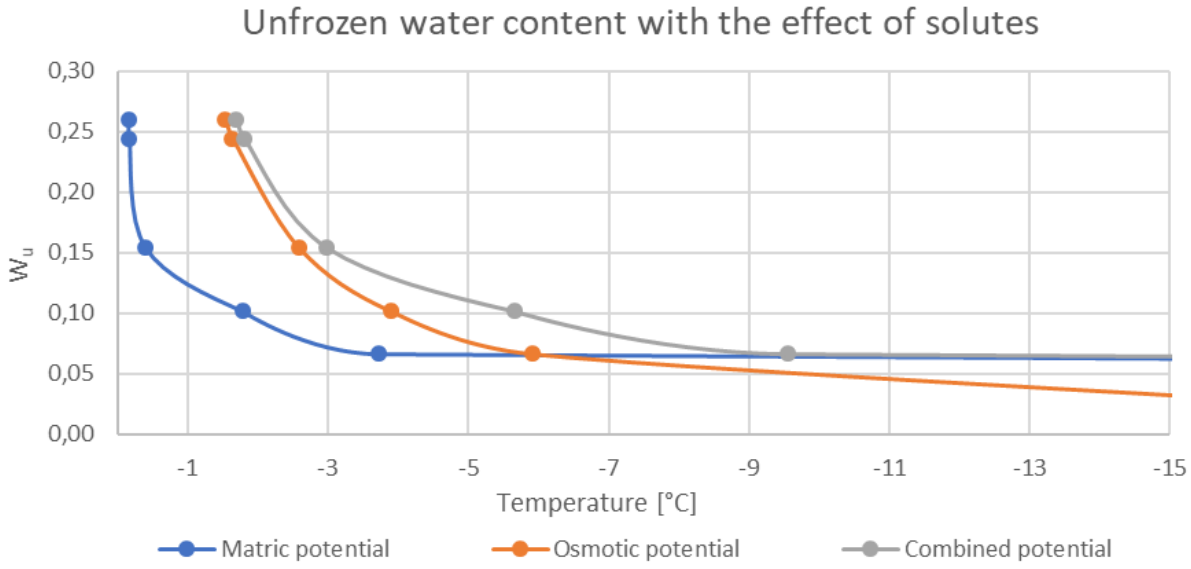

Figure 7.2: *Curve of unfrozen water content calculated from osmotic potential and matric potential, including the combined line for sample 5.*

Figure 7.2 shows the freezing point curves estimated for matric potential, osmotic potential and the combined curve for sample 5. The combined curves give the SFCC and the calculated curves are shown in Figure 7.3. At full saturation the matric potential is close to zero. As saturation decrease the ice entry value is reached and the pore water starts to freeze. Saturation decreases, and the matric potential of the pore water decreases. For a fully saturated sample with solutes in the pore water the matric potential is much lower than the osmotic potential at initial freezing. At some point the matric potential will be larger than the osmotic potential and will then be

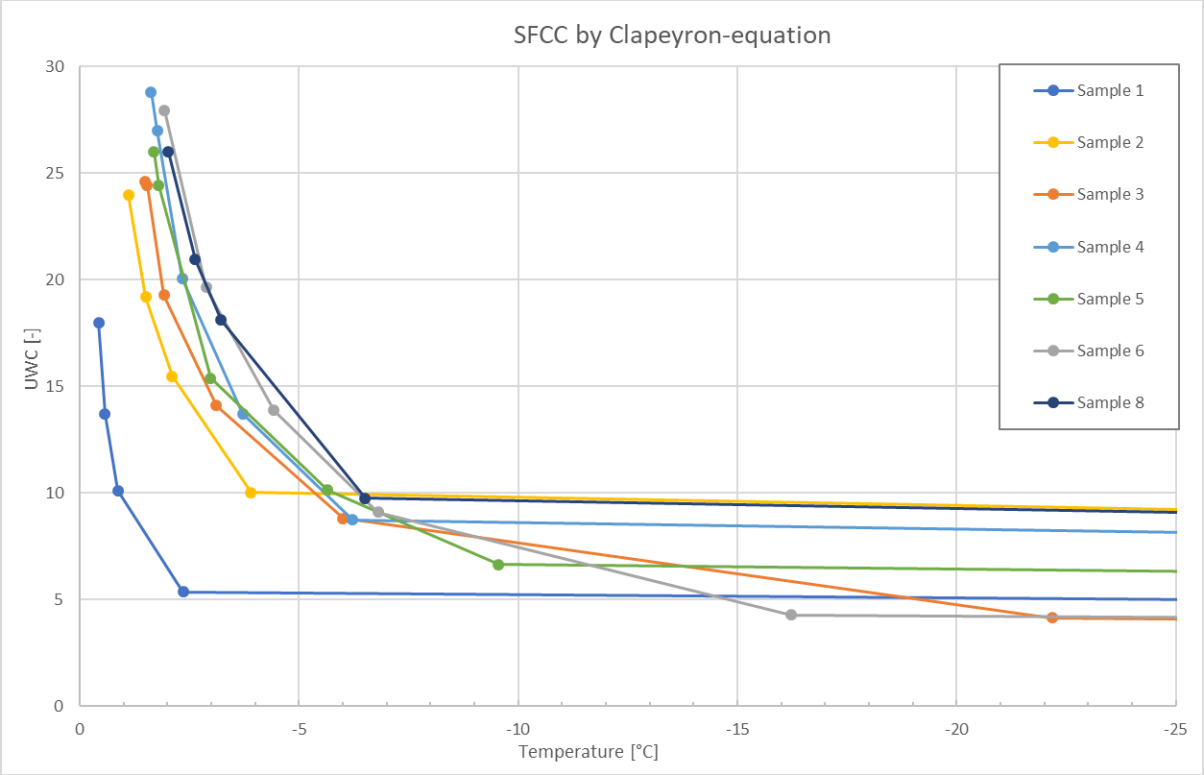

Figure 7.3: *The SFCC calculated for the soil samples with the generalized Clapeyron equation.*

the dominating potential that keeps part of the pore water unfrozen at negative temperatures. When the saturation is high, the osmotic potential is much larger than the matric potential and the combined freezing effect is just slightly higher than the effect due to osmotic potential. As saturation deceases, the matric potential increases and the osmotic potential decreases so that the combined water potential effect become greater than the osmotic potential. The combined potential continues to exceed the matric potential to a temperature of approximately –10°C where the combined curve equals that of the matric potential. When the matric potential exceeds the osmotic potential the effect of the osmotic potential is insignificant on the amount of unfrozen water.

With alterations of the matric potential and the salinity in a couple of samples, the FP estimated with Equation 4.33 fits well with the measured FP values. This method gives a better fit than with the method by Istomin et al. (2017) which underestimates the freezing point depression. Enlarged versions of the curves shown in Figure 7.1 and 7.3 can be found in Appendix C and give a clearer image of the deviation in the estimated freezing points by the two methods. The SFCC is estimated in a simpler way compared to that explained in the article by Zhou et al. (2018). The reason for this is that the method requires determination of curve fit parameters from experimental tests. Experimental tests on UWC were not performed in this study. The estimated SFCC in Figure 7.3 can be compared to the curves in Figure 7.4. The UWC curves in Figure 7.4 are for a Morin clay with different solute contents and show both experimental and calculated values. A pore water salinity of 30 ppt equals 0.5 mol/L and the estimated curves should be compared to the curve with 0.5 mol/L or be below this curve. At water content of 0.2 the FP estimated by Zhou et al. (2018) is about 1°C to 2°C lower than the estimated curve from testing. This can be because of a larger content of fines in the Morin clay than in the clayey silt from UNIS East. For the Morin clay with a solute content between 0.2 mol/L to 0.5 mol/L the

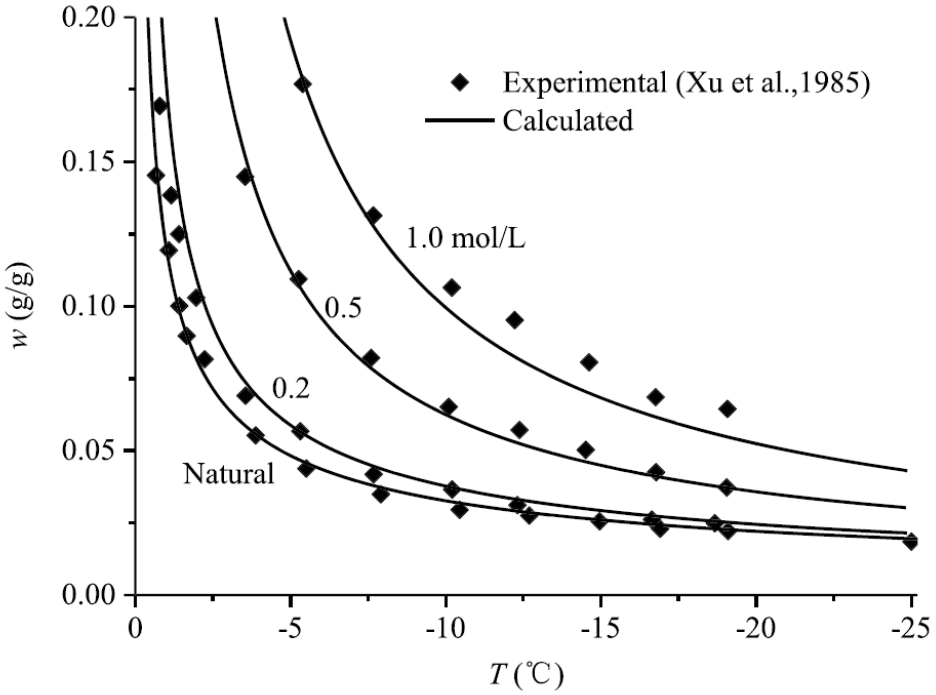

Figure 7.4: *Relationship between unfrozen water content and temperature from experiments and calculations on Morin clay (Zhou et al., 2018).*

UWC it estimated to be between 0.04–0.07 at –10°C. Sufficient data for water potential at low water contents have not been obtained. For the curves that lack data points for water potential lower than 10% water content the estimated UWC is too high at –10°C compared to the curves in Figure 7.4. Sample 3, 5 and 6 have data points around 0.05 of UWC and for these SFCC the UWC is about 7% at –10°C. This shows that with enough data points at low water contents the estimated soil freezing characteristic curves are in agreement with the curves estimated by Zhou et al. (2018), but seem to give slightly higher values of UWC at the same temperature. Furthermore, the UWC curve by Zhou et al. (2018) shows that at –25°C the UWC can be about 3% for a soil sample with solute content of 0.5 mol/L. The estimated curves for sample 3 and 6 converge to 5% UWC at –25°C. It is difficult to obtain accurate dew point measurements of soil with low water content because the change in water potential is very large compared to the change in water content. In addition, too few tests were performed at samples with low water content. Therefore, the estimation of the UWC at low temperatures with Equation 4.33 inherits uncertainty. The calculation method must be tested with more water potentials at lower water content to check if the method gives the desirable accuracy at low water content as well. Figure (Zhou et al., 2018) can be used for comparison of the results at low water content and may give an indication of what the results should be for unfrozen water contents below –10°C.

7.2 Thermal Properties as Functions of Temperature

7.2.1 Volumetric Heat Capacity

The volumetric heat capacity is calculated by Equation 3.7. When the UWC curve is established the amount of frozen and UWC at the different temperatures are known and used in the calculations. The volumetric heat capacities for water and ice are known, but soil minerals can take various values that are not determined. By rearranging Equation 3.7, the volumetric heat capacity of soil is obtained by

$$c_s = \frac{c_v - c_w w_u \rho_{dry}}{\rho_{dry}} \tag{7.2}$$

and then this equation is used with the measured average unfrozen volumetric heat capacity for the soil, the measured water content and the dry density. That gives the required c_s for the soil. The range of the calculated c_s for the soils of the present study was found to be 0.2 kJ/kg°C to 0.85 kJ/kg°C. The measurements with low values are believed to be too low and the higher values fit better. Therefore, the value 0.71 kJ/kg°C which is similar to the heat capacity for bentonite clay seems to fit well and will be used in the estimations of volumetric heat capacity (Andersland & Ladanyi, 2004). Figure 7.6 shows the comparison of measured and calculated values of the volumetric heat capacity. For sample 1 to 3, the three upper most samples in Figure 7.6, the measured values are lower than the calculated values. The measured and calculated value fit better for sample 4 to 8, but the calculated frozen values tend to be lower than the measured. Figure 7.5 shows an example of the calculated curve for temperature dependent volumetric heat capacity determined by using Equation 3.7 and the estimated unfrozen water content curve. The change in amount of water and ice in the soil at different temperatures is the most significant factor for the change in the volumetric heat capacity with temperature.

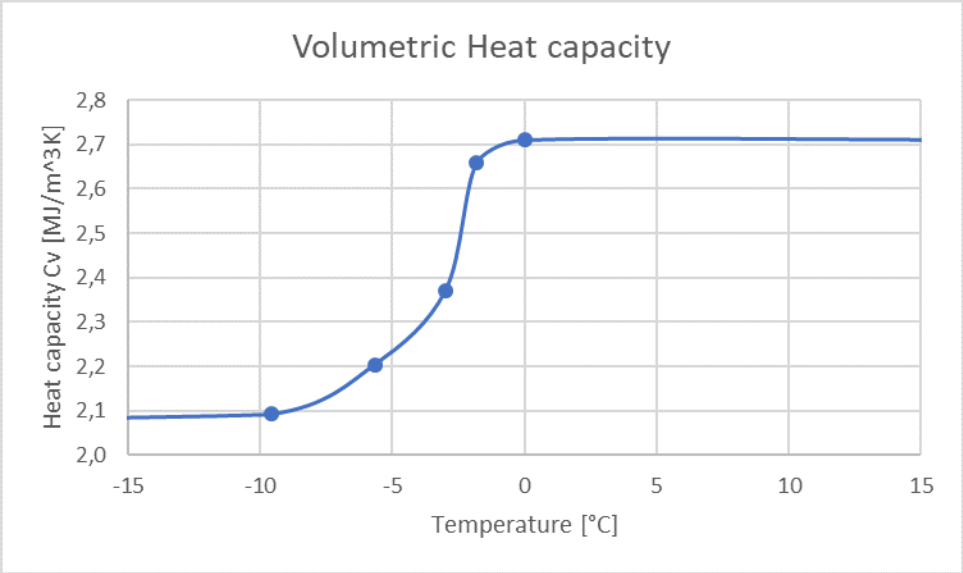

Figure 7.5: *The estimated curve for heat capacity with temperature for sample 5.*

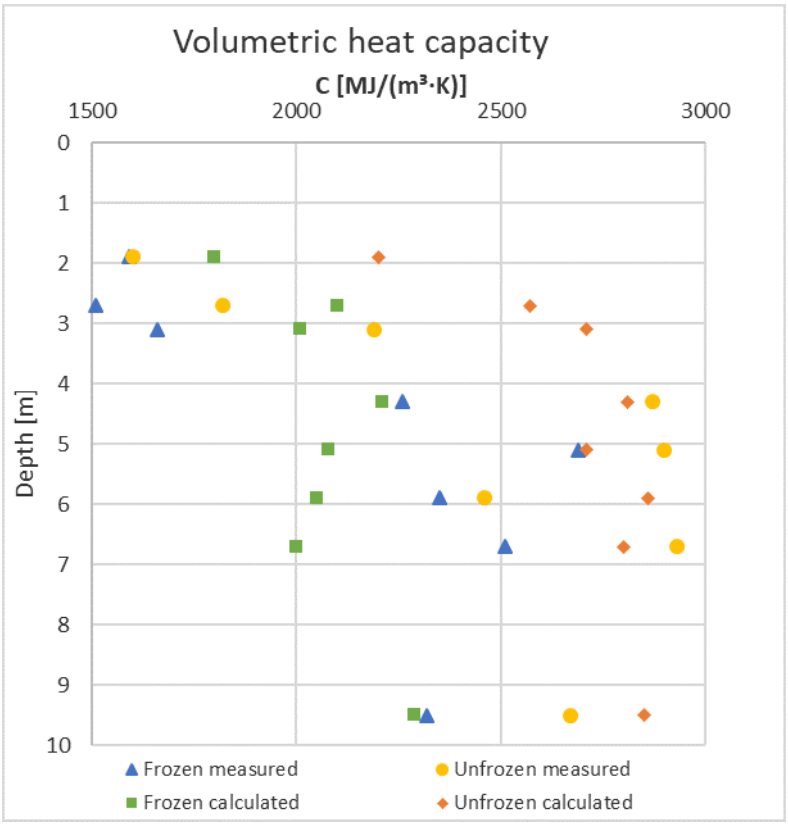

Figure 7.6: *The values calculated for volumetric heat capacity based on UWC estimations is compared to measured values.*

7.2.2 Thermal Conductivity

The thermal conductivity is estimated by the empirical formulations by Kersten and Johansen presented in Subsection 3.2.2. The thermal conductivity for soil particles depends on the mineral content. The mineral content has not been determined for the present soils, and the lack of this value can give uncertainty in the use of the empirical formulation. A value of 2.2 W/mK was used as suggested by Andersland and Ladanyi (2004). The values measured with the TR–1 and SH–1 sensors are compared with the values found from the empirical estimates. The unfrozen values are from measurements with soil at 20°C and the frozen values are measured with soil at –18°C. Johansen's method includes the amount of unfrozen and frozen water content. To obtain comparable results a value of 2% UWC at –18°C was chosen as an approximation. The results by the Johansen method is sensitive for changes in the UWC. Figure 7.8 and Figure 7.9 show the comparison of frozen and unfrozen values of thermal conductivity. The estimated values with Kersten's formulation give higher values than with Johansen's formulation and they differ with approximately 0.2 W/mK which is 10% deviation if the value of real thermal conductivity is around 2 W/mK. For sample 1, 2 and 3, the measured thermal conductivities were significantly lower than for the other samples. For these samples the estimated values were higher than the measured. For sample 3 to 8 there were a slight tendency that the measured values were higher than the estimated values. The measurements with the TR–1 sensor tend to be 0.1 W/mK to 0.2 W/mK higher than with the SH–1 sensor. A clear trend of what measurement method or estimation method that gave the most correct value for thermal conductivity was not found. It would be necessary to control the results with measurements performed with

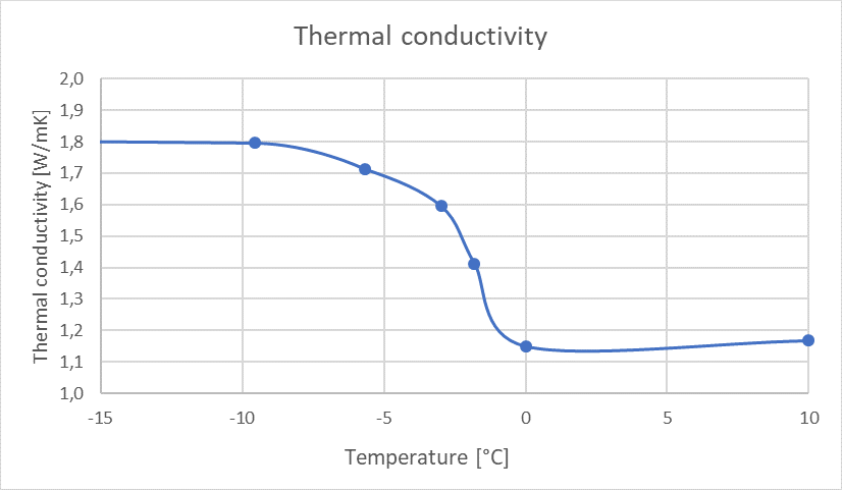

Figure 7.7: *The estimated curve for thermal conductivity with temperature for sample 5.*

a more accurate method to evaluate what test give best results. However, in lack of other more precise methods, the empirical formulation by Johansen was used to establish the curve relating thermal conductivity to temperature because it includes the amount of UWC. The SFCC developed with the Clapeyron equation was used to determine the frozen and UWC at different temperatures. Figure 7.7 shows how the estimated thermal conductivity change with temperature for sample 5.

7.3 Salinity and Freezing Point Depression

The investigations by Bing and Ma (2011) on the FP of saline soil show that the FP of soil decreases as the salt content increases and that at the same salt content the FP for clay soil is lower than for sandy soil. A soil with larger content of fines will have a lower FP, because of smaller soil grains and larger specific surface area. It is very important to determine the salinity in the soil since the osmotic potential from the solute content contributes to depressing the freezing point by up to several degrees below zero. The depression of the FP is highly important when looking at the ground thermal regime since the permafrost can thaw at negative temperatures. With a freezing point depression of –2°C, permafrost temperature of –3°C is relatively warm. The measured freezing point depression increases with the increase in the salinity and coincides with the findings by Bing and Ma (2011). The freezing point depression shifts the UWC curve to more negative temperatures and this implies that the UWC will become higher at more negative temperatures than without salt present. This affects the mechanical behaviour of the soil such as reducing the strength and increase the creep rate.

Figure 7.10 compares the salinity measurements from this experimental work and that done by Gilbert et al. (2019). Since the salinity is found as mass of salt in the solution to the mass of pore water in the soil sample, the salinity is very sensitive to water content in the sample. This can be the reason why deviations in salinity around the same depth are seen. More measurements are needed in order to perform a proper sensitivity analysis of the salinity to water content.

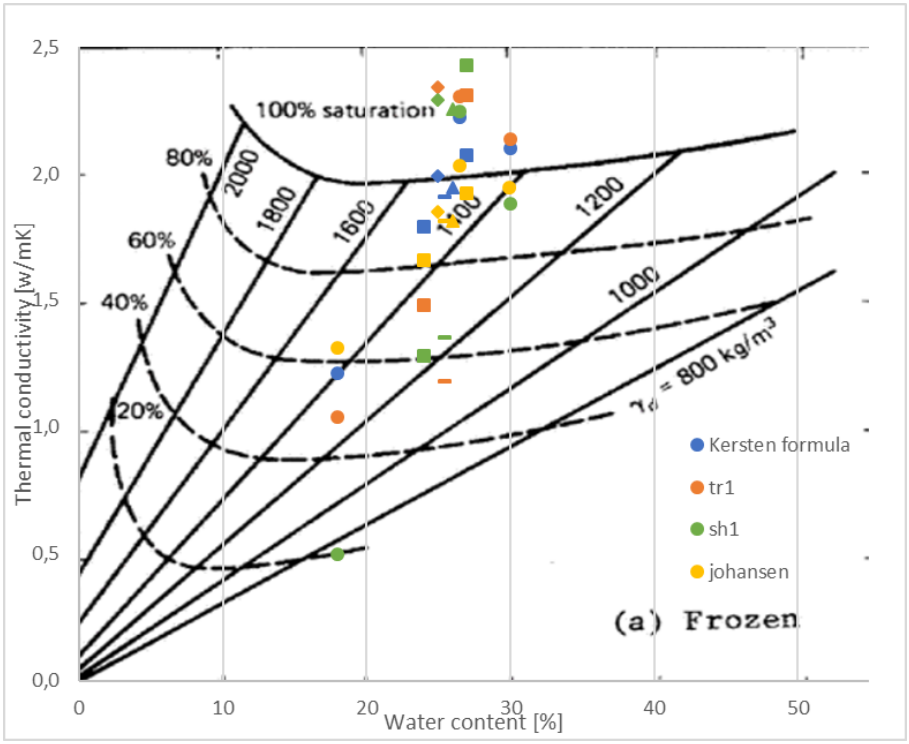

Figure 7.8: *Comparison of measured and calculated values for frozen thermal conductivity in the Kersten diagram. The different estimation types are differentiated by colour. The different samples are given different symbols in the diagram.*

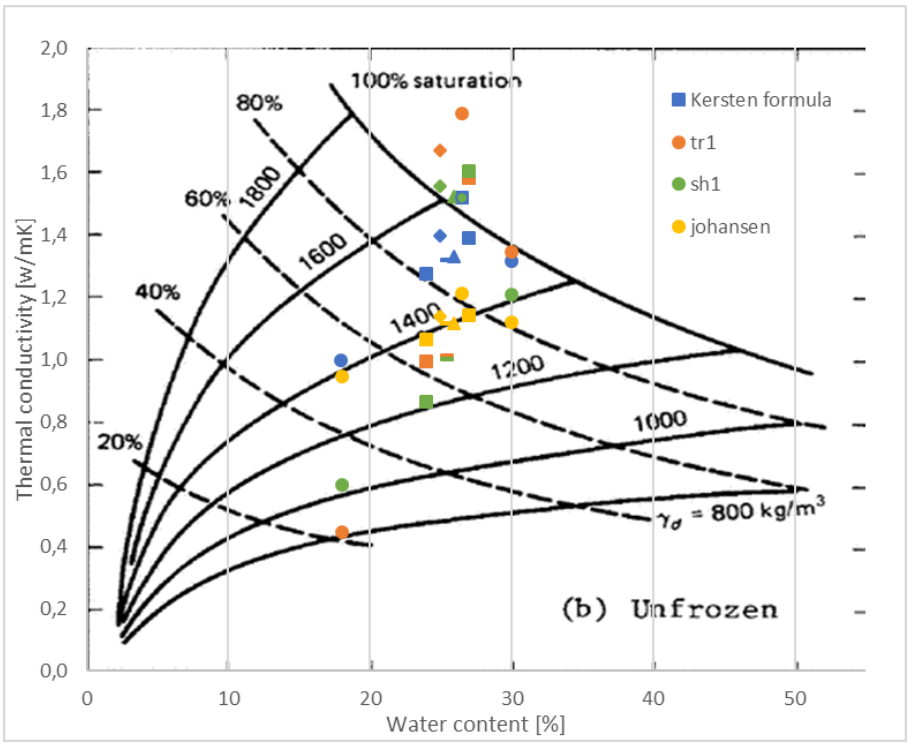

Figure 7.9: *Comparison of measured and calculated values for unfrozen thermal conductivity in the Kersten diagram. The different estimation types are differentiated by colour. The different samples are given different symbols in the diagram.*

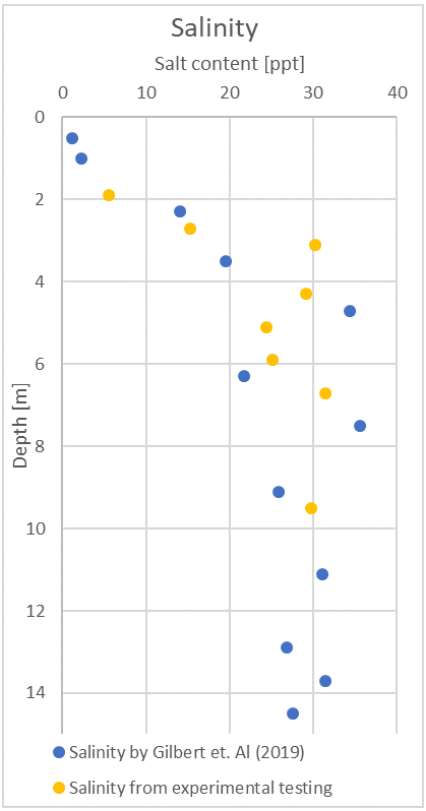

Figure 7.10: *Comparison of salinity measurements.*

7.4 Verification of Calculations

A model of a soil sample is set up in a Temp/W analysis in the program Geostudio 2018. Figure 7.11 shows a section of the model and it is 5 cm in diameter and 10 cm long. The thermal conductivity with temperature and UWC with temperature curves are used in the model. The model uses volumetric water content and the frozen and unfrozen volumetric heat capacities as input parameters. The model is given an initial state of 22°C before it is cooled by applying this temperature to the boundary condition. It is cooled by applying a boundary condition of –18°C on the outer sides of the sample. The boundary condition representing the core of the sample is kept as a closed boundary so that no temperature is applied, but can change according to the cooling from the outside. The temperature in the core of the sample is plotted as a function of time (Figure 7.11). The plot shows that the temperature decreases down to the FP which is determined where the rate of temperature change slows down and the curve is almost horizontal. After some time, the rate of temperature change and increases again. The freezing process is much faster in the modelled sample than in the measured samples. The measured sample was wrapped in cling film and aluminium foil and there will be air in between the layers. Measurements were performed in a freezing room with a temperature of –18°C. The wrapping will give some insulation and the freezing process will slow down because of this. Because of convection in the room and heating of the air around the sample, it is likely that the boundary condition of –18°C is too low. These are some reasons why the modelled freezing curve has a much faster cooling rate. However, the curve shows that the core temperature will drop to the FP where the cooling rate slows down for a while. This clearly indicates that the thermal properties function established for the material behave as it should. The model could

have been altered to better represent the real time measurements. The actual conditions for the measurements are not studied in detail and to model them would be using estimations to approach more similar results. Hence, the similarities between the freezing curves are seen as sufficient verification. Measurements of the FP could be performed in a liquid bath for better control of the boundary conditions.

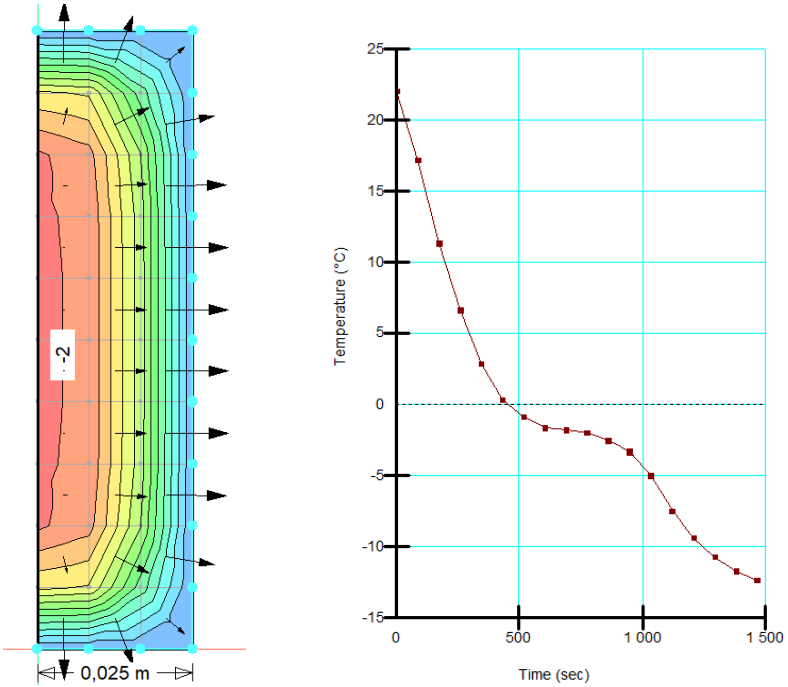

(a) (b)

Figure 7.11: *(a) A soil sample is modelled and the figure shows a stage in the cooling process where the core temperature is –2°C. (b) Graph showing the simulated temperature change in the core of the sample.*

Chapter 8

Modelling the Ground Thermal Regime

A model approximates reality and the applicability of results from simulations depends on how well the simplified model represent the natural phenomenon. A finite element method (FEM) based model can be used to simulate and predict future behaviour in the ground thermal regime in permafrost soil. Simplifications of the natural conditions must be done to set up the model and these simplifications can be based on measured data or suitable parameters from theory. A model should be able to give results that are compatible with the natural situation. For example, a ground thermal model should be able to replicate a temperature profile from thermistor string temperature measurements to verify that the model gives approximately the same temperature profile. A model with a better fit to measured data is likely to give more precise indications in simulations of future behaviour in the ground thermal regime. Predictions of the temperature in permafrost soil and the future active layer thickness (ALT) are important in an engineering perspective for the engineers to be able to design infrastructure that can withstand predicted temperature changes or restore infrastructure that will be affected by temperature changes in the ground. The strength and bearing capacity of the frozen soil will be reduced and the creep rate will increase with higher permafrost temperatures. Changes in the upper 10 to 20 m of the frozen ground are the most important when concerning infrastructure. The model should give predictions of how much the ALT will increase over time and how the temperature profile will develop under different climate scenarios.

8.1 Model Setup

The software GeoStudio 2018 with the TEMP/W module was used to model the ground thermal regime at the UNIS East site that was described in Section 5.1. A 2–dimensional (2–D) model was set up for the thermal analysis, although only vertical heat flow was considered. This was done by closing the vertical boundaries such that no heat transfer occurred along these. The model represents a 1 m wide and 30 m deep soil column. The element size was 0.25 m times 0.25 m and could be decreased if more precise predictions of change by depth were needed. The TEMP/W model is based on the law of energy conservation, where the total energy is conserved unless energy is added or subtracted from the system (GEOSLOPE International Ltd, 2017). In the soil porous medium the rate of change in thermal energy is determined by sensible and

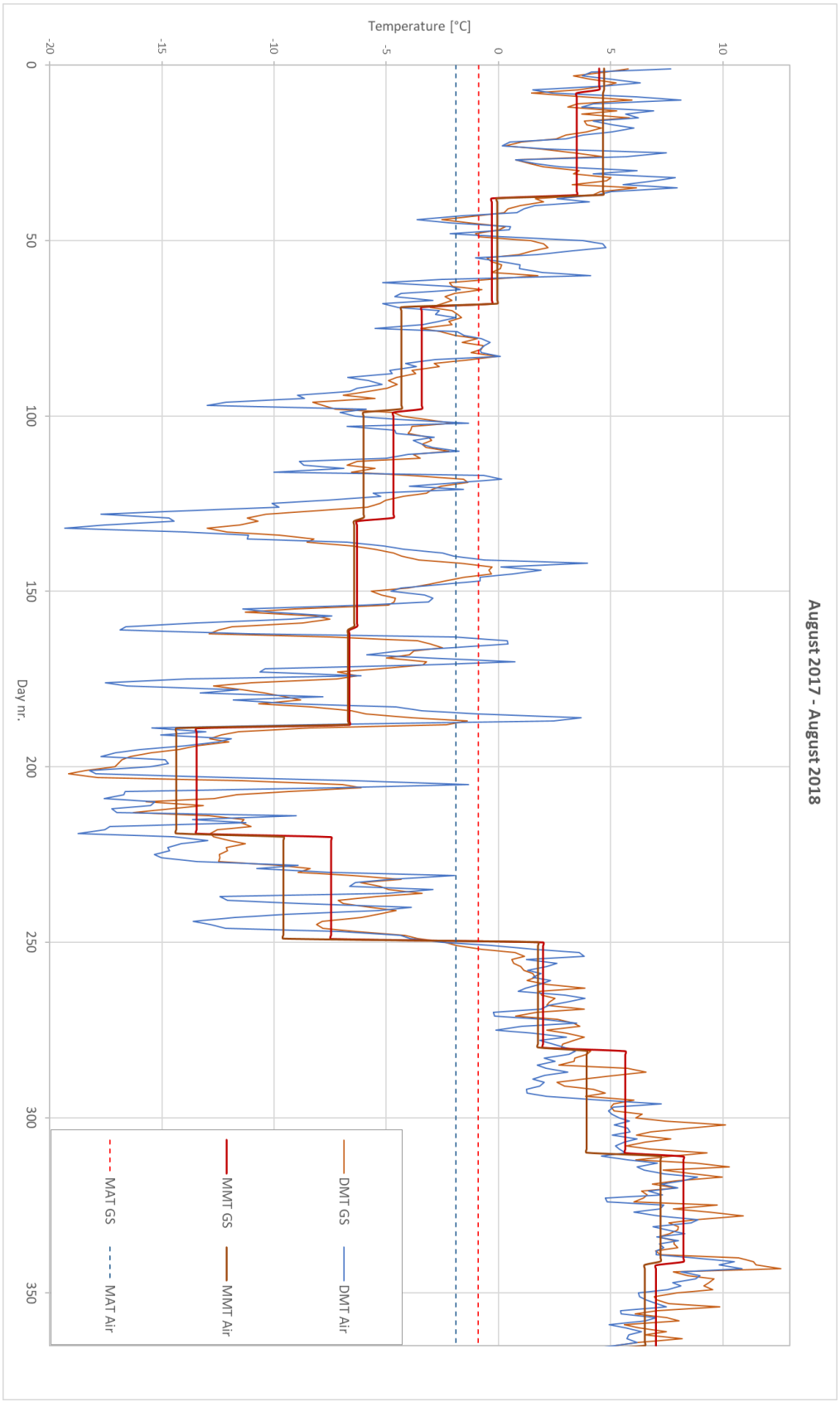

Figure 8.1: *Curves of average daily temperatures, average monthly temperatures and average yearly temperatures for 2017–2018 for measured air temperatures and ground temperatures measured at 0 m depth.*

latent heat. The sensible heat is defined by the volumetric heat capacity. The latent heat is the energy needed for fusion of ice to water. In this model the heat transfer happened by conduction. The conduction is the ability to transmit heat in response to the temperature gradient (GEOSLOPE International Ltd, 2017). The soil properties were defined and were important for the rate of change in thermal energy in the model. Water flow and volumetric change (frost heave) were not included or analysed in the model.

To model the ground thermal regime input parameters for the soil material and the boundary conditions must be defined. In this model temperature data from the thermistor strings presented in Subsection 5.1.5 was used and meteorological data from the Adventdalen site was used. Figure 5.1 shows the location of the UNIS East and the Adventdalen sites. Figure 8.1 shows temperature observations from 25th of August 2017 to April 2019 from thermistor measurements at 0 m depth and meteorological observations of AT 2 m above ground. Daily mean temperatures show the day to day variation. The monthly average temperatures are shown as step functions and the mean annual temperature shown as a line for air and ground temperatures.

To begin with, boundary conditions were applied to the model to set up an initial temperature profile. The initial state should replicate today's situation. The bottom boundary condition was adapted from the thermistor string measurements and was set to be –3.9°C, equal to temperature at 30 m depth. At the ground surface in the model, the mean annual air temperature (MAAT) of –1.9°C was applied as a boundary condition. When the boundary conditions were applied, a steady state thermal analysis was run to get the temperature distribution in the soil.

Furthermore, after the temperature profile was set up by the steady state analysis a transient thermal analysis was performed to simulate temperature changes in the ground thermal regime over time. The bottom boundary condition with a fixed temperature was removed and replaced by a closed boundary. That means that no heat is added or extracted at this boundary. A temperature curve representing the annual temperature variations at ground surface (GS) was applied at the top. The GS condition was the most important curve for the rate of change in temperature in the modelled ground thermal regime. The temperature curve for one year applied at GS was repeated for many years to achieve a "steady state". A steady state was reached when the change in temperature in the profile between two consecutive years was small. The ground thermal regime simulated after 10 years was used as an initial state for further simulations. To model how the temperature profile will behave under a climate change scenario with rising temperatures, the boundary condition was changed according to the predictions of rise in air temperatures (AT). The model then indicated how the temperature profile and active layer (AL) respond to the changes in temperature at ground surface.

8.1.1 Soil Parameters

Soil is a heterogeneous material and the properties vary within the soil. In geotechnics the main task is to predict values that can be used to represent the soil to make calculations of stability, settlements or like in this case temperature change in the ground. To be able to model the soil, it is divided into different layers where the parameters are determined for each layer and should represent the soil material within that layer. TEMP/W has three different material models; full thermal, coupled convective and simplified thermal. In this analysis the full thermal model is used. The input parameters needed for the full thermal model is thermal conductivity as a function of temperature, unfrozen water content as a function of temperature, the frozen and unfrozen volumetric heat capacity and the insitu volumetric water content. These parameters are determined from the results of the experimental testing of soil samples from UNIS East.

The unfrozen water content (UWC) and the thermal conductivity as functions of temperature are found from calculations based on these experimental results as explained in Chapter 7. The calculated UWC curves are also used to obtain the frozen and unfrozen volumetric heat capacity. For some of the curves it was necessary to extrapolate the curves to have a curve defined for the relevant temperatures. The soil parameters used in the model are shown in Table D.1, the soil freezing characteristic curve for each soil sample is given in Appendix C and the estimated curves for thermal conductivity are given in Appendix D. The temperature for phase change can be defined for the analysis. The phase change temperature would be the initial freezing point measured in the soil samples. In the model one value must be determined for the whole soil column, but the freezing point varied for all tested samples. However, the curves for UWC determines the amount of water that is frozen and unfrozen at different temperatures. This will in turn affect the volumetric heat capacity that is directly found by knowing the amount of each substance. The rate of change in latent heat of fusion per change in °C is controlled by the unfrozen volumetric water content – temperature curve (GEOSLOPE International Ltd, 2017). Therefore, it is not necessary to change the temperature of phase change since it is controlled by the UWC curve defined for each layer.

The upper soil layer represents the 2.5 m thick coarse gravelly sand layer at the site. Below this layer there are 7 different layers of clay and silt samples. Layer number two from the top is 0.5 m thick and layer three to six are 1 m thick. Layer 7 is 2 m thick and represents the layer of 7 m to 9 m depth. The bottom layer from 9 m to 30 m depth is represented by properties for sample 8. Gilbert et al. (2019) tested soil samples below 10 m depth at the UNIS East site and found that the soil composition changes slightly with depth. The results from the previous testing did not include dew point measurements and cannot be used in obtaining the curves for temperature dependent properties. Therefore, for simplification the results for sample 8 are used for the depth below 10 m in the present simulations. The soil properties for the different layers in the model are presented in Appendix C.

8.1.2 Ground Surface Boundary Condition

The ground surface temperature (GST) is not easy to measure directly and a function approximating the GST must be established to use in the model. Influencing factors make the GST different from AT. Amount of radiation absorbed in the ground, degree of air turbulence, availability of water for evaporation, the thermal conductivity of the ground surface layer and micro climatic conditions are influencing factors on the GST (Williams & Smith, 1989). Air temperatures are affected by convective heat flow and change at a higher rate than GST. Figure 8.1 shows that the amplitude of AT from Adventdalen and the temperature measurements at 0 m depth (referred to as ground temperatures) from UNIS East differ several times through the year and the amplitude of AT is higher than the GST in both summer and winter. The MAAT is –1.9°C and for ground temperatures at 0 m depth the mean annual temperature is –0.9°C. The MAAT can differ with 5°C to 6°C in one or two years in this area and the difference in MAAT and mean annual temperature at GS can be explained by the energy balance at the surface (Isaksen et al., 2000). The monthly average temperatures for ground temperatures are higher than the average AT in almost all months. The insulating effect from snow cover can give rise to difference in ground and air temperatures and keep the soil warmer than AT. During summer the exposed ground surface absorbs radiation and GST can be higher than AT. This effect is enhanced in the Arctic region because of the midnight sun. In addition, the pipes where thermistor strings are placed extend above ground surface and is exposed to the surrounding air (Figure 8.2). The pipe can be heated up and this can affect the temperature of the air inside

the pipe and may have influenced the temperature measurements in the top of the pipe. The thermistor at 0 m can, if it is in direct contact with the tube wall, be heated by direct sun radiation on the pipe. The fact that it is air inside the pipe can cause convection. This can also cause the thermistor readings to deviate from the actual soil temperatures, but this effect has not been proven.

Figure 8.2: *Snow cover conditions around a borehole at the UNIS East site in March 2019.*

To simulate the GST in the model a temperature curve must be defined in Temp/W for the upper boundary. The curves for daily average and monthly average temperatures for ground temperatures and air temperatures from Figure 8.1 are applied as GS boundary condition. The curve for a year is repeated for 10 years to check which simulation that gives best fit with the measured temperature profile. Both daily and monthly temperature curves show that the AT gives a temperature profile with slightly colder temperatures in the model in the upper 10 m than the real temperatures. Below 10 m the predicted temperatures are almost identical to the measured temperatures. The AL estimated with ground temperatures is about 20 cm thicker than with AT. The AL is found to be approximately 1 m from simulations with AT as boundary condition. The AL from thermistor measurements is between 0.8 m to 1 m and this is best simulated by the AT boundary condition. Therefore, with the uncertainties in ground temperatures, the AT will be used in further simulations. The AT with mean annual temperature will be used to avoid the big spikes in daily average temperatures and simplifies the process with adding the future temperature increase. Predictions of future temperature raise in air temperatures can be directly added to the AT used in the model. A surface-n factor could have been calculated and it is possible to add such a n-factor in the model. This is not done because it is difficult to determine the appropriate n-factor with the correct wind speed, vegetation cover and snow cover and know how it will change from year to year and how these conditions will become in the future.

8.1.3 Bottom Boundary Condition

Because of the heat flux from Earth's interior temperatures will increase more or less linearly under the depth of zero annual amplitude (ZAA), as Figure 2.2 shows. The heat flow from Earth's interior yield temperature gradients of 1°C per 22 m to 160 m (Andersland & Ladanyi, 2004). The geothermal gradient limits the thickness of the permafrost layer from below. At greater depths the geothermal gradient will have a significant impact on the temperatures in the ground. In this study the geothermal heat flux is not included in the bottom boundary condition as temperature perturbations of deep permafrost is not the main topic. However, this could have been attempted as a heat flux can be imposed on the boundaries in Temp/W. The impact of the geothermal gradient on the near-surface-permafrost is however small. In the study of ground surface-temperature reconstruction by Isaksen et al. (2000), it was shown that the temperature gradient was about constant at 0.025°C/m down to 45 m depth and then increased below this and was 0.037°C/m at 90 m depth. Present data from ground temperature measurements can be used in inversion modelling of deep permafrost to provide paleoclimatic information for the last one or two centuries (Isaksen, 2001). The model can be used to look at temperature perturbations from the surface and down to depths where the thermal gradient will have a significant impact on the ground temperatures. If the boundary condition at the bottom of the model is fixed to a constant temperature, energy will have to be removed from the bottom of the model to keep the temperature constant. With a closed bottom boundary condition the temperature at the bottom will be able to change over time. This is used in the TEMP/W model after applying the initial condition. The MAAT applied at the ground surface is higher than the temperature measured at 30 m depth. There are no annual temperature fluctuations at 30 m depth since this is below the depth of ZAA, but the temperature can increase over time with increase in heat transported to this depth. If the MAAT would be constant over many years, the ground would warm to this temperature. The upper part warms first, and it would take time to warm the soil further down. The fact that the MAAT is warmer than the permafrost temperature below ZAA indicates that the permafrost has formed under colder conditions and that the present MAAT is warm.

8.1.4 Climate Scenarios

For the period 1971–2000 the MAAT for the Svalbard Airport series was –5.9°C (Hanssen-Bauer et al., 2019). This is several degrees lower than the MAAT measured at the Adventdalen site in 2017–2018. It is evident that there has been a warming during the last 20 years. A report about past, present and future climate in Svalbard was published earlier this year and give predictions of how the climate will change under different climate gas emission scenarios (Hanssen-Bauer et al., 2019). Predictions for how future climate will be are based on the Coupled Model Intercomparison Project (CMIP5) by the International Panel on Climate Change (IPCC) and the global climate and emission models from this project and other regional climate models are implemented to get a specific analysis for Svalbard (Hanssen-Bauer et al., 2019). Future scenarios are based on how greenhouse gas emissions will develop and are described as Representative Concentration Pathways (RCP). Three different pathways or scenarios for how emissions will develop have been established; RCP2.6 drastic cuts from 2020; RCP4.5 reductions are made after 2040; RCP8.5 business as usual. These scenarios, based on global climate models without downscaling, are estimated to cause an increase in MAAT of 3°C, 6°C and 10°C respectively from the period 1971–2000 to 2071–2100 (Hanssen-Bauer et al., 2019). Temperature change is larger during the winter months than in the summer.

Table 8.1: *The change in temperature in °C from the median of ESD predictions for Svalbard land area following the RCP2.6 and RCP8.5 scenarios for the period 1971–2000 to 2071–2100. The seasons are abbreviated with the initial characters of the months, so DJF is winter, MAM is spring, JJA is summer and SON is fall. (Adapted from Hanssen-Bauer et al., 2019).*

Season	**RCP 2.6** [°C]	**RCP 8.5** [°C]
Annual	3.8	9.5
December, January, February	5.8	15.1
March, April, May	3.2	8.3
June, July, August	1.4	4.2
September, October, November	4.8	10

In the report different models are used to downscale the global model and include impact of local phenomenon, such as sea ice coverage. In this work the temperatures based on empirical statistical downscaled (ESD) projections from global CMIP5 models and the RCP scenarios are used. ESD takes into account both geographical systemic effects and large-scale conditions (Hanssen-Bauer et al., 2019). Predictions are done for different land areas in Svalbard, and the results are divided into medium (median), low (5% percentile) and high (95% percentile) of the absolute change in air temperatures using the 1971–2000 period. To apply the future change in AT in the TEMP/W model the medium ESD predictions for Svalbard land area are used. Simulations will be done with an RCP2.6 and RCP8.5 scenario. The projected temperature change from the report are temperature changes from 1971–2000 to 2071–2100 and is a change for a 100-year period. The change in annual MAAT is given and the average increase for each season divided into periods of three months is given as shown in Table 8.1. To implement these temperature changes into the surface temperature curve in the TEMP/W model the temperature for a month will be increased with 1/10 of the projected temperature for that month every 10th year. The temperature is added to the monthly average AT from the Adventdalen series. This is done from the initial model of 2018 and continued for 100 years to 2118 where temperatures have increased with the values given in Table 8.1. That means that The MAAT with RCP2.6 scenario will increase with a total of 3.8°C and the RCP8.5 scenario with 9.5°C and applying this to the MAAT for Adventdalen in 2018 will give a MAAT of 1.9°C and 7.6°C respectively in 2118.

8.2 Model Results

8.2.1 Initial Model

Model results are plotted together with the temperature profile from thermistors measurements to compare the model results to the actual conditions. It is desirable that the model reproduce a similar temperature profile to the measured. Also, the temperature profile from model simulations should not change significantly from one year to the next when the same boundary conditions are used. Figure 8.3 shows temperature profiles adapted from simulations with the monthly average temperatures from 2017–2018 applied at GS. Simulations for the three first years show that down to about 8 m depth the first year is warmest the profiles shift slightly towards colder temperatures over time. Below 9 m the temperatures are colder during the first year of simulations but move towards warmer temperatures. The difference is largest around

12 m depth and there is almost no difference at 30 m depth. When comparing the temperature profiles from the three first years to the tenth year, the same situation is seen, but with a larger difference in temperature. At 5 m depth and 12 m depth the difference between the first and tenth year is approximately 0.5°C. Furthermore, the temperature fluctuations go deeper during the first years. The air temperatures for 2017–2018 from Adventdalen have a MAAT of –1.9°C. The temperature at 30 m is –3.9°C. The average temperature at the top is warmer than the temperatures in the soil below. If the average temperature at the top is kept constant, the ground below will be warmed towards the average temperature at GS. A complete steady state will not be achieved before the whole profile has reached the average temperature at GS. A simulation was run to check how long time it takes to reach this steady state. After 100 years the temperature at 30 m increased with about 0.8°C. After 500 years, the temperature approached –1.9°C. Hence, it takes a very long time before the temperatures at around 30 m depth increase. With the initial model after 10 years the temperature at 30 m has not changed and is still –3.9°C and can therefore be used as an initial condition.

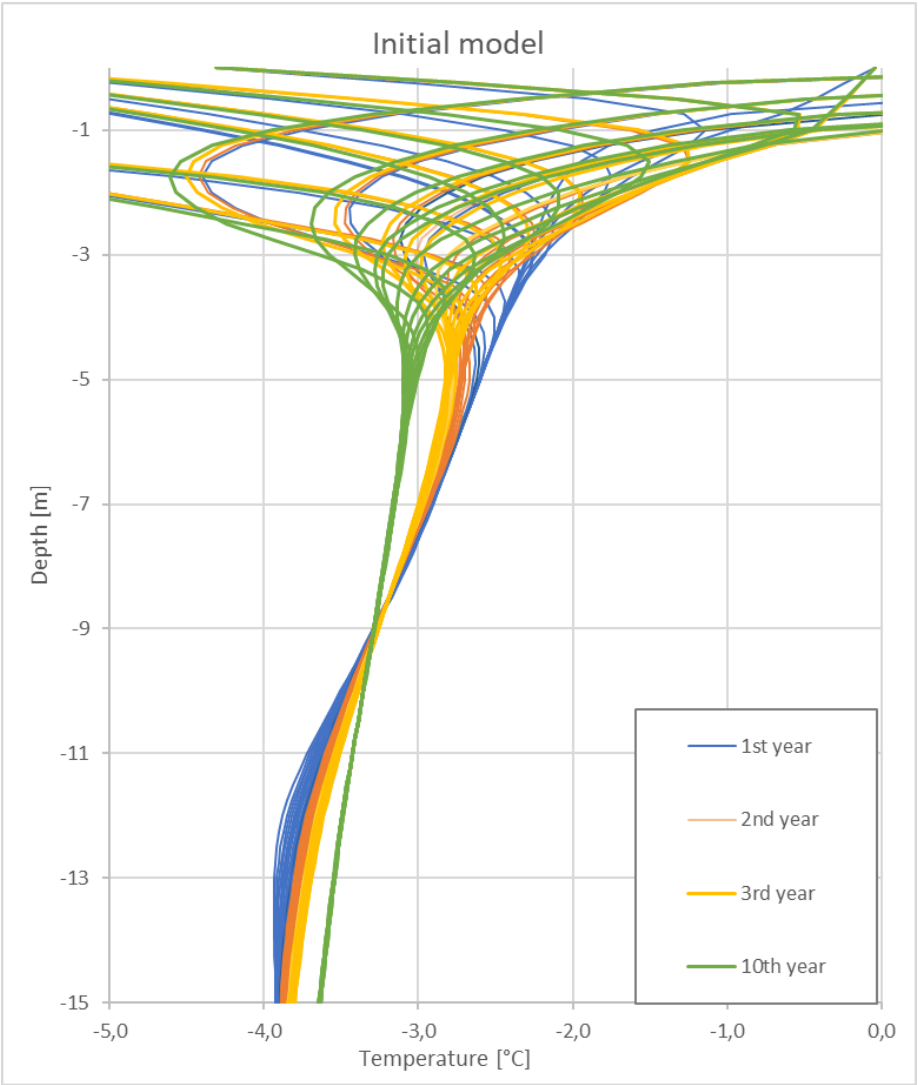

Figure 8.3: *Temperature profiles from model simulations for a 10 year period, the same ground surface temperature curve is applied. The curves are shown for the 1st, 2nd, 3rd and 10th year.*

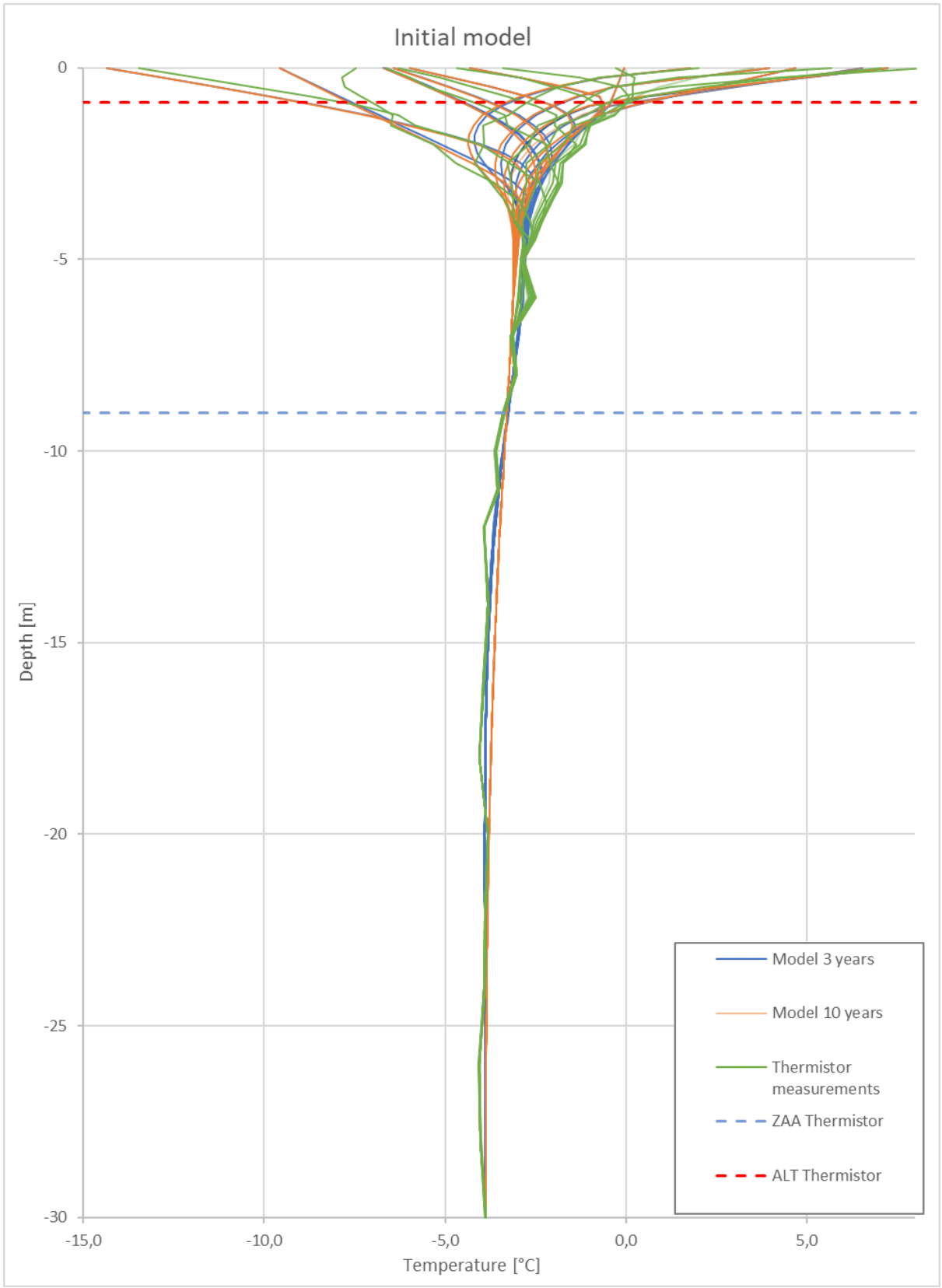

Figure 8.4: *Comparison of the temperature profile from thermistor measurements and model simulations for the 3rd and 10th year. For the model simulations average air temperatures for 2017–2018 are applied. Depth of ZAA and ALT for the thermistor profile is indicated.*

In Figure 8.4 the model simulations for third and tenth year are compared with the temperature profile from thermistor measurements. The irregularities of the thermistor temperature profile make it difficult for precise comparison with the smooth profiles from simulations. However, it can be observed that from about 1 m to 5 m depth the thermistor measurements are warmer than the predictions by the model. The simulated temperature variations in the upper part of the soil and the almost constant temperatures below 5 m depth seem to fit well with the thermistor profile. The difference between the profiles from simulations and from measurements are small, and both the 3rd year and 10th year curves are seen as a sufficient fit with the thermistor curve. The future predictions will be applied to the model after it has run for 10 years and will be referred to as the initial state.

In Figure 8.4 the AL and ZAA found from thermistor measurements are indicated as lines. AL thickness is at 0.9 m depth from thermistor measurements and at 1 m depth in the model after 10 years run time. The ZAA is at 9 m in the thermistor profile, determined by where there is less than 0.1°C change throughout the year. In the model this is at 7 m. The temperature at the bottom of the profile (30 m) is –3.9°C for both thermistor and model. The comparison of temperature profiles shows that the simulated profile fit well with the measured temperature profile and this is an indication that the model can be used to simulate the present and future conditions of the ground thermal regime.

8.2.2 Future Ground Temperature Profiles

The projections for future ground temperature profiles are found by performing model simulations where the climate scenarios presented in Subsection 8.1.4 are applied as temperature increase in the average monthly temperatures applied at GS in the model. The monthly average is increased with 1/10 of the projected temperature changes every 10th year. This is a simplification as the temperature change will not happen stepwise, nor linearly, but it is done in a stepwise way here as to be able to predict how the ground thermal regime could develop.

First, the RCP2.6 scenario was applied as a temperature curve at GS for 100 years. The temperature profile after 50 years and 100 years with simulation of the RCP2.6 scenario is shown in Figure 8.5. The orange profile shows the initial profile which represent how the conditions are today. The blue profile is the temperature profile after 50 years with the RCP2.6 scenario and from the profile it is seen that the ALT will increase with 0.5 m. That is an average increase of 1 cm/year. The depth of ZAA decrease and change from 7 m to 5 m. The temperature at 30 m will increase with 0.4°C from –3.9°C to –3.5°C. As Figure 8.5 shows, winter temperatures increase significantly more than summer temperatures. The trumpet curve shifts toward the right and warmer temperatures. The shift of the curve is larger in the upper meters than at the bottom, but after 50 years the near-surface-permafrost is still frozen. 50 years with emissions from the RCP2.6 scenario is not critical for the ground thermal regime.

As Figure 8.5 shows, the changes in the ground temperatures are a lot more drastic after 100 years with the RCP2.6 scenario. The temperature profile indicates a large increase in ALT, with 4.3 m increase from the initial state in 2018. The rate of increase in ALT increase from 1 cm/year for the first 50-year period (2018–2068) to 7.6 cm/year the second 50-year period (2068–2118). The depth to ZAA increase drastically from 7 m depth to a depth of 17.5 m. The temperature at 30 m depth has increased to –3.0°C. This is almost 1°C increase from the initial year.

Secondly, the RCP8.5 scenario was applied to the model. Figure 8.6 shows the temperature

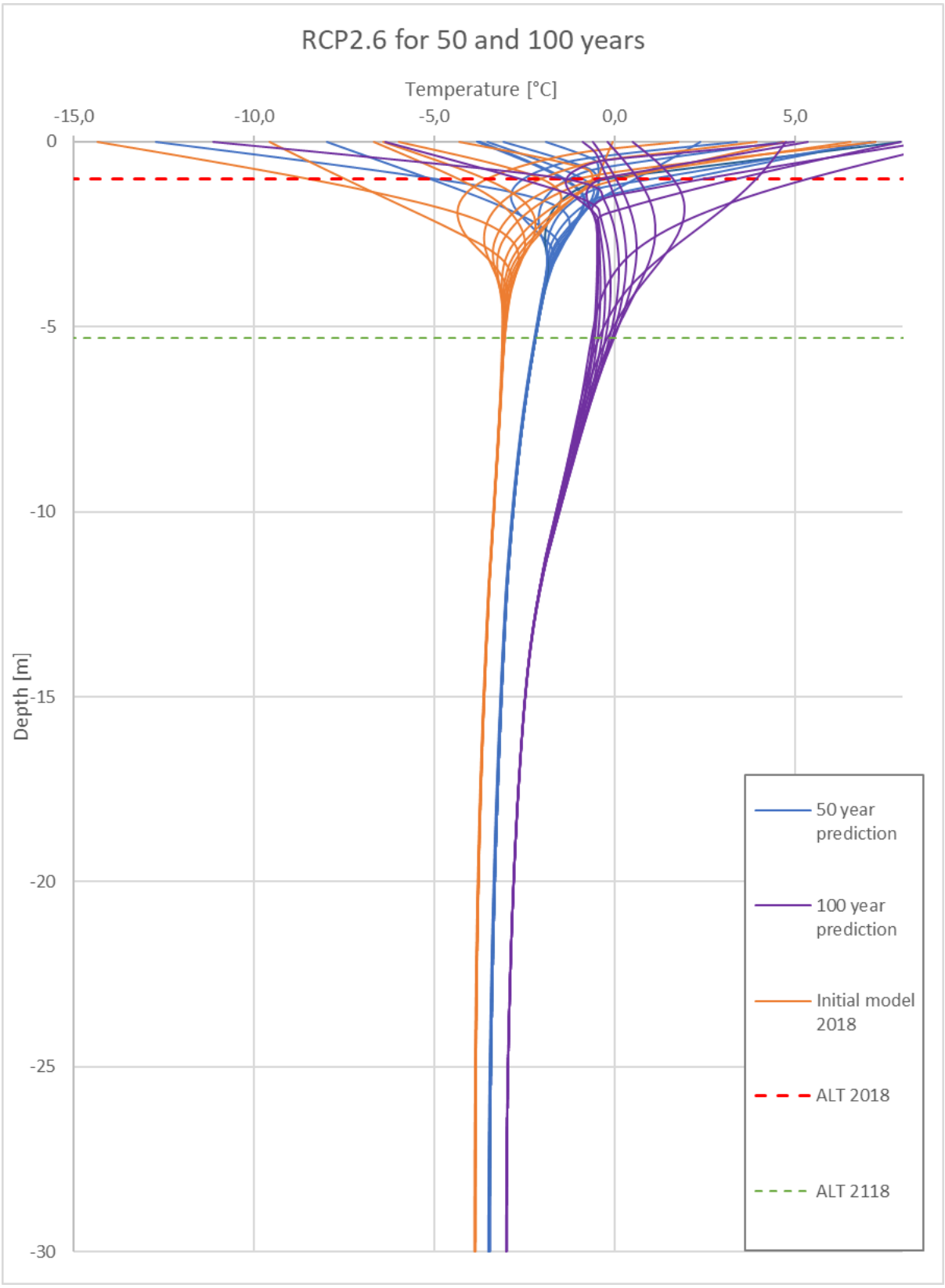

Figure 8.5: *Ground temperature profiles, initial state and situation after 50 years and 100 years applying emission scenario RCP2.6.*

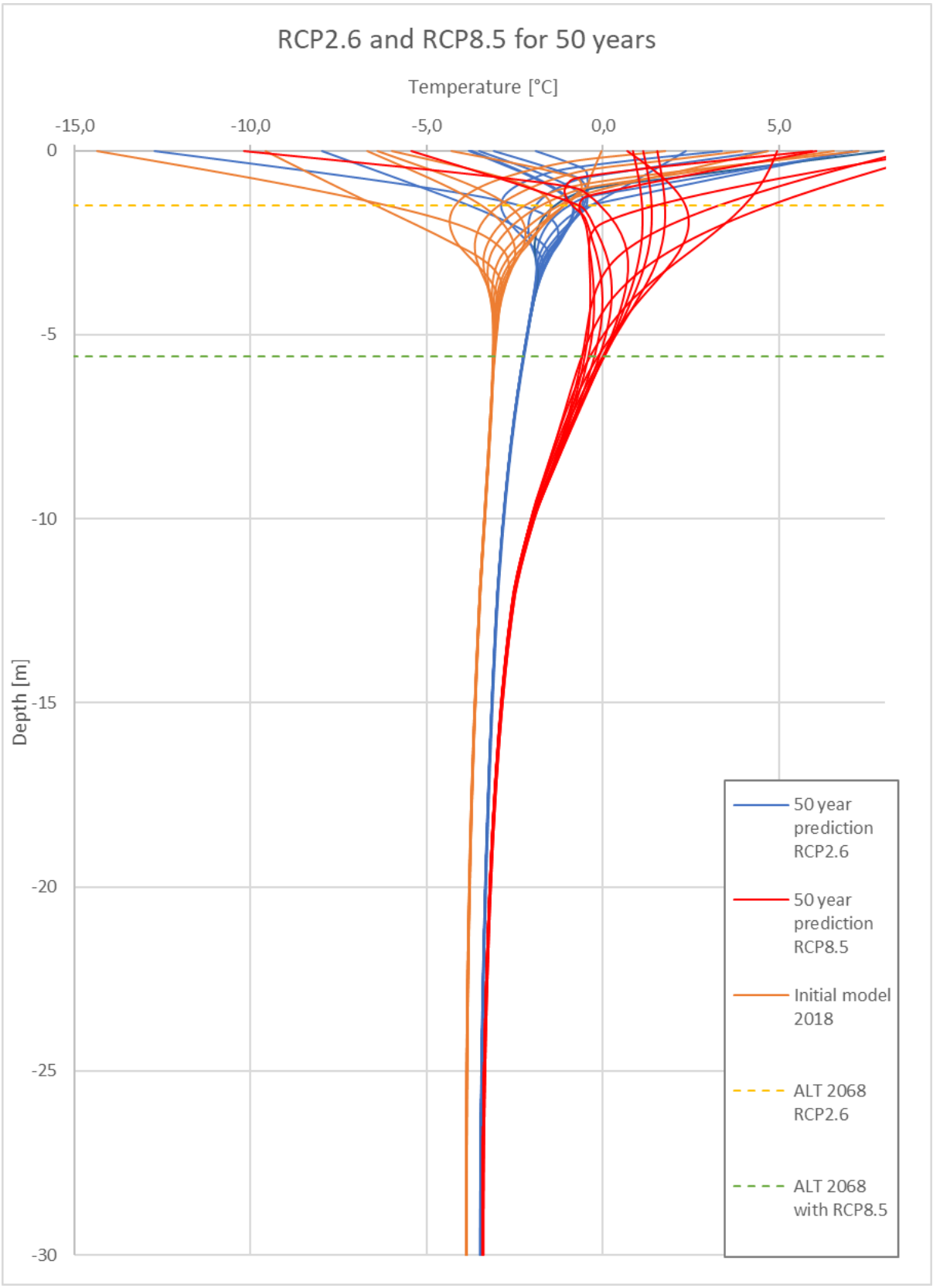

Figure 8.6: *Ground temperature profiles, initial state and situation after 50 years using emission scenarios RCP2.6 and RCP8.5.*

profile after 50 years from simulation with the RCP2.6 and RCP8.5 scenarios. The temperature profile after 50 years with RCP8.5 is similar to the profile after 100 years with RCP2.6. The difference is that the RCP8.5 scenario has a slightly larger shift in the top of the profile, but the temperatures at 30 m depth has not changed as much as after 100 years with the RCP2.6 scenario. The change at 30 m depth is almost the same after 50 years with RCP 2.6 and 8.5 and is –3.5°C. The RCP8.5 scenario give an ALT increase of about 10 cm/year.

8.2.3 Sensitivity Analysis

A sensitivity analysis was performed to evaluate the model sensitivity to changes in the soil parameters. This is done by changing the freezing point (FP) of the soil material and the UWC curve and the thermal conductivity curve is adapted accordingly. First, the FP is increased with 1°C, which means that the FP is increased from approximately –2°C to –1°C. Another analysis is done by decreasing the FP with 1°C and shifting the curves to a FP approximately at –3°C. The simulations are run with the boundary conditions of air temperatures for the RCP2.6 scenario for simulation with original properties and properties with shift in temperatures. For the scenario where the UWC curve and thermal conductivity is shifted by adding 1°C the temperature where freeze and thaw occur in the soil is shifted, as shown in Figure 8.7. With a positive shift the FP occur at a higher temperature which means that less heat is needed to warm the soil at negative temperatures because it's mostly ice that needs to be heated and the phase change and addition of latent heat happen at a higher temperature. The depth of annual temperature fluctuations is larger for the scenario with shifted temperatures. This is because most of the thermal energy is used to heat ice instead of contributing to phase change of ice when the FP temperature is increased. When less heat is needed for phase change the temperature fluctuation goes deeper. This is also the reason why the deep permafrost (20–30 m) is warming up at a faster rate than in the original profile. Less heat is needed to warm up ice and when the UWC and FP is shifted to higher temperatures, the ice must be warmed to higher temperatures before the need of latent heat will slow down the warming. For the original temperature profile temperatures are much closer to the melting point. The rate of warming is slower because latent heat is needed to melt the ice before further warming can happen. Less heat is available to heat the soil below where the phase change occurs and thus temperatures change less below the AL. Increasing the FP and UWC would give a less critical state of the permafrost since present temperatures would be further away from the melting point and more warming must occur to reach a critical state.

Another sensitivity analysis was performed by shifting the UWC curve and the thermal conductivity curve with –1°C. A negative shift changes the FP so that it is lower than it was before. This means that most of the phase change happen at a lower temperature and a lot of latent heat must be added to melt all the ice at a lower temperature than before. When the ice is melted the permafrost has thawed and further warming of the soil will happen at a faster rate above the FP. The critical temperature concerning soil strength will be lower. Figure 8.8 shows that since the critical temperature is lower, the upper part warms faster once the freezing point depression is reached. Deeper down, the temperature change happens at a slower rate since the temperature is closer to the melting point and more latent heat is needed for temperature increase since a larger amount of ice must be melted. The initial and shifted curve are similar in the upper part of the profile, but the melting point is at a lower temperature for the shifted curve, which means that the soil in the shifted curve has thawed to a greater depth and the temperature fluctuations go down to this depth. In the thawed depth, only water is cooled

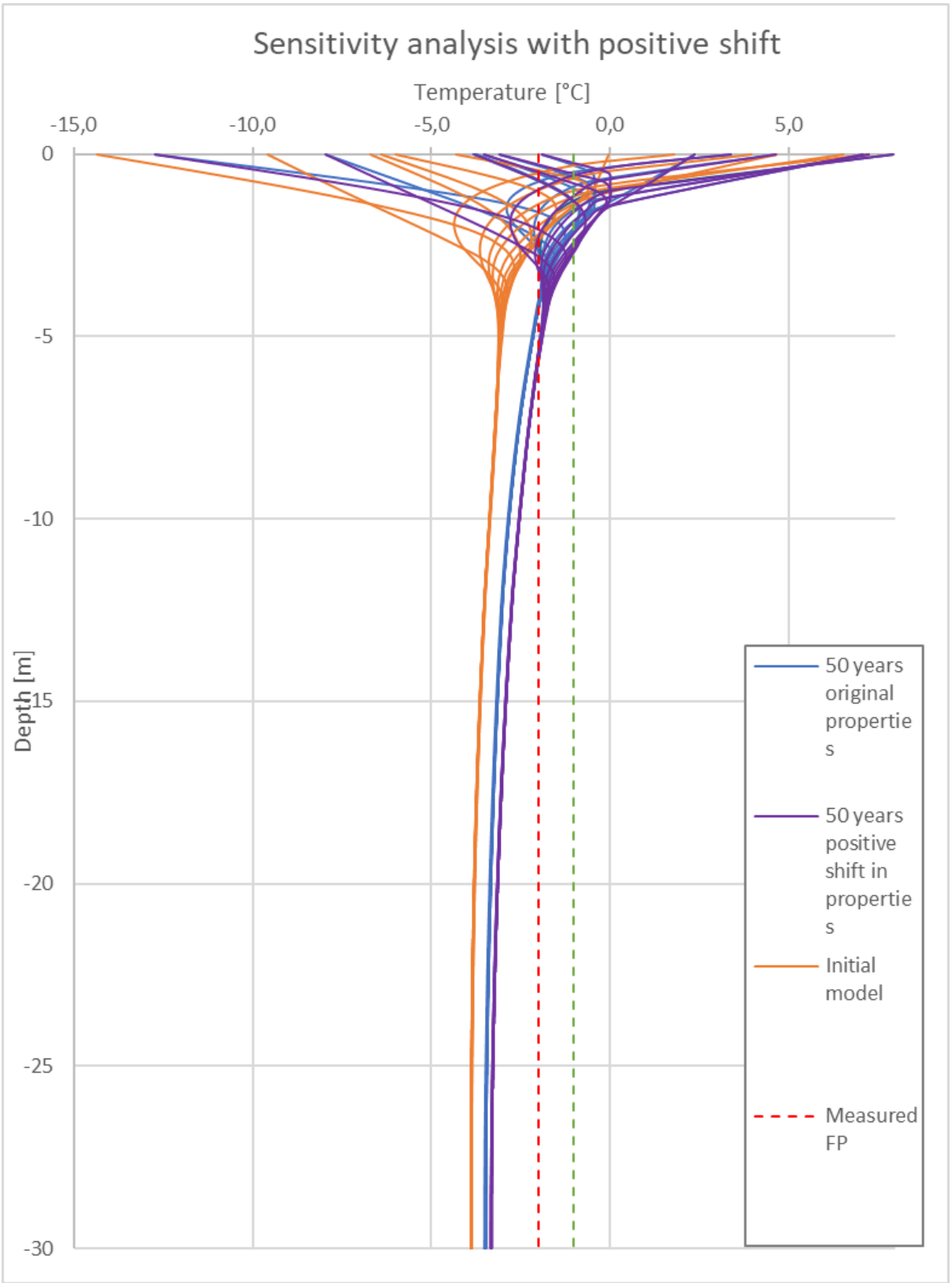

Figure 8.7: *Increasing the temperature of the UWC curve and thermal conductivity by +1°C shows the sensitivity of soil model to change in soil properties. The RCP2.6 scenario is used as boundary condition over 50 years.*

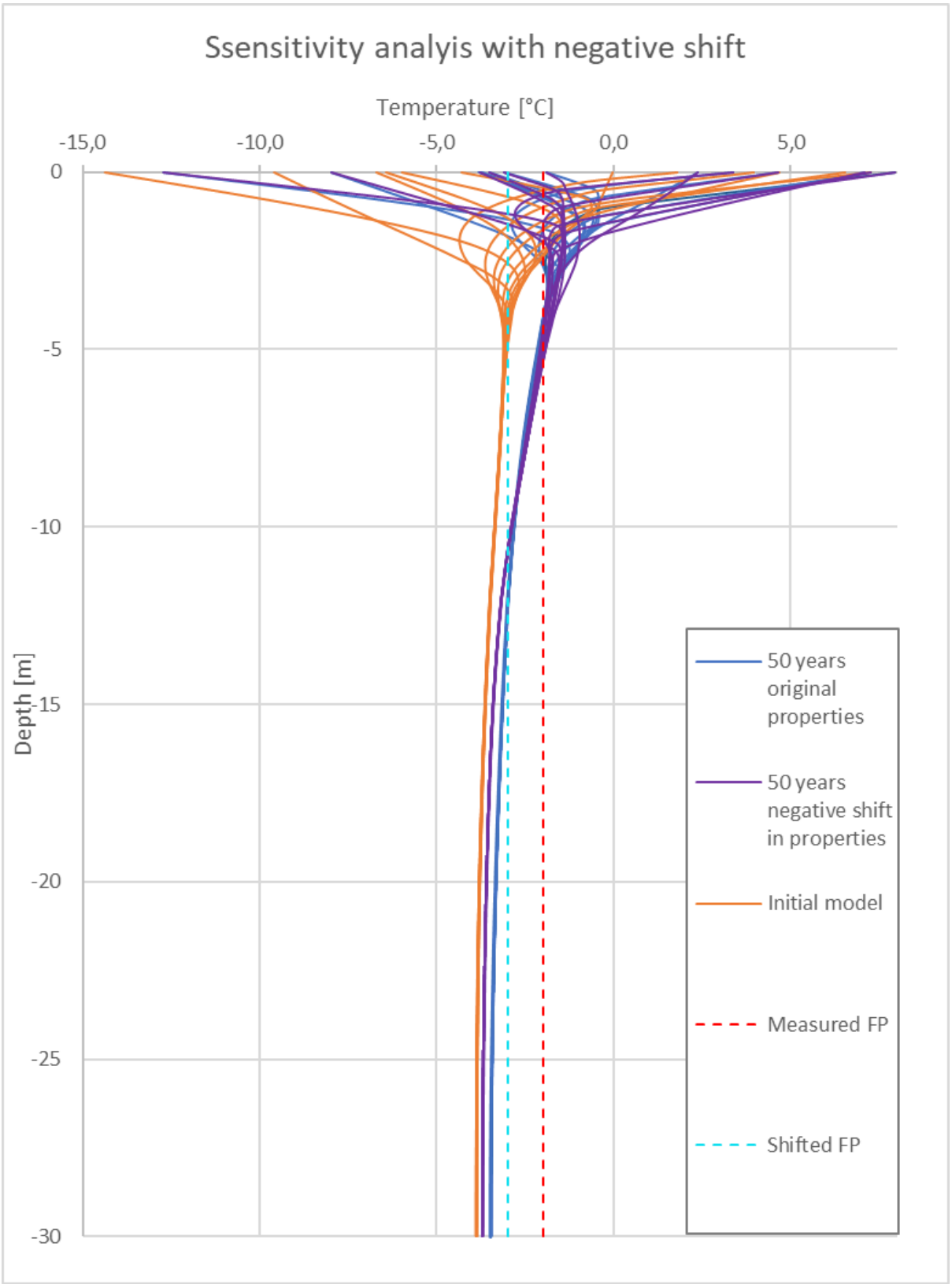

Figure 8.8: *Increasing the temperature of the UWC curve and thermal conductivity by –1°C shows the sensitivity of soil model to change in soil properties. The RCP2.6 scenario is used as boundary condition over 50 years.*

and thawed. A negative shift of the curves would give a more critical state of the present permafrost since the present state would be closer to the melting point, the AL would be thicker and bearing capacity of existing piles would be drastically less than it is today.

8.3 Discussion

The emission scenarios RCP2.5 and RCP8.5 predicts increase in AT and the model simulations give an indication of how AT will affect the ground thermal regime. Increase in AT cause higher MAAT and the top of the ground temperature profile shifts toward right and warmer temperatures near the surface. The predictions for AT estimates that winter and spring temperatures will increase more than summer and autumn temperatures. This is clearly seen at the GS in Figure 8.5 where the difference in negative temperatures are much larger than for the positive temperatures between the three different profiles. With the RCP2.6 most months that previously had average monthly temperatures below 0°C will continue to be negative, the exception is that October temperatures will be positive after 50 years and November temperatures will be positive after 100 years. The increase in temperatures will cause a big change in freezing index. For the initial scenario with MAAT of –1.9°C, the freezing index is 1434°C days and the thaw index 729°C days. After 50 years with RCP2.6 scenario the freezing index is 1002°C days and thawing index 988°C days. After 100 years with RCP2.6 scenario the freezing index is 586°C days and thawing index 1263°C days. The freezing and thawing indexes indicate the duration and magnitude of days respectively below and above 0°C. After 50 years the thawing index has increased, and some warming of the near-surface-permafrost occur, but there is still a significant amount of freezing during the year which slows the rate of warming. After 100 years the thawing index is much larger than the freezing index and this is clearly reflected in the temperature profile. The permafrost is completely thawed down to 6 m depth and temperatures at depths down to 10 m are close to the melting point.

The ALT increase with 0.5 m under RCP2.6 scenario after 50 years. The ALT is found as the depth where temperatures reach at or above 0°C. The FP in the soil is below 0°C due to the fine-grained soil and the salt content in the pore water. That means that the permafrost is thawed below 0°C and that the ALT is larger than what first indicated. With a FP of –2°C the ALT increase with additional 0.5 m. The freezing point depression also mean that the temperatures are closer to the melting point and that less warming must occur before the permafrost is thawed. It is very important to consider the salinity of the soil and the freezing point depression to see where the critical temperature in the permafrost is. The ALT should be found based on this temperature. The bearing capacity of piles founded in this soil will decrease because there will be a higher amount of UWC (unfrozen water content) in the soil and the AL has increased which means that the length where the pile is carried is reduced. However, the soil is still frozen below 2 m depth and with piles of approximately 10 m the warming after 50 years is not very critical for engineering considerations. Design life is often 50 years for establishment of new infrastructure. In comparison, the ground conditions are critical in an engineering perspective after 50 years with emission scenario RCP8.5 or after 100 years with RCP2.6 scenario. Then the permafrost down to 7–8 m depth has thawed if we consider the FP to be –2°C. With a pile length of 10 m, the whole length of the pile would be in soil with temperatures close to the melting point. It is likely that a house founded on these piles would experience loss of bearing capacity, large settlements and stability problems. For the near-surface-permafrost, the RCP2.6 and RCP8.5 give very different outcomes after 50 years. The RCP2.6 does not give drastic change, while with RCP8.5 the situation after 50

years is very critical for infrastructure. It would be necessary to increase pile lengths or use other foundation methods if infrastructure were to be placed in the soil that will experience this change in the ground thermal regime. Below 10 m depth the difference between the two scenarios are insignificant. The soil is still frozen below 10 m depth.

It is of interest to observe how the ALT change in the model. An increase in ALT and degradation of near-surface-permafrost is critical for infrastructure in permafrost areas. From the predicted RCP2.6 scenario the AL will increase with 0.5 m from 1 m to 1.5 m. This is an increase of 1 cm/year. The increase is much greater for the next 50 years. Then the increase is 7.6 cm/year to a depth of 3.8 m below the initial ALT. A borehole in lower Adventdalen has from 2000–2017 had an increase in AL of 0.6 cm/year and comparing to this the prediction of 1 cm/year for 50 years with temperature increase seem reasonable. The soil conditions in lower Adventdalen differ from the UNIS East site but consist of layers characterized as silt and clay (Gilbert et al., 2019) and can be compared to the UNIS East site in this matter. In a bedrock borehole at Kapp Linne ALT has been observed to increase with 6.2 cm/year the last ten years (Hanssen-Bauer et al., 2019). The heat conduction in bedrock is very different from that in a fine-grained soil and should not be directly compared. Calculations by Instanes and Rongved (2017) on the ground conditions in Longyeardalen suggest an ALT increase from 1.5 m to 2.5 m by the end of the century with a RCP4.5 emission scenario. They emphasize that warming rates are efficiently reduced due to the high ice content in the fine-grained material and the amount of latent heat that must be added for melting the ice. The projected ALT at the end of the 100-year scenario is high, 5.3 m, compared to the findings by (Instanes & Rongved, 2017). At the UNIS East site, the upper 2.5 m consist of coarser material. The measured water content in these samples was lower than in the samples below. This can be wrong because the samples were not intact and might not contain the original water content when the sample is tested. With less ice present the warming will happen faster and this can cause an overestimation of the warming rate in the top layer of the soil. In the model the water content is lower in the top 2.5 meter and can be one of the reasons why the ALT is so large at the end of the scenario. Furthermore, it is important to observe how the temperature profile in the near-surface region will develop and to depths where infrastructure will interfere (around 10 m depth). At 10 m depth temperatures increase with 0.5°C from –3.3°C to –2.8°C in the 50-year scenario and increase with 1.8°C to –1.5°C in the 100-year scenario. For the temperature at 30 m the temperatures increase from –3.9°C to –3.5°C and –3°C. The prediction of temperatures below 10 m coincide with findings by (Instanes & Rongved, 2017). They found that temperatures below 10 m will increase slower and at 20 m depth temperatures will increase from –4°C to between –2°C to –3°C by 2100.

The rate of warming of soil is different at different temperatures. At very low temperatures most of the water in the soil is frozen and most of the thermal energy goes into warming the ice. When temperatures increase part of the ice must be melted to heat the soil. The UWC curve describes how much ice that must be melted at different temperatures. When temperatures increase towards the melting point, the rate of warming decrease. This can be explained because the UWC curve is steep close to the FP and the amount of ice that must be melted increase as temperatures get closer to the FP. The reason why the rate of temperature change decrease when more ice must be melted is that large amounts of of latent heat are needed for the phase change of ice to water. The thermal energy goes into the phase change instead of increasing the temperatures. When the melting point is reached the rate of warming increase considerably, because all thermal energy goes into heat increase and additional latent heat of fusion is not needed.

The effect of energy consumption at phase change was tested by altering the value of latent heat in the model. The model with the temperature curve for 2017–2018 was run with different values for the latent heat for 500 years. In the first simulation the value for latent heat of fusion was 334 kJ/kg and for the second simulation the value was adjusted to 100 kJ/kg. For the first simulation with the original latent heat of fusion the bottom temperature increased with 0.8°C over 100 years and for the second simulation the increase was 1.5°C at 30 m depth. The increase was almost twice as large when the latent heat of fusion is reduced. After 500 years the bottom temperature in the first simulation had not yet reached the MAAT applied at the top, but was –2.1°C. With the altered latent heat of fusion, the temperature at 30 m depth reached that of the MAAT (–1.9°C) already after 300 years.

The model of the ground thermal regime in permafrost soil set up in TEMP/W is as discussed, a simplification of the real soil profile and approximations are done to be able to perform simulations of different scenarios. The soil is modelled based on experimental investigations and calculations. These may differ from the real soil profile. The soil is represented by investigations of soil down to 10 m depth. More experiments of the soil below this depth should have been performed for a better approximation of the soil profile. In addition, the influence of salt on the freezing point depression and thus the thermal properties are very important. This study has found some indications on how salt content, freezing point depression and thermal properties are related. Further studies need to be performed for more precise determination.

The GS boundary condition is very important for how the ground thermal regime is simulated in the model. It should be further investigated how to best approximate GST in the model. The boundary conditions should be based on average temperatures from measurements over a longer time period than was used in this project. It would also be beneficial to have longer time series of thermistor measurements for a better view on how the real ground thermal regime develop and for better comparison with model results.

Chapter 9

Conclusions and Recommendations for Further Work

9.1 Summary and Conclusions

Thermal properties of soil can be determined as functions of temperature and establishing the curve of unfrozen water content is important in this process. Measurements of thermal properties with the KD2 Pro give values for unfrozen and frozen thermal conductivity and volumetric heat capacity, but measurements with the probe fail to give accurate measurement results at the freezing point (FP) temperatures and about 5°C below the FP. Values for thermal conductivity measured by the probe and values estimated with soil properties from index testing used in empirical formulations are compared, and the empirical formulations does not seem to correlate with measurements. Kersten's empirical formulation predicts thermal conductivity values about 0.2 W/mK higher than with the Johansen formulas. The empirical formulation by Johansen depend on correct determination of unfrozen water content. There is an indication that measured values are higher than those determined by empirical formulations, but this trend is inconsistent.

The unfrozen water content is determined by a generalized Clapeyron equation with measurements of soil water potential, salinity of soil samples and water content. When two phases coexist, the chemical potential of these two phases must be in equilibrium. When unfrozen water exists in soil at negative temperatures, the unfrozen water must be in equilibrium with the pore ice. The water potential of the unfrozen water is used to determine the temperature of this coexistence which is the FP. First, the FP caused by the matric potential from adsorption and capillary forces is calculated. Secondly, the FP caused by the osmotic potential is calculated. Furthermore, the FP caused by both matric and osmotic potential is calculated. The FP calculated with the Clapeyron equation agrees well with measured freezing points. For the saline permafrost soil, the salinity is the most important factor for the freezing point depression. With a salinity of about 30 ppt the FP is depressed with approximately 2°C. The osmotic potential caused by the solutes in the pore water decrease when temperatures decrease. The matric potential increase when the saturation decrease as more water is transformed to ice. The osmotic potential is the dominating potential at the FP, but for the soil from UNIS East, it was found that between –5°C and –10°C the matric potential exceeds the osmotic potential. The osmotic potential is negligible when it is exceeded by the matric potential. The matric potential is the reason why part of the pore water remains unfrozen even at temperatures below –10°C.

Estimations show that 5% of the water content can still be unfrozen at –10°C. The estimation of the water content is more uncertain at negative temperatures below this. Direct measurements of the unfrozen water content below the FP were not performed and it is therefore difficult to evaluate the estimated curve of unfrozen water content, but estimations show good agreement with unfrozen water content curves estimated by (Zhou et al., 2018).

When the curves for unfrozen water content are calculated, a function relating volumetric heat capacity and temperature can be directly calculated since the amount of substance at each temperature is known. The empirical formulation by Johansen includes amount of frozen and unfrozen water content in the estimations and is used to establish the temperature dependent thermal conductivity curve. A model based on the estimated functions for unfrozen water content and thermal properties has been set up in the finite element program Geostudio 2018 and the TEMP/W analysis tool is used. The thermal conductivity values from empirical formulation deviate from the measured values, but the deviation is considered to have no major influence on the results in the model. The predictions of the ground temperature profile at the UNIS East site in 50 years under a RCP2.6 scenario show that the active layer will increase with about 0.5 m and that the near-surface-permafrost will still be frozen, and the conditions are not critical when concerning infrastructure. After 100 years with emission scenario RCP2.6 or 50 years with emission scenario RCP2.6 simulations indicate thawing of the near-surface-permafrost down to about 6 m depth and ground temperatures are close to the melting point down to 10 m depth. These are very critical conditions, and it is not likely that existing infrastructure can sustain these changes. The permafrost below 10 m depth will take a considerably longer time to warm and thaw, but temperatures will increase also below 10 m depth. The results from simulations with different scenarios give a big variation in the outcome. It is therefore important to use the most likely scenario of future emissions and climate change when predicting change in the ground thermal regime for engineering considerations.

A sensitivity analysis of how the rate of temperature change in the ground is affected by change in the FP and SFCC is performed. The shift of the FP determines the starting point and shift of the SFCC curve, and the shift of the SFCC will cause a shift in the curve relating thermal properties to temperature. The AL should be determined at the temperature of the initial FP and this is below 0°C for saline and fine-grained soil. The main reason why it is important to have the freezing point depression and the SFCC determined correctly is that they determine the amount of latent heat needed to melt the amount of ice determined by the curve. The latent heat needed for phase change of ice to water slows the rate of warming. Therefore, the SFCC is very important in simulations of how the rate of temperature change in the ground thermal regime will happen. If the latent heat and phase change effect is not accounted for in a transient analysis, the rate of ground thermal change will be greatly over estimated. The effect of adsorption and capillary forces related to particle size and the effect of salt content are important in determination of the SFCC and these effects must be considered when modelling the ground thermal regime of permafrost soil.

9.2 Recommendations for Further Work

Further research within the topics presented in this thesis is necessary to further develop the methods used and more testing must be performed to be able to assess the applicability and effectiveness of the methods. Here are some recommendations on what needs to be done to advance in the field.

- A standard procedure for measurements of thermal properties with the KD2 Pro in frozen soil should be developed. The effect of phase change should be included in the device algorithm to be able to do measurements at and below freezing temperature. Extensive testing should be performed to obtain measurement data to verify the test. Measurement results should be compared with results from other methods of thermal properties, e.g. the guarded hot plate method, to validate the KD2 Pro as a sufficient measurement method. Effective medium theory should be investigated as a method for efficient estimation of thermal conductivity.
- A standard procedure for measurements of water potential should be developed. More testing with the WP4C Dew Point PotentiaMeter should be performed on different soil types to get a better understanding of the effect of solutes and fines on the pore water potential. Salinity measurements should be taken of the soil samples used in the potential measurements to obtain correct salinity and osmotic potential. It was difficult to distinguish the matric potential from the measured total potential and studies should be made to determine a way for more precise prediction of the matric potential.
- It is necessary to perform the estimation of the FP and unfrozen water content based on the matric and osmotic potential for more soil samples with variety in soil composition, water content and solute content to be able to validate the method. It is necessary to perform experimental testing to measure the FP and unfrozen water content in the samples used in the estimation to be able to verify if the method give precise predictions of these values.
- It should be attempted to take measurements of the GST, e.g. by placing a thermistor just below the surface and obtain continuous measurement series. This could give a better understanding of how air and ground surface temperatures are correlated. This correlation should be implemented in the model and would be a better approximation of the real conditions than with applying air temperatures. In addition, temperature curves applied as boundary conditions and temperature profiles from thermistors used for comparison should be based on average temperatures for several years rather than for a single year. This would give a better representation of the average temperatures at the site. It should be investigated how predictions of future climate change and rise in air temperatures could be implemented in a more precise way in the boundary conditions. Including the geothermal heat flux in the model could give a different outcome in the simulations and this effect will be important to include if permafrost temperatures at depths below ZAA are to be studied. Increasing the number of layers representing the soil will give more precise predictions of the ground thermal regime if that is found necessary.

References

Aleksyutina, D., & Motenko, R. (2017, 01). Composition, structure and properties of frozen and thawed deposits on the baydaratskaya bay coast, kara sea. *Earth's Cryosphere*, *21*, 13-25. doi: 10.21782/KZ1560-7496-2017-1(13-25)

Andersland, O. B., & Anderson, D. M. (1978). *Geotechnical engineering for cold regions.* McGraw-Hill Inc.

Andersland, O. B., & Ladanyi, B. (2004). *Frozen ground engineering* (second ed.). New Jersey: John Wiley & Sons.

Anderson, D. M., & Morgenstern, N. R. (1973, 07). Physics, chemistry, and mechanics of frozen ground: A review. In *North american contribution. 2nd international conference on permafrost, yakutsk, ussr* (p. 257-288).

Anisimov, O. A., & Nelson, F. E. (1995). Permafrost distribution in the northern hemisphere under scenarios of climatic change. *Global and Planetary Change*, *14*(1), 59–72.

Bing, H., & Ma, W. (2011). Laboratory investigation of the freezing point of saline soil. *Cold Regions Science and Technology*, *67*(1), 79 - 88. Retrieved from `http://www.sciencedirect.com/science/article/pii/S0165232X11000425` doi: https://doi.org/10.1016/j.coldregions.2011.02.008

Black, P. B., & Tice, A. R. (1989). Comparison of soil freezing curve and soil water curve data for windsor sandy loam. *Water Resources Research*, *25*(10), 2205-2210. Retrieved from `https://agupubs.onlinelibrary.wiley.com/doi/abs/10.1029/WR025i010p02205` doi: 10.1029/WR025i010p02205

Bratlie, U. H. H. (2018). *An experimental study of thermal properties of permafrost soils* (Unpublished master's thesis). Norwegian University of Science and Technology, Department of Civil and Environmental Engineering.

Brown, J., Ferrians, O. J., Heginbottom, J., & Melnikov, E. (1997). *Circum-arctic map of permafrost and ground-ice conditions.* Washington, DC: U.S. Geological Survey in Cooperation with the Circum-Pacific Council for Energy and Mineral Resources.

Campbell, G. S., Smith, D. M., & Teare, B. L. (2007a). Application of a dew point method to obtain the soil water characteristic. *Global and Planetary Change*, *14*(1), 59–72.

Campbell, G. S., Smith, D. M., & Teare, B. L. (2007b). Application of a dew point method to obtain the soil water characteristic. In T. Schanz (Ed.), *Experimental unsaturated soil mechanics* (pp. 71–77). Berlin, Heidelberg: Springer Berlin Heidelberg.

Decagon Devices, I. (2016). Operators manual kd2 pro [Computer software manual].

Decagon Devices, I. (2018). Operators manual wp4c [Computer software manual].

Engås, C. (2018). Første rettsak om gamle sykehuset. *Svalbardposten. Available at: https://svalbardposten.no/nyheter/forste-rettssak-om-gamle-sykehuset/19.10172 (access: 17. December 2018).*

Etzelmüller, B., Schuler, T. V., Isaksen, K., Christiansen, H. H., Farbrot, H., & Benestad, R. (2011). Modeling the temperature evolution of svalbard permafrost during the 20th and 21st cetury. *The Cryosphere Discuss*, *5*.

Farouki, O. T. (1981a). Evaluation of methods for calculating soil thermal conductivty. *CRREL Report*, *82-8*.

Farouki, O. T. (1981b). *Thermal properties of soils.* Hanover, New Hampshire: U.S. Army Cold Regions Research and Engineering Laboratory.

Farouki, O. T. (1981c). The thermal properties of soils in cold regions. *Cold Regions Science and Thechnology*, *5*(1), 67–75.

Førland, E. J., Benestad, R., Hanssen-Bauer, I., Haugen, J. E., & Skaugen, T. E. (2011). Temperature and precipitation development at svalbard 1900–2100. *Advances in Meteorology*, *2011*(1). (doi: 10.1155/2011/893790)

GEOSLOPE International Ltd. (2017). Heat and mass transfer modeling with geostudio 2018 (Second Edition ed.) [Computer software manual].

Gilbert, G. L., Instanes, A., Sinitsyn, A. O., & Aalberg, A. (2019). Characterization of two sites for geotechnical testing in permafrost: Longyearbyen, svalbard. *AIMS Geosciences*, *In press*(.). (.)

Gong, L., Wang, Y., Cheng, X., Zhang, R., & Zhang, H. (2013). A novel effective medium theory for modelling the thermal conductivity of porous materials. *International Journal of Heat and Mass Transfer*, *68*(1), 295–298.

Hanssen-Bauer, I., Førland, E., Hisdal, H., Mayer, S., Sandø, A., Sorteberg, A., ... Wong, W. K. (2019, 02). *Climate in svalbard 2100 - a knowledge base for climate adaptation* (Tech. Rep. No. 1/2019). NCCS. doi: 10.13140/RG.2.2.10183.75687

Hjort, J., Karjalainen, O., Aalto, J., Westermann, S., Romanovsky, V. E., Nelson, F. E., ... Luoto, M. (2018). Degrading permafrost puts arctic infrastructure at risk by mid-century. *Nature Communications*, *9*(5147).

Hong, W.-T., Jung, Y.-S., Kang, S., & Lee, J.-S. (2016, 12). Estimation of soil-water characteristic curves in multiple-cycles using membrane and tdr system. *Materials*, *9*, 1019. doi: 10.3390/ma9121019

Instanes, A., & Rongved, J. L. (2017). *Forventede klimaendringers paavirkning paa byggegrunn i longyearbyen-omraadet* (Tech. Rep.). Statsbygg Report Nr. IAS2171-1.

Isaksen, K. (2001). *Past and present ground thermal regime, distribution and creep of permafrost - case studies in svalbard, sweden and norway* (Dr. Scient.). University of Oslo.

Isaksen, K., Vonder Mühll, D., Gubler, H., Kohl, T., & Sollid, J. L. (2000). Ground surface-temperature reconstruction based on data from a deep borehole in permafrost at janssonhaugen, svalbard. *Annals of Glaciology*, *31*.

Øistein Johansen. (1975). *Thermal conductivity of soils* (Ph.D. diss). Norwegian Technical University, Trondheim; also, U.S. Army Cold Regions Reasearch and Engineering Laboratory Transl. 637, July 1977.

Istomin, V., Chuvilin, E., & Bukhanov, B. (2017, 12). Fast estimation of unfrozen water content in frozen soils. *Earth's Cryosphere*, *21*, 116-120. doi: 10.21782/EC1560-7496-2017-6(116-120)

Istomin, V., Chuvilin, E., Bukhanov, B., & Uchida, T. (2015, 09). A method for determination of water content in real and model porous media in equilibrium with bulk ice or gas hydrate.

Larsen, J. O. (2016). *Skredsikring og fundamentering i permafrost* (Tech. Rep.).

M. Anderson, D., & R. Tice, A. (1972, 01). Predicting unfrozen water contents in frozen soils from surface area measurements. *Highw Res Rec*, *393*, 12-18.

Nordli, O., Przybylak, R., Ogilvie, A. E., & Isaksen, K. (2014). Long-term temperature trends and variability on spitsbergen: the extended svalbard airport temperature series, 1898–2012. *Polar Research*, *33*(1). Retrieved from `https://doi.org/10.3402/polar.v33.21349` doi: 10.3402/polar.v33.21349

Nybo, M. S. (2017). *An experimental study of unfrozen water content in fine grained permafrost soils* (Unpublished master's thesis). Norwegian University of Science and Technology, Department of Civil and Environmental Engineering.

Pietrak, K., & Wisniewski, T. S. (2015). A review of models for effective thermal conductivity of composite materials. *Journal of Power Technologies*, *95*(1), 14–24.

Putkonen, J. (2003). Determination of frozen soil thermal properties by heated needle probe. *Permafrost and Periglacial Processes*, *14*(4), 343-347. Retrieved from `https://onlinelibrary.wiley.com/doi/abs/10.1002/ppp.465` doi: 10.1002/ppp.465

Riksantikvaren. (2018). Besok fredete kulturminner i longyearbyen. *Available at: https://www.riksantikvaren.no/Aktuelt/Nettutstillinger/Besoek-fredete-kulturminner-i-Longyearbyen (access: 17. December 2018).*

Standard Norge. (1994). *Iso 11265 soil quality - determination of the specific electrical conductivity* (Tech. Rep.).

Standard Norge. (2013). *Ns-en 1744 test for chemical properties of aggregates* (Tech. Rep.).

Standard Norge. (2015). *Ns-en iso 17892 geotechnical investigation and testing - laboratory testing of soil* (Tech. Rep.).

Standard Norge. (2018). *Ns-en iso 14688 geotechnical investigation and testing - identification and classification of soil* (Tech. Rep.).

Sun, H., Liu, S., & Qin, J. (2016, 01). Characterizing subzero-temperature thermal properties of seasonally frozen soil in alpine forest in the western sichuan province, china. *Journal of Water Resource and Protection*, *08*, 583-593. doi: 10.4236/jwarp.2016.85048

Tice, A. R., Burrous, C. M., & Anderson, D. M. (1978, 07). Determination of unfrozen water in frozen soil by pulsed nuclear magnetic resonance. In *3rd international conference on permafrost, alberta, canada* (p. 149-155).

UNIS. (2018). Unis-data.

Vegdirektoratet. (2016). *Håndbok r210 laboratorieundersøkelser* (Tech. Rep.). Statens vegvesen.

Watanabe, K., & Mizoguchi, M. (2002, 04). Amount of unfrozen water in frozen porous media saturated with solution. *Cold Regions Science and Technology*, *34*, 103-110. doi: 10.1016/S0165-232X(01)00063-5

Williams, P. J., & Smith, M. W. (1989). *The frozen earth* (first ed.). Cambridge: Press Syndicate of the University of Cambridge.

Zhou, J., Wei, C., Lai, Y., Wei, H., & Tian, H. (2018, 11). Application of the generalized clapeyron equation to freezing point depression and unfrozen water content. *Water Resources Research*, *54*. doi: 10.1029/2018WR023221

Appendix A

Acronyms

AL	Active Layer
ALT	Active Layer Thickness
AT	Air Temperature
ESD	Empirical Statistical Downscaling
FEM	Finite Element Method
FP	Freezing Point
GS	Ground Surface
GST	Ground Surface Temperature
MAAT	Mean Annual Air Temperature
MAT	Mean Annual Temperature
MAGT	Mean Annual Ground Temperature
SFCC	Soil Freezing Characteristic Curve
SWCC	Soil Water Characteristic Curve
UNIS	University Centre in Svalbard
UWC	Unfrozen Water Content
ZAA	Zero Annual Amplitude

Appendix B

Symbols

a	Water activity [-]
A	Area $[m^2]$
A_s	Surface temperature amplitude
A_z	Amplitude of attenuation with depth $[m]$
C	Mass solute content $[g/g]$
c	Molar concentration $[mol/l]$
c	Heat capacity $[kJ/kgK]$
c_v	Volumetric heat capacity $[MJ/m^3K]$
d	Diameter $[mm]$
i	van 't Hoff index $[-]$
I_{sf}	Freezing index $[°Cdays]$
I_{st}	Thawing index $[°Cdays]$
k	Thermal conductivity $[W/mK]$
K_e	Kersten number [-]
L	Latent heat $[kJ/kg]$
L_f	Latent heat of fusion $[kJ/kg]$
m	Molar mass of water $[g/mol]$
M	Molecular weight $[g/mol]$
m_s	Mass of solids $[g]$
m_w	Mass of water $[g]$
n	Porosity [%]
n_f	Surface n-factor [-]
p	Period [hours, days]

P	Pressure [MPa]
q	Rate of heat flow $[J/m^2s]$
Q	Heat flow $[J/s]$
R	Universal gas constant$[J/Kmol]$
S_r	Saturation [%]
t	Time [hours, days]
t_{eq}	Temperature at pore water-pore ice equilibrium [°C]
T	Temperature [°C]
T_0	Reference freezing point of water [$T_0 = 273.15$°C]
T_f	Freezing point of soil [°C]
T_f	Freezing point of nonsaline soil with total water content w_0 [°C]
T_m	Mean annual temperature [°C]
T_{ref}	Freezing point of soil at reference state [°C]
$T_{S,t}$	Ground surface temperature [°C]
T_z	Maximum and minimum temperature at given depth [°C]
$T_{z,t}$	Temperature variation at given depth [°C]
v	Volume fraction $[-]$
V	Total volume $[m^3]$
V_i	Volume of ice $[m^3]$
V_v	Volume of voids $[m^3]$
V_w	Volume of water $[m^3]$
w	Total water content $[g/g]$
w_i	Frozen water content $[g/g]$
w_u	Unfrozen water content $[g/g]$
X	Penetration depth of thawing $[m]$
z	Depth $[m]$
α_u	Thermal diffusivity $[m^2/s]$
γ	Unit weight of soil $[kN/m^3]$
γ_s	Density of the soil grain particles $[kN/m^3]$
γ_w	Density of water $[kN/m^3]$
η	Constant in the generalizen Clausius Clapeyron equation [MPa]
μ_w	Chemical potential $[MPa]$
Π_D	Donnan osmotic pressure $[MPa]$

ρ	Bulk density $[g/cm^3]$
ρ_d	Dry density $[g/cm^3]$
ϕ	Phase lag [hours, days]
ψ	Water potential [MPa]
ψ_m	Matric water potential [MPa]
ψ_o	Osmotic water potential [MPa]
ω'	Surface potential [MPa]

Appendix C

Results from Laboratory Testing and Calculation Results

C.1 Experimental Test Results

Table C.1: *Results from index testing. Density, dry density and particle density.*

Sampl ID	**Sample number**	$\boldsymbol{\rho}$ $[g/cm^3]$	$\boldsymbol{\gamma}$ $[kN/m^3]$	$\boldsymbol{\rho_d}$ $[g/cm^3]$	$\boldsymbol{\gamma_d}$ $[kN/m^3]$	$\boldsymbol{\rho_s}$ $[g/cm^3]$	$\boldsymbol{\gamma_s}$ $[kN/m^3]$
E5_03	1	1.77	17.4	1.5	14.8		
E5_05	2	1.85	18.1	1.49	14.6	2.59	25.4
E5_06	3	1.89	18.5	1.50	14.7	2.66	26.0
E5_09	4	1.93	18.9	1.52	14.9	2.65	26.0
E5_11	5	1.88	18.5	1.50	14.7	2.63	25.8
E5_13	6	1.88	18.5	1.45	14.3	2.63	25.8
E5_15	7	1.92	18.9	1.54	15.1	2.64	25.9
E5_22	8	1.98	19.4	1.58	15.5	2.64	25.9

Table C.2: *Results from index testing. Water content, porosity, saturation, salinity, organic content and freezing point.*

Sample number	**Depth** [m]	$\boldsymbol{w}$ [%]	$\boldsymbol{\theta}$ [%]	$\boldsymbol{n}$ [%]	$\boldsymbol{Sr}$ [%]	**Salinity** [ppt]	**Organic content** [%]	**Freezing point depression** [°C]
1	1.9	18	25	43	61	5.6	3.6	
2	2.7	24	36	44	80	15.3	4.8	–1.1
3	3.1	26	40	43	88	30.3	4.3	–1.5
4	4.3	27	41	43	94	29.1	4.4	–1.6
5	5.1	26	39	43	88	24.4	4.6	–1.8
6	5.9	30	43	45	95	25.2	4.2	–2.0
7	6.7	25	38	42	90	31.4	4.2	–2.1
8	9.5	26	40	40	99	29.7	4.3	–2.0

Table C.3: *Average values for the frozen and unfrozen thermal conductivity.*

Sample number	**Thermal conductivity** $[W/mk]$				**Volumetric heat capacity** $[MJ/m^3k]$	
	TR–1		SH–1		SH–1	
	k_uf	k_f	k_uf	k_f	$c_{v,uf}$	$c_{v,f}$
1	0.8	1.15	0.48	0.57	1.60	1.47
2	0.84	1.48	0.82	1.28	1.82	1.51
3	0.85	1.18	1.00	1.35	2.19	1.66
4	1.55	2.31	1.60	2.4	2.87	2.26
5	–	–	1.50	2.25	2.88	2.69
6	1.35	2.14	1.20	1.88	2.73	2.35
7	1.65	2.35	1.54	2.30	2.93	2.51
8	1.75	2.30	1.52	2.25	2.74	2.32

C.2 Calculation of Unfrozen Water Content

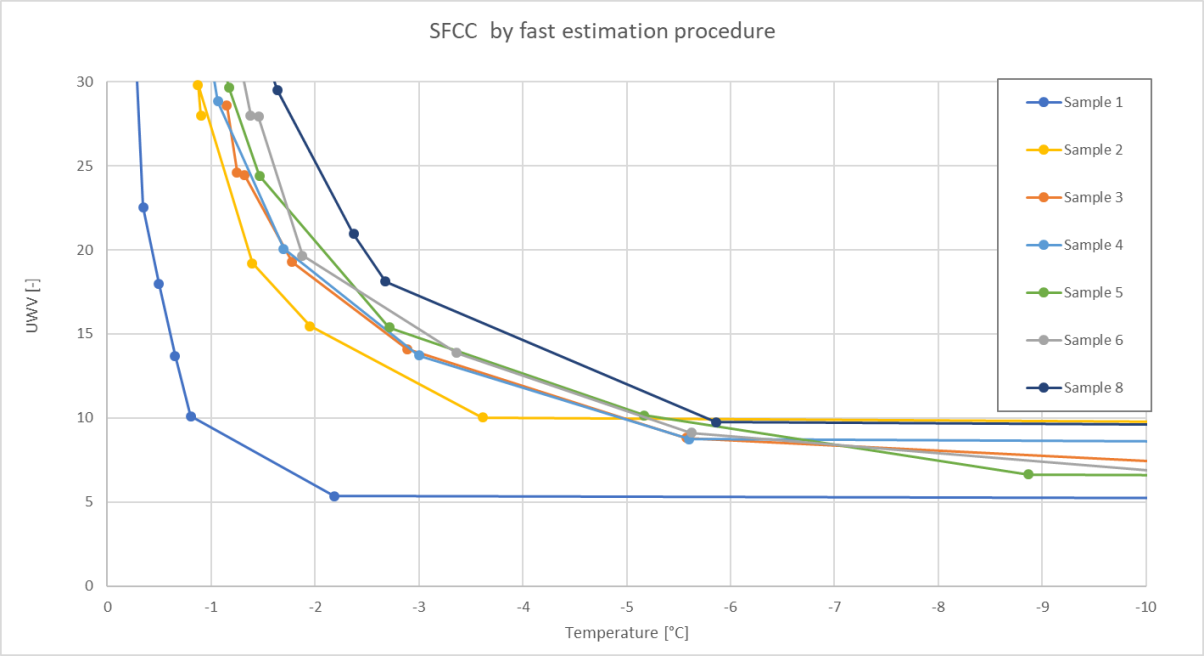

Figure C.1: *The SFCC calculated with the fast estimation of UWC by (Istomin et al., 2017).*

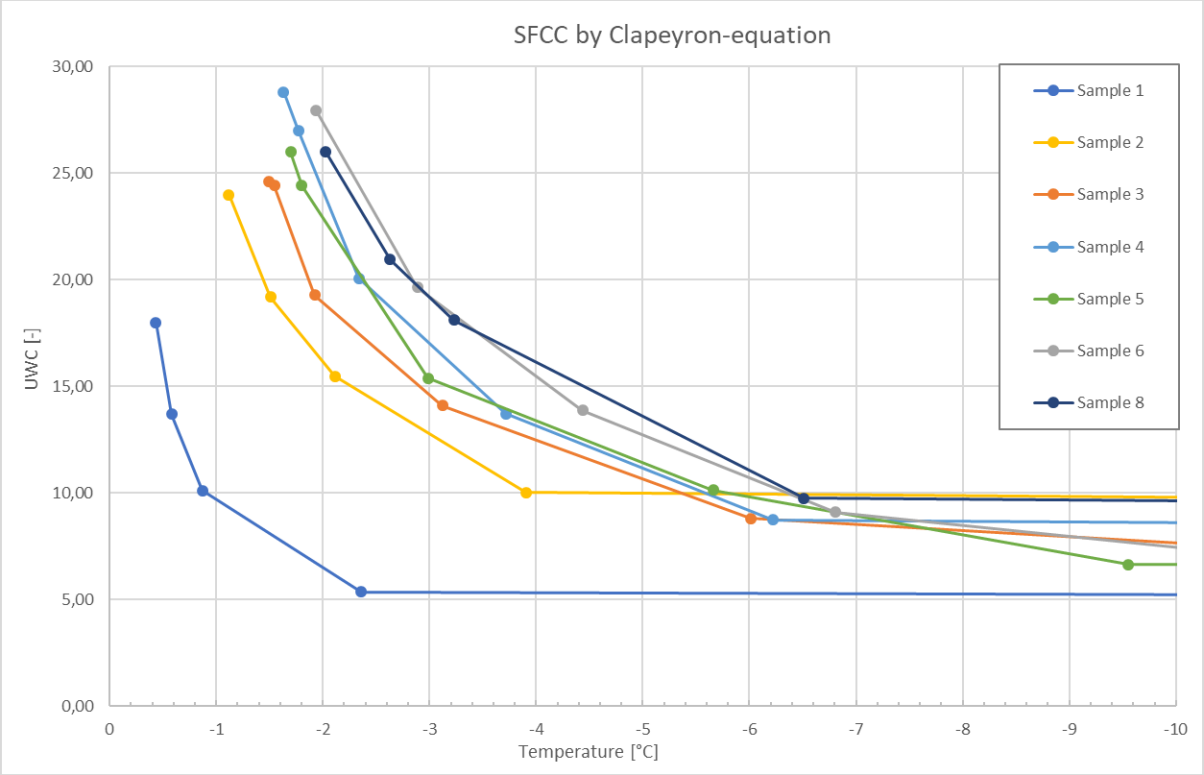

Figure C.2: *The SFCC calculated for the soil samples with the generalized Clapeyron equation.*

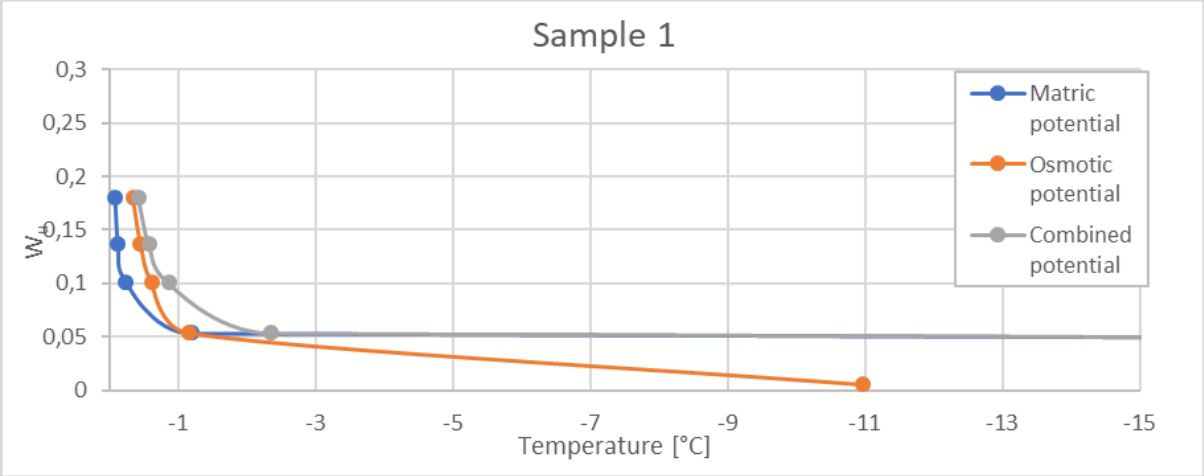

Figure C.3: *The curve of unfrozen water content calculated from osmotic potential, matric potential and total water potential for sample 1.*

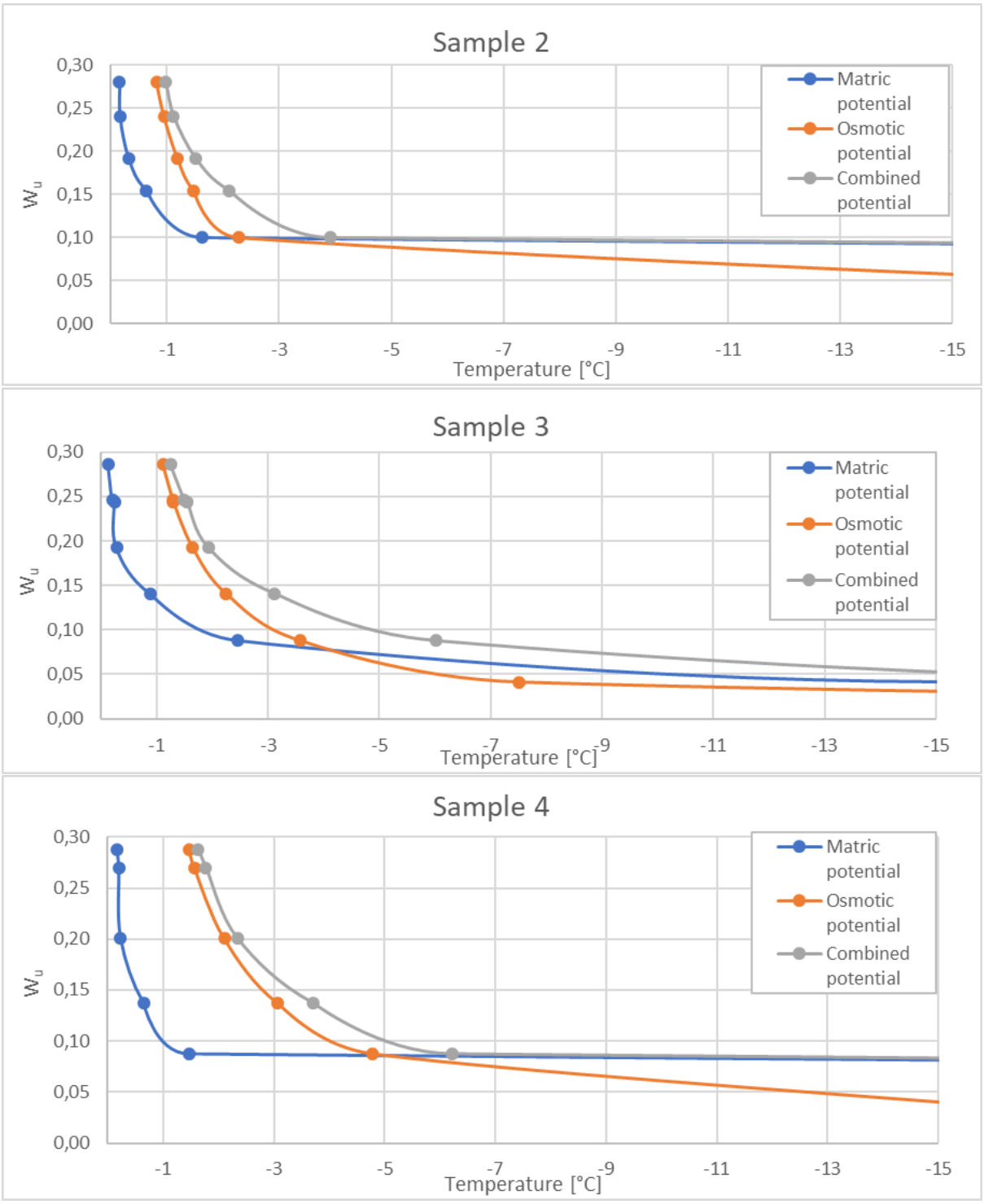

Figure C.4: *The curve of unfrozen water content calculated from osmotic potential, matric potential and total water potential for sample 2–4.*

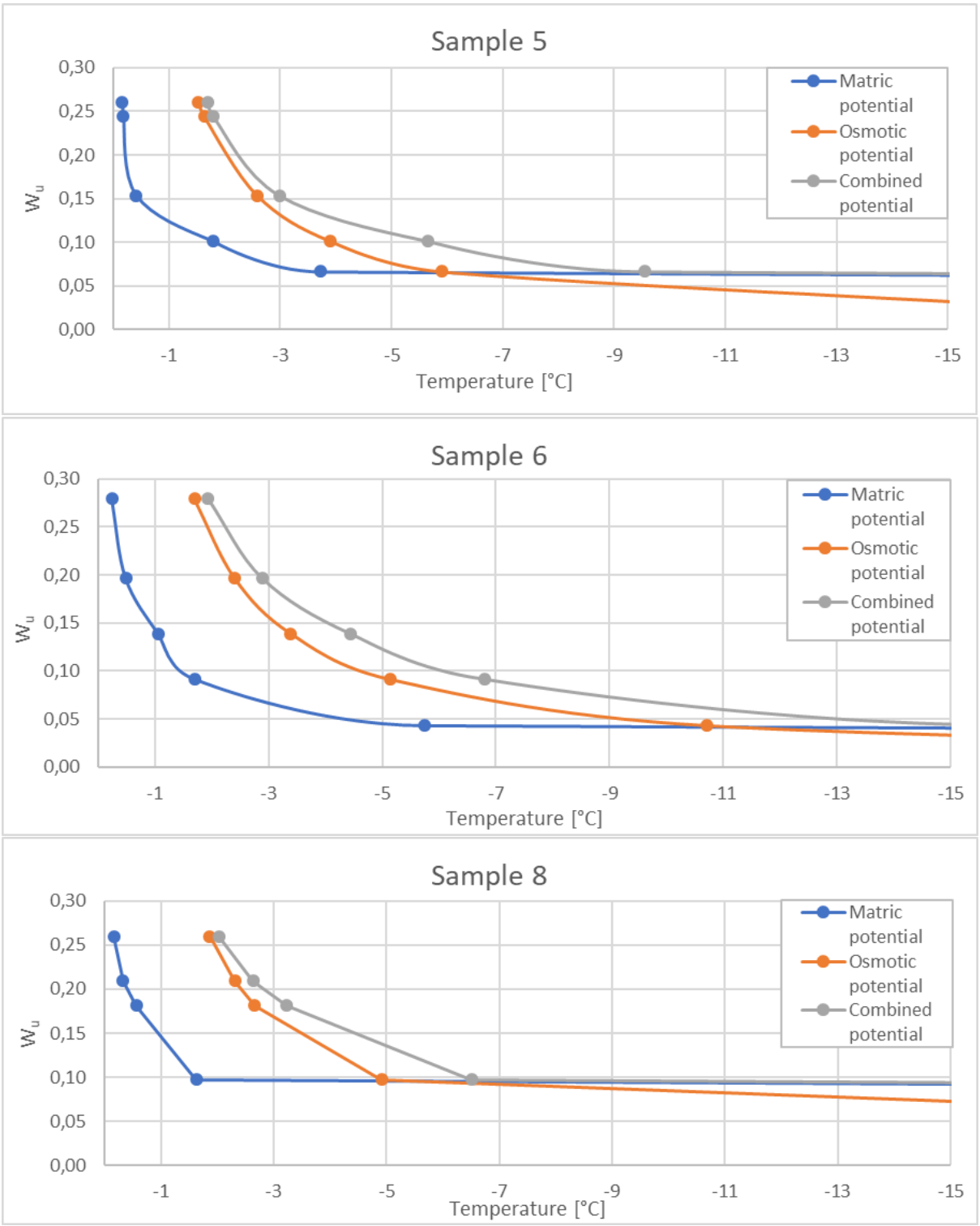

Figure C.5: *The curve of unfrozen water content calculated from osmotic potential, matric potential and total water potential for sample 5, 6 and 8.*

Appendix D

Geothermal Model Proposition

D.1 Soil Parameters for Modelling

Table D.1: *Soil properties used as input parameters in the model of the ground thermal regime at UNIS East set up in Geostudio 2018.*

Sample	**Volumetric Water Content**	**Volumetric Heat Capacity** $kJ/m^3/°C$	
		Unfrozen	**Frozen**
1	0.25	2200	1800
2	0.36	2570	2100
3	0.40	2710	2010
4	0.41	2810	2210
5	0.39	2710	2080
6	0.43	2860	2050
7	0.38	2860	2050
8	0.40	2850	2290

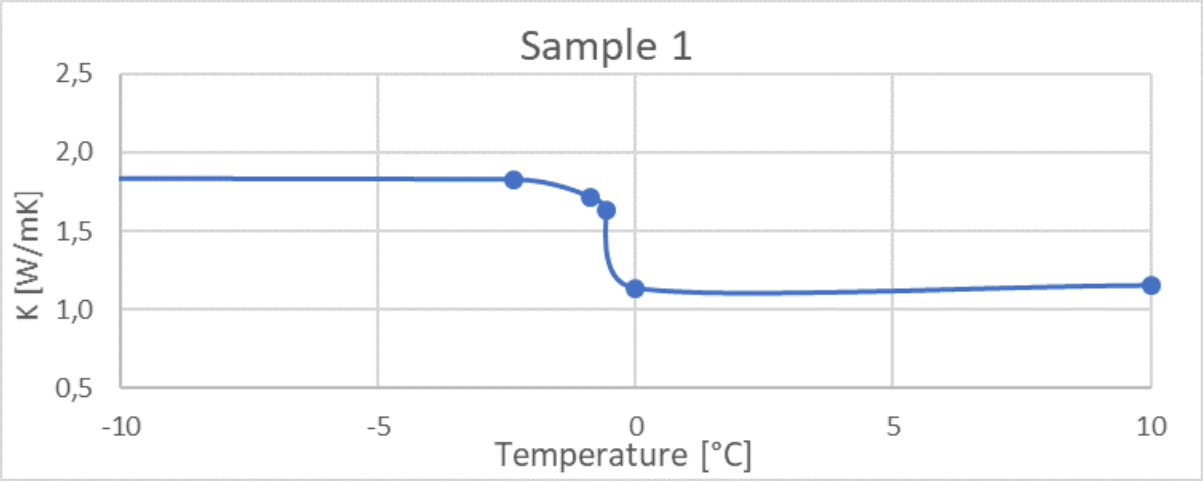

Figure D.1: *The curve for sample 1 relating thermal conductivity to temperature calculated by the Johansen's empirical formulation with the estimated SFCC.*

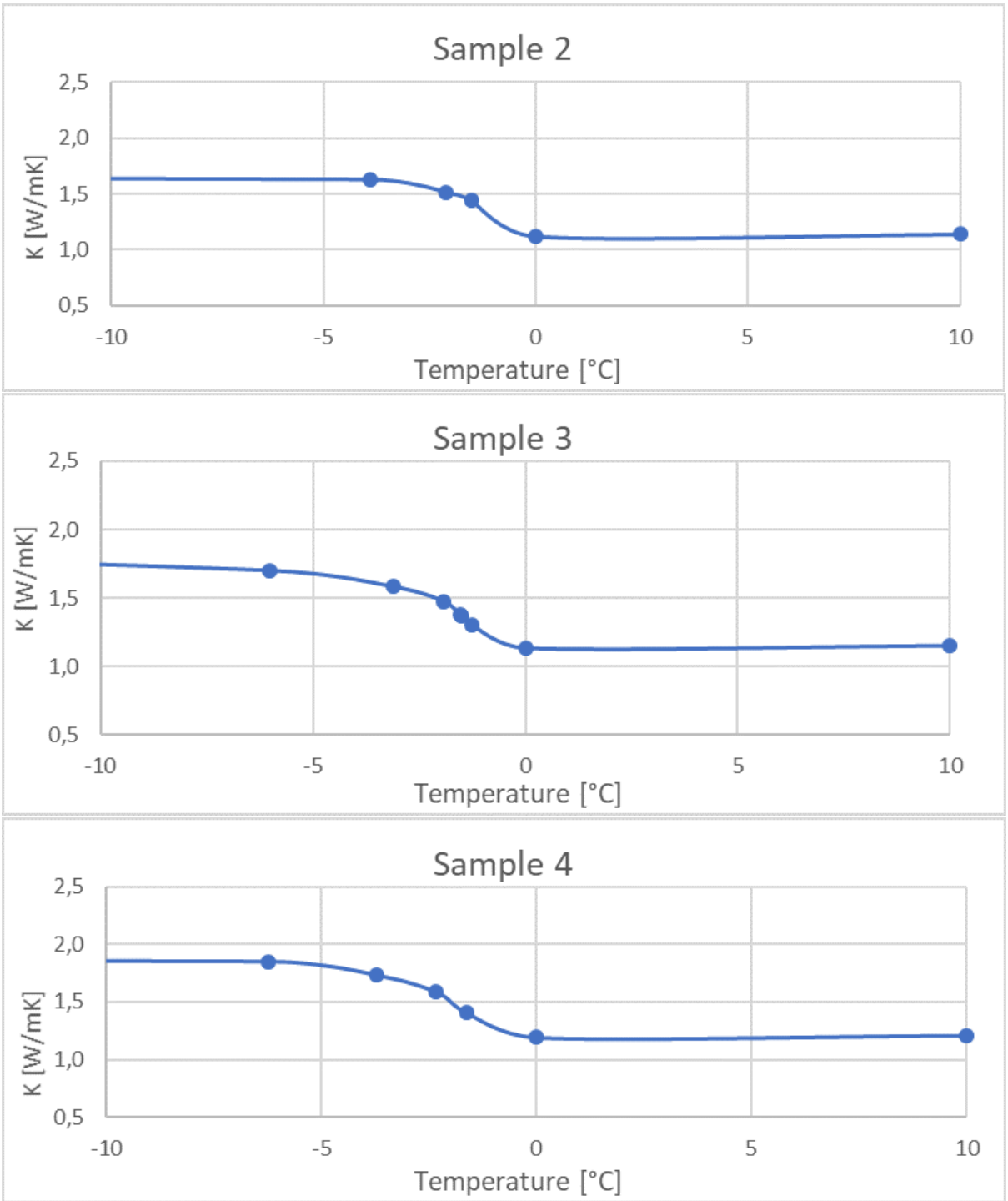

Figure D.2: *The curve for sample 2–4 relating thermal conductivity to temperature calculated by the Johansen's empirical formulation with the estimated SFCC.*

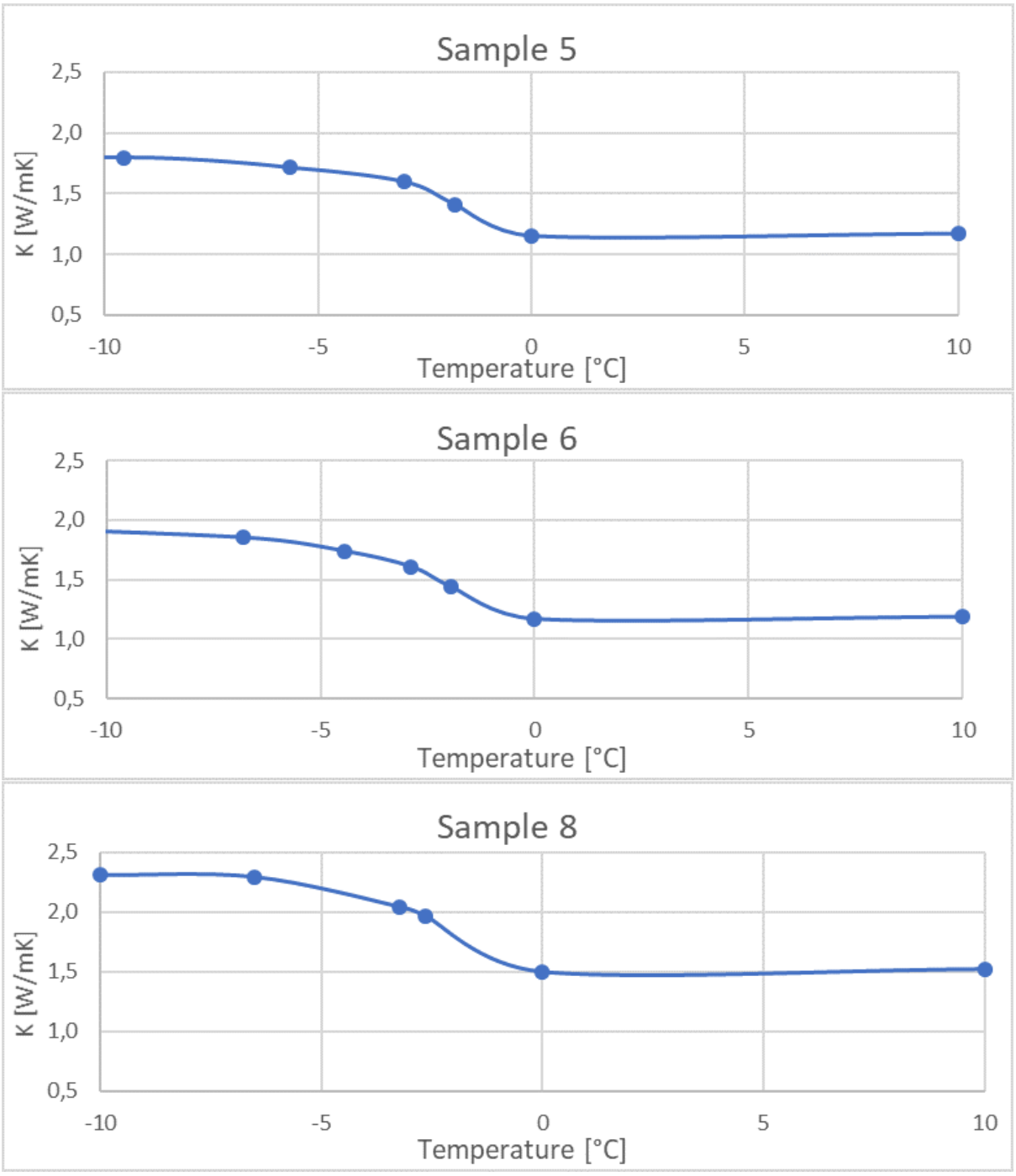

Figure D.3: *The curve for sample 5, 6 and 8 relating thermal conductivity to temperature calculated by the Johansen's empirical formulation with the estimated SFCC.*

D.2 Model Profiles

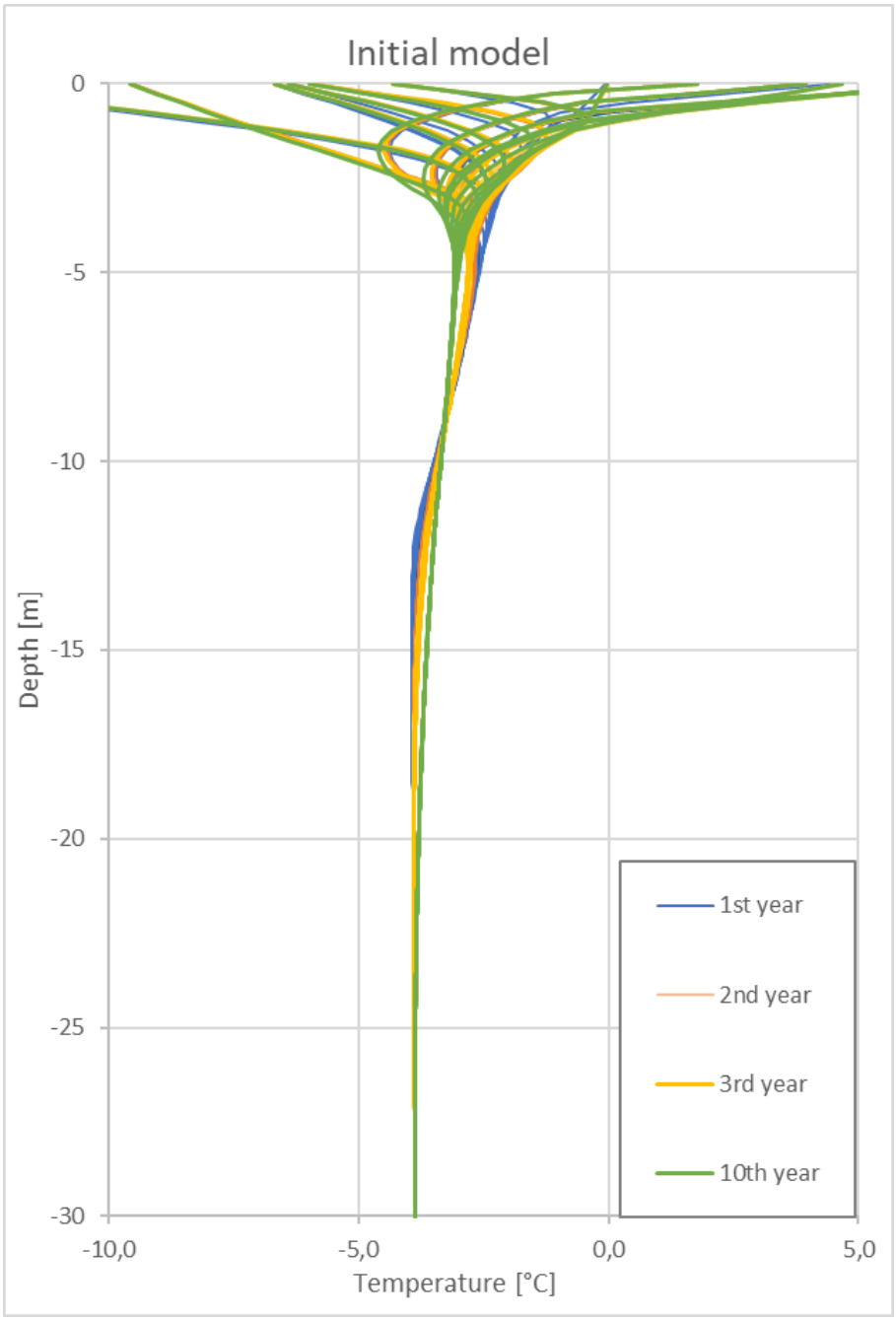

Figure D.4: *Temperature profiles from model simulations. The same temperature curve is applied at GS over several years. The curves are shown for the 1st, 2nd, 3rd and 10th year.*

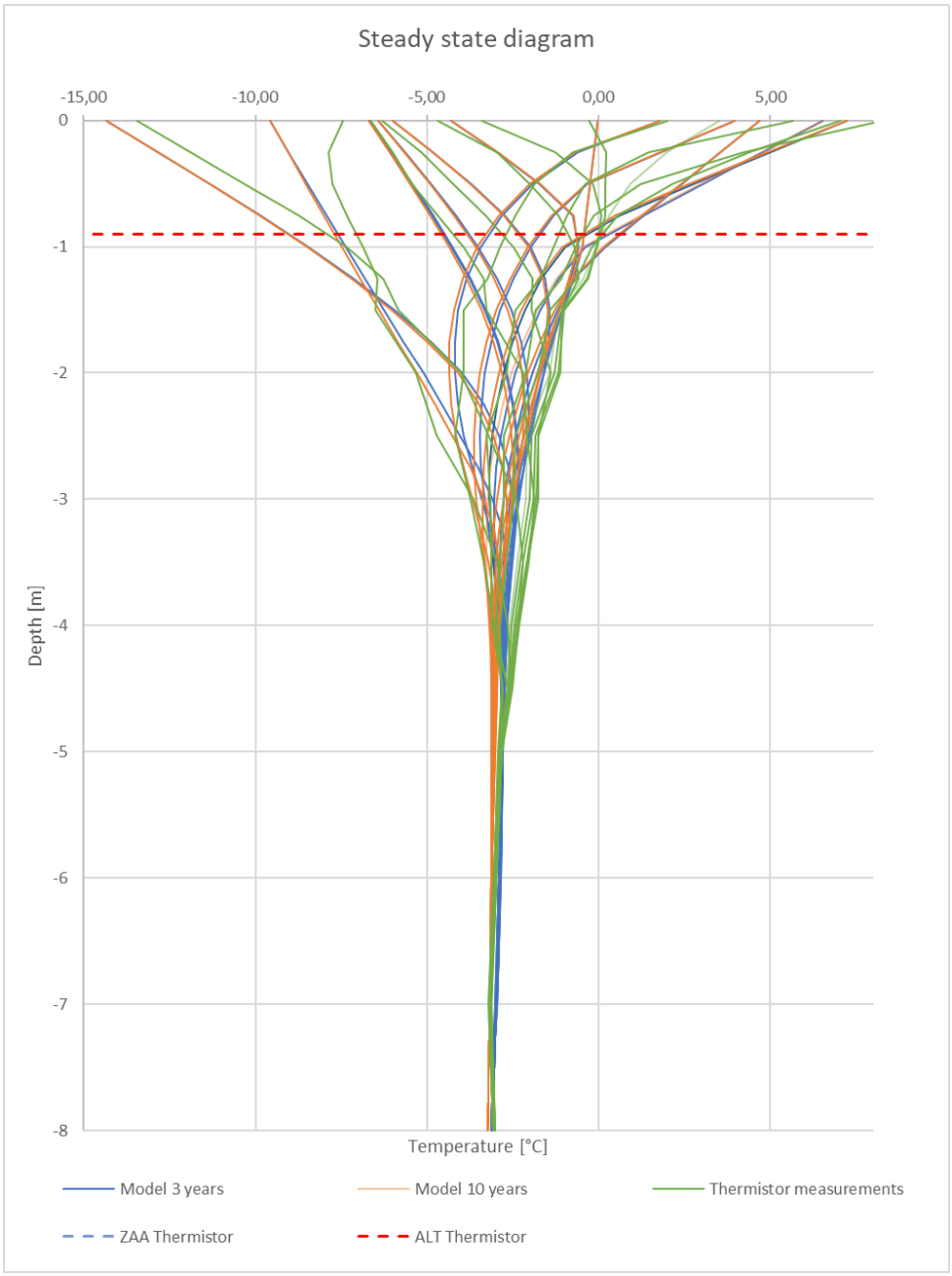

Figure D.5: *Comparison of the temperature profile from thermistor measurements and model simulations for the 3rd and 10th year. For the model simulations average air temperatures for 2017–2018 are applied. Depth of ZAA and ALT for the thermistor profile is indicated.*

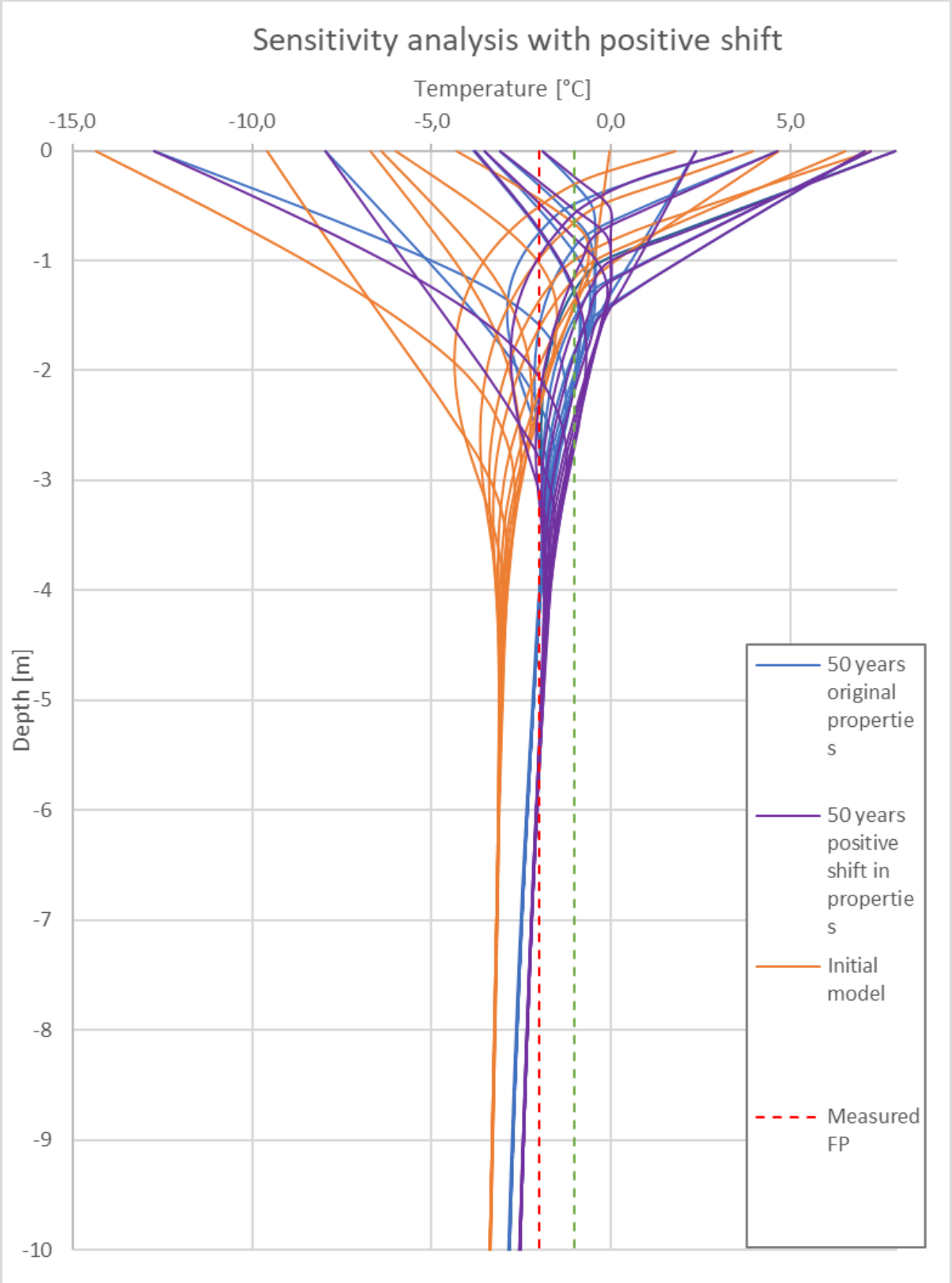

Figure D.6: *Increasing the temperature of the UWC curve and thermal conductivity by +1°C shows the sensitivity of soil model to change in soil properties. The RCP2.6 scenario is used as boundary condition over 50 years.*

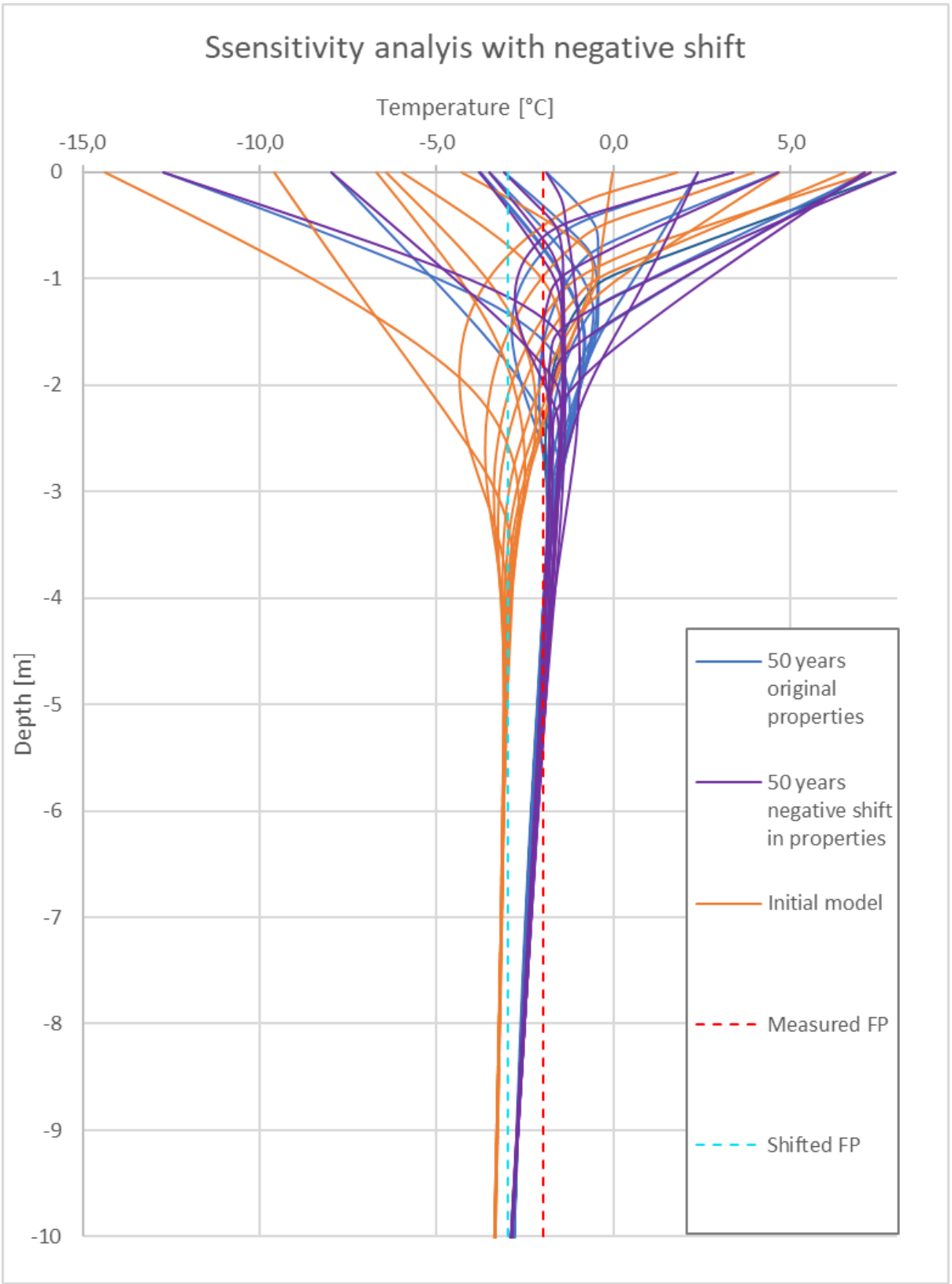

Figure D.7: *Increasing the temperature of the UWC curve and thermal conductivity by –1°C shows the sensitivity of soil model to change in soil properties. The RCP2.6 scenario is used as boundary condition over 50 years.*